



# UNIVERSITÀ DEGLI STUDI DI TRIESTE

## XXVIII CICLO DEL DOTTORATO DI RICERCA IN

INGEGNERIA E ARCHITETTURA – INDIRIZZO INGEGNERIA  
MECCANICA, NAVALE DELL'ENERGIA E DELLA PRODUZIONE

### **Experimental study and numerical simulation of the behaviour of viscoelastic materials to reduce the vibrations on board ships**

Settore scientifico-disciplinare: ING-IND/02

PHD STUDENT  
**PEDRO NICOLAS  
MENDOZA VASSALLO**

PHD PROGRAM COORDINATOR  
**PROF. DIEGO MICHELI**

THESIS SUPERVISOR  
**PROF. MARCO BIOT**

**ACADEMIC YEAR 2015/2016**



## **Acknowledgments**

This PhD thesis would not have been possible without the help and contribution from several people I would like to thank and mention.

I would like to thank CSNI S.c.a.r.l. for the preparation of the test specimens and prototypes without which the experimental part of the research would not have been possible.

I am very grateful to all of my professors for their guidance, especially my supervisor prof. Marco Biot, for his patience and support and also, to my colleagues for their inspiration and technical advice.

Many thanks go to all my friends for their unconditional support.

Special thanks go to my family for their sacrifices and encouragement, and to my love, Réka, for her love, attention and support especially in these past few months.



## **Riassunto**

Al giorno d'oggi, il rumore e le vibrazioni sono i fattori principali per valutare i livelli di comfort a bordo delle navi. Nel caso delle navi di lusso, quali navi da crociera e mega-yacht, gli elevati livelli di comfort richiesti sono raggiunti attraverso la mitigazione del rumore e delle vibrazioni generate dalle sorgenti a bordo. In questa tesi sono stati studiate la riduzione delle vibrazioni a bordo delle navi con l'applicazione di materiali viscoelastici mediante l'utilizzo di pavimenti flottanti e l'applicazione di materiali viscoelastici sulle strutture.

Per quanto riguarda i pavimenti flottanti, sono stati condotti diversi studi per dimostrare la loro efficacia nell'isolamento delle strutture riceventi sulle navi, come le cabine passeggeri, e anche per valutare le loro prestazioni. Tuttavia, esiste una mancanza di metodi di progettazione per controllare la capacità dei pavimenti flottanti per ridurre i livelli di rumore strutturale e nonché le procedure standard per testare il loro Transmission Loss. Nel caso dell'applicazione di materiali viscoelastici, sono stati condotti diversi studi per il loro utilizzo nei settori aerospaziale e automobilistico, dimostrando la loro efficacia per ridurre i livelli di rumore strutturale e vibrazioni. Nonostante

l'applicazione di materiali viscoelastici nell'industria marittima da diversi anni, il loro utilizzo si basa principalmente sull'esperienza dei cantieri navali e dei subappaltatori. In mancanza di una procedura standard per la progettazione di queste soluzioni di smorzamento, occorrerebbe effettuare ulteriori ricerche per generare modelli matematici e procedure di progettazione per consentire ai progettisti navali di simulare più accuratamente gli effetti di questo trattamento sulle strutture marine.

Per quanto riguarda i pavimenti flottanti, è stata sviluppata una procedura per la progettazione di nuovi pavimenti flottanti per applicazioni marine, con l'obiettivo di migliorare le loro capacità di isolare le strutture riceventi da un rumore strutturale. La procedura utilizza nella prima fase simulazioni con elementi finiti per ottimizzare il materiale resiliente da utilizzare per il disaccoppiamento della struttura ricevente dalla struttura vibrante, nonché il profilo strutturale che supporta il materiale resiliente. Le configurazioni ottimali vengono quindi fabbricate in prototipi per realizzare prove di laboratorio per convalidare i modelli agli elementi finiti, per identificare le risonanze del pavimento flottante e per valutare i livelli di Transmission Loss. I risultati dell'attività di ricerca mostrano l'efficacia della procedura proposta e sottolineano l'importanza dei test sperimentali per convalidare l'esito delle simulazioni numeriche. Per quanto riguarda l'applicazione di materiali viscoelastici a bordo le navi, si propone un metodo

per eseguire prove di laboratorio per la misurazione del Loss Factor di materiali viscoelastici applicati su lastre rettangolari, utilizzando lo stesso background teorico dello standard ASTM E756, senza ricorrere ad attrezzature altamente precise e costose. Questo studio rappresenta il punto di partenza per la base di una ricerca congiunta a lungo termine tra Memorial University of Newfoundland, l'Università di Trieste e CSNI S.c.a.r.l., che ha come obiettivo finale la definizione di un approccio razionale per un'applicazione ottimale dei materiali viscoelastici nelle strutture marine per meglio controllare il rumore strutturale a bordo delle navi.





## **Abstract**

Nowadays, noise and vibrations are the main factors for evaluating comfort levels on board ships. In the case of luxury vessels, such as cruise ships and mega-yachts, the required high levels of comfort are achieved through the mitigation of noise and vibrations generated by onboard sources. In this thesis the reduction of vibrations on board ships with the application of viscoelastic materials by means of the use of floating floors and the application of viscoelastic materials on the structures are studied.

Concerning floating floors, several studies have been undertaken to demonstrate their effectiveness in isolating the receiving structures in ships, such as the passenger cabins, and also to evaluate their performance. However, there is a lack of design methods for controlling the capability of floating floors to diminish structure borne noise levels, as well as standard procedures to test their Transmission Loss. In the case of the application of viscoelastic materials, several studies have been done for their use in the aerospace and automotive fields, proving their effectiveness to reduce the structure borne noise and vibration levels. Despite the application of viscoelastic materials in the maritime industry for several years, their use is based mainly on the

experience of shipyards and sub-contractors. There is still a lack of a standard procedure for the design of these damping solutions, which is why, more research should be carried out in order to generate mathematical models and design procedures to allow ship designers to simulate more accurately the effects of this treatment on marine structures.

Regarding the floating floors, a procedure has been developed for the design of new floating floors for marine applications, with the objective to improve their capabilities of isolating the receiving structures from structure borne noise. The procedure first uses Finite Element simulations to optimise the resilient material to be used for the decoupling of the receiving structure from the vibrating structure, as well as the structural beam supporting the resilient material. The optimal configurations are then built into prototypes for laboratory tests to validate the Finite Element models, to identify the floating floor resonances and to evaluate the Transmission Loss levels. The results of the research activity show the effectiveness of the proposed procedure and emphasise the importance of the experimental tests to validate the outcome of the numerical simulations. On the subject of the application of viscoelastic materials on board ships, a method is proposed to perform laboratory tests for the measurement of the Loss Factor of viscoelastic materials applied on rectangular plates, using the same theoretical background of the ASTM E756 standard, without recurring to highly precise and costly equipment. This study

represents the starting point for the base of a long term joint research among the Memorial University of Newfoundland, the University of Trieste and CSNI S.c.a.r.l., that has as final objective the definition of a rational approach for an optimal application of viscoelastic materials in marine structures to better control the structure borne noise on board ships.



# Table of Contents

Riassunto.....	i
Abstract.....	vii
Nomenclature.....	xv
List of Figures.....	xix
List of Tables.....	xxvi
Introduction.....	1
THEORETICAL BACKGROUND.....	5
1 Vibration damping and control.....	5
1.1 Linear viscous damping.....	5
1.1.1 Equation of motion for a SDOF system.....	6
1.2 Representations of damping.....	7
1.3 Loss Factor.....	9
1.4 Complex modulus model.....	9
1.5 Effects of temperature and frequency.....	11
1.5.1 Effects of temperature.....	11

1.5.2 Effects of frequency.....	12
METHODS .....	13
2 Passive vibration control.....	13
2.1 Control of vibration by added damping .....	14
2.2 Control of vibration by resilient isolation .....	17
3 Measures of damping.....	19
3.1 Complex modulus measurement .....	20
3.1.1 Unconstrained layer configuration .....	21
3.1.2 Constrained layer configuration .....	27
3.1.3 Half-power bandwidth method .....	34
4 Motion Transmissibility.....	37
5 Floating Floor performance indicators .....	39
5.1 Transmission Loss .....	39
5.2 Insertion Loss .....	41
6 Floating floor optimisation .....	43
6.1 Background .....	43
6.2 Optimisation procedure .....	44
EXPERIMENTAL SETUP .....	49

7	Floating floors experimental procedures .....	51
7.1	Configuration Optimisation.....	52
7.1.1	Configurations .....	52
7.1.2	Material selection .....	53
7.1.3	Design load .....	54
7.1.4	Design constraints.....	54
7.2	Numerical simulations.....	55
7.2.1	Finite element model description .....	55
7.2.2	Finite element static simulations results .....	62
7.2.3	Finite element dynamic simulation results .....	63
7.3	Static laboratory tests .....	65
7.3.1	Static laboratory tests: Setup .....	66
7.3.2	Static laboratory tests: Results.....	67
7.4	Dynamic laboratory tests.....	68
7.4.1	Dynamic tests setup: Measurement of resonant frequencies... ..	68
7.4.2	Dynamic tests results: Resonant frequencies.....	70
7.4.3	Dynamic tests setup: Measurement of Transmission Loss .....	71
7.4.4	Dynamic tests results: Transmission Loss .....	73

7.5 Conclusion.....	76
8 Plate structure .....	79
8.1 Excitation system .....	85
8.2 Acquisition system .....	90
8.3 Data processing .....	93
8.4 Windowing .....	94
8.5 Results .....	97
RESULTS AND DISCUSSION .....	109
9 Resilient Mounts.....	109
10 Material characterisation .....	111
CONCLUSIONS .....	115
REFERENCES .....	119



# Nomenclature

## Latin symbols

$A$	Absorption area of receiving room ( $\text{m}^2$ )
$A(\omega)$	Accelerance ( $\text{a/F}$ )
$c$	Damping coefficient
$d$	Static deflection (m)
$D$	Flexural rigidity ( $\text{Pa}\cdot\text{m}^3$ )
$e$	Young modulus ratio
$E$	Young modulus (Pa)
$f$	Frequency (Hz)
$G$	Shear modulus (Pa)
$g$	Shear parameter
$h$	Thickness ratio
$H$	Plate thickness (m)
$i$	Imaginary unit
$I$	Second moment of inertia ( $\text{m}^4$ )
$IL$	Insertion Loss (dB)
$k$	Stiffness
$k$	Dimensional eigenvalue
$L$	Plate length (m)
$L_p$	Sound pressure level (dB)
$L_v$	Average velocity level (dB)
$m$	Mass (kg)

$M$	Mechanical mobility
$P$	Compression load (N/m <sup>2</sup> )
$Q$	Quality factor
$r$	Frequency ratio
$S$	Radiating surface (m <sup>2</sup> )
$t$	Time (s)
$T$	Motion transmissibility
$TL$	Transmission Loss (dB)
$U$	Strain energy
$v$	Motion velocity (m/s)
$W_d$	Energy loss
$W_{radiated}$	Sound power radiated (W)
$X(\omega)$	Receptance (x/F)
$Y$	Structural parameter
$Z_u^*$	Bending stiffness ratio: unconstrained layer configuration
$Z_c^*$	Bending stiffness ratio: constrained layer configuration

**Greek  
symbols**

$\varepsilon$	Normal strain
$\zeta$	Damping coefficient
$\eta$	Loss Factor
$\lambda$	Dimensionless frequencies
$\nu$	Poisson ratio
$\xi$	Eigenvalue
$\pi$	Pi
$\rho$	Density (kg/m <sup>3</sup> )

$\sigma$	Normal stress (Pa)
$\sigma_e$	Radiation efficiency
$\tau$	Shear stress (Pa)
$\phi$	Shear strain
$\psi$	Time or phase lag (s)
$\omega$	Frequency (rad/s)

### **Abbreviations**

ASTM	American Society for Testing and Materials International
CLD	Constrained Layer Damping Configuration
DMA	Dynamic Mechanical Analysis
DMTA	Dynamic Mechanical Thermal Analysis
FEM	Finite Element Method
FFT	Fast Fourier Transform
FLD	Free Layer Damping Configuration
FRF	Frequency Response Function
HVAC	Heating Ventilating and Air Conditioning
MDOF	Multi Degree Of Freedom
NVL	Ship Noise and Vibration Laboratory
RKU	Ross Kerwin Ungar
SDOF	Single Degree Of Freedom



## List of Figures

Figure 1 – One degree of freedom system with viscous damper, the Voigt-Kelvin model.....	6
Figure 2 – Harmonic excitation and response for a viscoelastic solid.....	7
Figure 3 – Hysteresis loop for a viscoelastic material .....	8
Figure 4 – Effects of temperature in the complex modulus properties behaviour of a typical viscoelastic material.....	11
Figure 5 – Effects of frequency in the complex modulus properties behaviour of a typical viscoelastic material.....	12
Figure 6 – Unconstrained layer with extensional damping configuration ....	15
Figure 7 – Constrained layer with shear damping configuration.....	17
Figure 8 – Continuous floating floor (1) and resiliently mounted floating floor (2).....	18
Figure 9 – Representation of a free layer damping system.....	22
Figure 10 – Representation of a constrained layer damping system .....	28
Figure 11 – Half-power bandwidth method .....	36
Figure 12 – SDOF system suspended on a moving platform .....	38

Figure 13 – Typical transmissibility curve of a damped SDOF system with support motion .....	38
Figure 14 – Transmission Loss curve of a damped SDOF system .....	40
Figure 15 – Transmission Loss curves of two damped SDOF systems with the same inertia, $m$ , and damping, $c$ , but different stiffness. ....	46
Figure 16 – Typical floating floor grillage considered as case study, with a detail of the beam section .....	52
Figure 17 – Transverse section of the supporting beams with the resilient elements in the original open configuration, and the new closed configuration .....	53
Figure 18 – Finite element model of a floating floor module with continuous resilient element application .....	56
Figure 19 – Finite element model of a floating floor module with discontinuous resilient element application .....	56
Figure 20 – Open beam section configuration mesh .....	57
Figure 21 – Resilient material mesh used for the open beam section configuration .....	57
Figure 22 – Resilient material and closed beam mesh used for the closed beam section configuration .....	58
Figure 23 – Portion of the module depicting the design load applied on each shell element on the top part of the beam section with light blue vectors ....	59

Figure 24 – Central part of the base module depicting the unitary force applied to one of the central nodes for the dynamic simulations with a light blue vector ..... 60

Figure 25 – Extremity of the base module showing the read-out node for the frequency transfer function measurement with an orange rhombus ..... 60

Figure 26 – Portion of the module depicting the fixed base boundary condition applied to the lower nodes of the solid elements of the resilient material .... 61

Figure 27 – Portion of the module depicting the symmetry constraint in the Y axis applied to one of the extremities of the module along the Y axis ..... 62

Figure 28 – Linear static simulation of the original floating floor module, showing the deformation and fringe of the structure ..... 62

Figure 29 – Mobility FRF of the dynamic simulation taken on the base module, log-log scale ..... 64

Figure 30 – Mobility FRF of the dynamic simulation taken on the base module, lin-log scale ..... 64

Figure 31 – A floating floor prototypes built after the numerical simulations ..... 66

Figure 32 – Setup of the static deflection tests undertaken in laboratory on the floating floor prototypes ..... 67

Figure 33 – Experimental apparatus used for the measurement of the damped natural frequencies of the floating floor prototypes..... 69

Figure 34 – Accelerance functions in the vertical direction of the floating floor modules.....	71
Figure 35 – Scheme of the experimental setup for the measurement of the Transmission Loss of the floating floor prototype modules .....	72
Figure 36 – Experimental apparatus used for the measurement of the Transmission Loss of the floating floor prototype modules .....	73
Figure 37 – Transmission Loss curves of the floating floor prototype modules .....	75
Figure 38 – Different configurations for the measurement of damping characteristics of non-self-supporting damping materials .....	79
Figure 39 – Dependence of system Loss Factor ( $\eta c$ ) of a plate with a viscoelastic layer application, on the relative thickness and modulus of the viscoelastic layer.....	81
Figure 40 – Setup for the Experimental Modal Analysis.....	82
Figure 41 – Final test setup with suspended elastic connections of plate specimen .....	85
Figure 42 – Impulse Hammer APtech AU02-6135.....	86
Figure 43 – Mode 1: 41.8 Hz.....	87
Figure 44 – Mode 2: 43.6 Hz.....	87
Figure 45 – Mode 3: 98.3 Hz.....	87
Figure 46 – Mode 4: 115.1 Hz.....	87



Figure 47 – Mode 5: 118.9 Hz .....	87
Figure 48 – Mode 6: 149.9 Hz .....	87
Figure 49 – Mode 7: 176.8 Hz .....	87
Figure 50 – Mode 8: 215.9 Hz .....	87
Figure 51 – Mode 9: 234.6 Hz .....	88
Figure 52 – Mode 10: 286.6 Hz .....	88
Figure 53 – Mode 11: 316.7 Hz .....	88
Figure 54 – Mode 12: 329.9 Hz .....	88
Figure 55 – Mode 13: 351.0 Hz .....	88
Figure 56 – Mode 14: 382.7 Hz .....	88
Figure 57 – Mode 15: 425.4 Hz .....	88
Figure 58 – Mode 16: 439.2 Hz .....	88
Figure 59 – Mode 17: 441.9 Hz .....	89
Figure 60 – Mode 18: 533.9 Hz .....	89
Figure 61 – Mode 19: 570.1 Hz .....	89
Figure 62 – Mode 20: 595.4 Hz .....	89
Figure 63 – Suitable impact areas indicated in red shade .....	90
Figure 64 – Final impact location, point “b” .....	90
Figure 65 – Acquisition system elements .....	91
Figure 66 – Initial accelerometer locations along the base plate .....	92
Figure 67 – Accelerometer locations .....	93

Figure 68 – Typical time response before and after application of an exponential window .....	95
Figure 69 – Time response, Acceleration ( $m/s^2$ ) vs Time (s), used for the initial general identification of peaks, where windowing is needed to force the response to decay .....	96
Figure 70 – Time response, Acceleration ( $m/s^2$ ) vs Time (s), used for the zooming technique, where windowing is not needed due to the natural decay of the response .....	96
Figure 71 – Accelerance frequency response function of 2mm Base Plate (BP2).....	97
Figure 72 – Accelerance frequency response function of 5mm Base Plate (BP5).....	98
Figure 73 – Comparison of the Accelerance of BP2 and PL2-FLD .....	98
Figure 74 – Comparison of the Accelerance of BP2 and PL4-FLD .....	99
Figure 75 – Comparison of the Accelerance of BP5 and PLS0.5-CLD.....	100
Figure 76 – Modal Loss Factor ( $\eta$ ) of PL2-FLD specimen .....	101
Figure 77 – Modal Loss Factor ( $\eta$ ) of PL4-FLD specimen .....	101
Figure 78 – Modal Loss Factor ( $\eta$ ) of PLS0.5-CLD specimen .....	102
Figure 79 – Comparison of the Accelerance of BP5 and PVA-FLD .....	103
Figure 80 – Comparison of the Accelerance of BP5 and PVB-FLD .....	103
Figure 81 – Comparison of the Accelerance of BP5 and PVC-FLD .....	104

Figure 82 – Comparison of the Accelerance of BP5 and PVD-FLD .....	104
Figure 83 – Modal Loss Factor ( $\eta$ ) of PVA-FLD specimen .....	105
Figure 84 – Modal Loss Factor ( $\eta$ ) of PVB-FLD specimen .....	106
Figure 85 – Modal Loss Factor ( $\eta$ ) of PVC-FLD specimen .....	106
Figure 86 – Modal Loss Factor ( $\eta$ ) of PVD-FLD specimen .....	107
Figure 87 – Transmission Loss curves of the floating floor prototype modules .....	109
Figure 88 – Obtained Loss Factor of Plastigel .....	112
Figure 89 – Comparison graph between the Loss Factor obtained with DMA tests performed on Plastigel, Viscogel and Sylomer, and the Loss Factor calculated with the methods presented in this work .....	113

## List of Tables

Table 1 – Different configurations of floating floor supporting hollow beam taken into account for the optimisation process.....	54
Table 2 – Results of the linear static finite element analyses of the different configurations of the floating floor modules .....	63
Table 3 – Configurations selected for prototype construction after the numerical simulations .....	66
Table 4 – Results for the static deflection tests performed on the floating floor module prototypes undertaken in the laboratory .....	67
Table 5 – Measured damped natural frequency of the floating floor prototype modules tested.....	70
Table 6 – Characteristics of Base Plate 1 .....	83
Table 7 – Characteristics of Base Plate 2 .....	83
Table 8 – Specimens tested .....	84

## **Introduction**

The study of the improvement of comfort aboard ships by means of reducing the noise and vibration levels is a subject that is being studied for several years, including the research and development of the standards that define a comfortable ship or cabin [1] [2] [3] [4], the identification and isolation of the vibration sources [5] [6] [7] [8], the prediction of the vibration levels transmitted on board ships [9], the isolation of the receiving entities [10] [11] [12], and so on. These studies are of great importance since noise and vibration are not only a key factor to high passenger comfort, but they are also an issue of concern since they can affect the health of the crew members [13] [14] [15].

The first approach for controlling noise and vibrations aboard ships, is to isolate the sources of vibrations, which is done generally by resiliently mounting the sources [8]. The second approach, when the first is not enough, or not effective in all the frequency range of interest, is to isolate the receiving entities. The methods of isolation vary according to the receiving entity. Floating floors are an effective solution to mitigate impact noise and structure borne noise [16]. However, in certain cases, these solution methodologies are not suitable or efficient in the mitigation of the structure borne noise in the

frequency range of 20 Hz to 250 Hz [17]. For these situations, another treatment used to isolate the receiving areas is the addition of damping layers on the structures [12] [18].

In spite of the existence of numerous research activities and intentions to study methods for diminishing the vibrations perceived by the passengers and crew on board ships [2] [3] [4] [10] [16], there is still a lack of international standards [12] for asserting the quality of structure borne isolation and of specific design methodologies for controlling the capability of floating floors to mitigate the structure borne noise levels perceived in habitable areas aboard ships.

On the other hand, several studies on the application of damping layers have been made for the aeronautic, automotive, and even railway industries [19] [20], and this type of treatment has been used in the maritime industry for several years [21], but their application is mainly based on the experience of shipyard and sub-contractors.

The aim of this thesis is to study, develop and advise methods to passively control noise and vibration on board ships with the use of floating floors, and to investigate and propose methods to study the damping effects of viscoelastic materials involved in the noise and vibration mitigation on board ships through the application of damping layers.

In the first part of this thesis, a brief theoretical presentation on some of the existing damping models, and the behaviour of viscoelastic materials with the variation of environmental effects like temperature and frequency. Finally, the complex modulus model is chosen for its ease of the representation when using the fractional derivative model.

In the second part, some of the more common existing methods for diminishing the vibrations are explained. The two selected methods are the control of vibration by added damping, and by resilient isolation. Following their presentation, the theory behind these methods, the parameters that they measure and the way in which they will be put into practice is explained. In the end of this part, an optimisation procedure to improve the vibration mitigation capabilities of floating floors is explained.

In the third part, the experiments undertaken to measure the damping capacities of the two methods under study are shown. The two methods have different procedures and requirements, so they are explained separately, but following the similar working procedures.

In the last parts of the thesis, the final results are presented, showing the final Transmission Loss curve of the designed floating floors, and one of the resulting material Loss Factors obtained.





# **THEORETICAL BACKGROUND**

## **1 Vibration damping and control**

All mechanical systems have determined mass and stiffness properties, that contribute strongly to their vibrational behaviour. The mass and stiffness of the system will determine the location of the resonant frequencies of the system. If the resonant frequencies cannot be avoided during the design phase by controlling the stiffness and mass characteristics, or by isolating the system from the vibration sources, then the remaining option is to add damping to the system. Damping is a phenomenon by which mechanical energy is dissipated in dynamic systems, is also defined as any means of dissipating some fraction of the energy given to the system at the resonance frequency by an external force [22] [23].

### **1.1 Linear viscous damping**

In engineering, linear viscous damping is the method mostly adopted, because the equations of motion are simple and linear, and so analytical solutions can be relatively easily obtained for a wide range of problems. The classical viscous damper is a device that creates force at each end which

oppose the relative velocity between its ends, and their magnitude is proportional to this relative velocity [23].

### 1.1.1 Equation of motion for a SDOF system

An idealised SDOF system with linear viscous damping, as shown in Figure 1, has the following equation of motion:

$$m \frac{d^2 x}{dt^2} + c \frac{dx}{dt} + kx = f(t) \quad (1)$$

This is known as the Voigt-Kelvin Model.

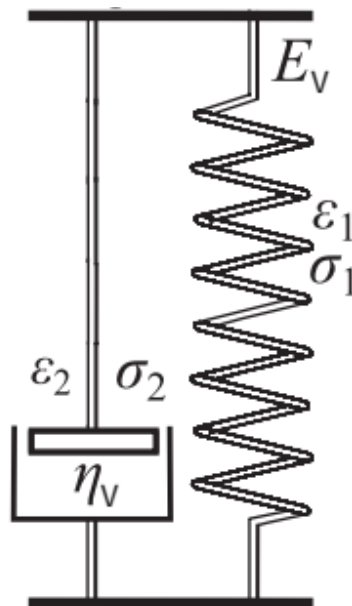


Figure 1 – One degree of freedom system with viscous damper, the Voigt-Kelvin model.

## 1.2 Representations of damping

Working in the frequency domain, is very convenient for most engineering and scientific applications and study of vibrational behaviour of materials. When this is the case, we have that the strain-time and the stress-time histories are harmonic, but there is a time or phase lag ( $\psi$ ) between the strain and the corresponding stress, as seen in Figure 2.

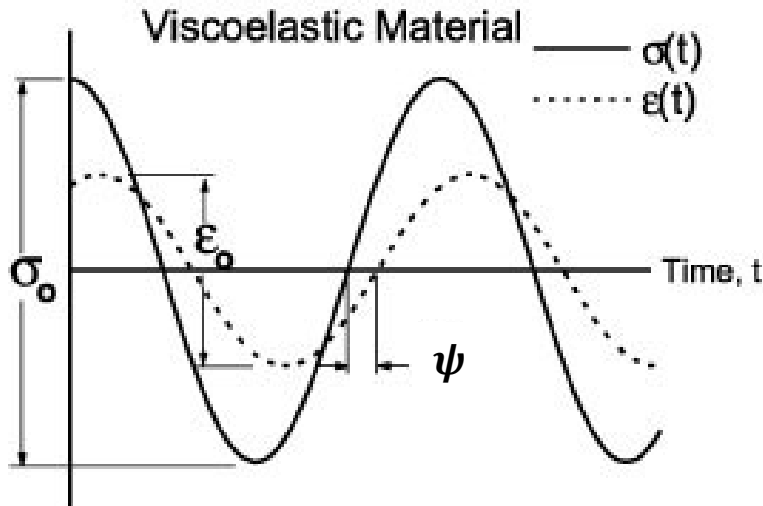


Figure 2 – Harmonic excitation and response for a viscoelastic solid

This is because for a viscoelastic solid, there is a  $90^\circ$  phase lag between the displacement and the velocity. This implies that for a viscoelastic solid, there is a velocity dependent term in the stress-strain relationship which, for  $\tau(t) = \tau_0 \sin(\omega t)$  and  $\phi = \phi_0 \sin(\omega t - \psi)$ , after some algebraic manoeuvre takes the following form:

$$\tau(t) = \frac{\tau_0}{\phi_0} \cos \psi \phi(t) + \frac{\tau_0}{\phi_0 |\omega|} \sin \psi \frac{d\phi(t)}{dt}$$

And considering  $G = (\tau_0/\phi_0) \cos \psi$  and  $\eta = \tan \psi$ , we have:

$$\tau = G\phi + \frac{G\eta}{|\omega|} \frac{d\phi}{dt} \quad (2)$$

Similarly, for extensional deformation we have:

$$\sigma = E\varepsilon + \frac{E\eta}{|\omega|} \frac{d\varepsilon}{dt} \quad (3)$$

This is the equation that describes the ideal elliptical hysteresis loop behaviour of a viscoelastic material, shown in Figure 3.

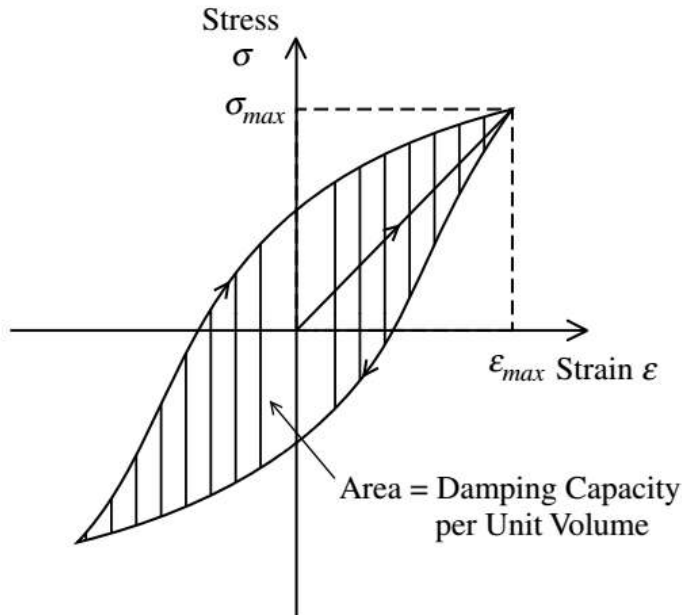


Figure 3 – Hysteresis loop for a viscoelastic material

### 1.3 Loss Factor

The damping properties of materials can be represented in many different ways, depending on the system under study and the area of application [24]. One of these energy units is the loss factor ( $\eta$ ), which is defined as the energy loss per radian ( $W_d/2\pi$ ) divided by the strain energy ( $U$ ):

$$\eta = \frac{W_d}{2\pi U} \quad (4)$$

### 1.4 Complex modulus model

The complex number model represents the stresses and strains in terms of the complex exponential function, defined as:

$$e^{i\omega t} = \cos \omega t + i \sin \omega t \quad (5)$$

Now, if we represent the strain by  $\phi = \phi_0 \exp(i\omega t)$ , then the strain rate  $d\phi/dt$  becomes simply  $i\omega t$ , and equations (2) and (3) become:

$$\tau = G\phi + \frac{G\eta}{|\omega|} i\omega\phi = G \left( 1 + i\eta \frac{\omega}{|\omega|} \right) \phi$$

$$\sigma = E\varepsilon + \frac{E\eta}{|\omega|} i\omega\varepsilon = E \left( 1 + i\eta \frac{\omega}{|\omega|} \right) \varepsilon$$

But since  $\omega$  must be positive at all times, because otherwise the dissipative term would be adding energy instead of subtracting it in each cycle,

we have that the expressions reduce to the following complex modulus relationships for shear and extensional stresses respectively:

$$\tau = G(1 + i\eta)\phi \quad (6)$$

$$\sigma = E(1 + i\eta)\varepsilon \quad (7)$$

The complex modulus, is easily and better represented, as has been studied and shown in recent years [25] [26] [27], with the fractional derivative model, which when applied to the frequency domain gives us the complex modulus  $E^*$  as:

$$E^* = E(1 + i\eta) = E' + E'' \quad (8)$$

$$G^* = G(1 + i\eta) = G' + G'' \quad (9)$$

Where  $E'$  and  $G'$  are the storage modulus, which are a measure of the stiffness of the material, and  $E''$  and  $G''$  are the loss moduli, that are a measure of the capacity of the material to dissipate energy.

## 1.5 Effects of temperature and frequency

### 1.5.1 Effects of temperature

The complex modulus properties of viscoelastic materials depend strongly on temperature, in ways particular to the composition of the material. Each viscoelastic material has a range of useful temperatures, that divide into three zones, the low temperatures glassy region, the transition region, and the higher temperatures rubbery region, as can be seen in Figure 4.

For a viscoelastic material, the softening temperature where the modulus begins to decrease, is very low and often below room temperature. Over the softening temperature, the modulus decreases rapidly and the loss factor increases to a maximum and then falls again, in what is known as the transition region. At temperatures above the transition region the modulus is low, and eventually the material disintegrates as the temperature rises [23].

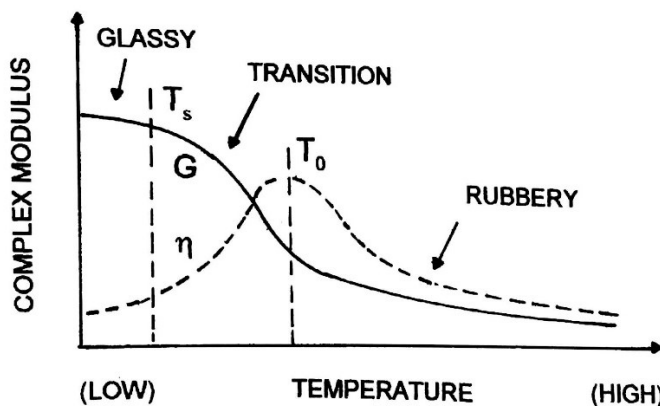


Figure 4 – Effects of temperature in the complex modulus properties behaviour of a typical viscoelastic material

### 1.5.2 Effects of frequency

The effects of frequency on the complex modulus properties of viscoelastic materials can be very strong, although qualitatively inverse to that of temperature. As the frequency increases, the behaviour of the viscoelastic material is as when the temperature decreases, as shown in Figure 5.

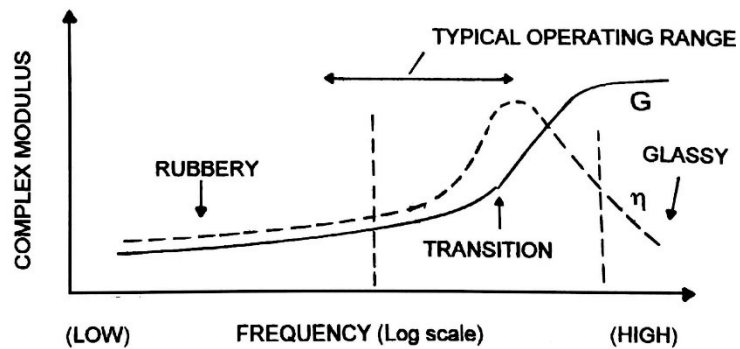


Figure 5 – Effects of frequency in the complex modulus properties behaviour of a typical viscoelastic material



## **METHODS**

### **2 Passive vibration control**

Passive vibration control involves the modification of the structural parameters of a vibrating system, this being stiffness, mass and damping, to adequate the response of the system to its dynamic environment. These modifications can consist of basic structural changes, or the addition of passive elements such as masses, springs, fluid dampers or damped rubbers. The mission of these elements is to react passively in opposition to the deflections, velocities or accelerations forced on them by vibrations. None of these passive elements require external intervention to mitigate the vibrations, other than the interaction with their immediate passive neighbouring elements or structural components.

Active vibration control systems rely on an external power source to activate devices that will act on the system to effectively generate vibrations of such sign that the negative effects of the initial vibration affecting the system are cancelled, or diminished. Since these control systems require the use of sensors, computer terminals, controllers, and several other electronic

equipment, they are costlier than passive methods, and are chosen only when the gain is worth the expenses [22].

In either way, the first approach should always be to reduce the vibration input from the main sources.

However, when dealing with the source does not sufficiently mitigate the vibration levels perceived by the end user, other passive vibration control methods must be chosen. There are four basic different approaches [28]:

- Vibration control by structural design
- Vibration control by localised additions
- Vibration control by added damping
- Vibration control by resilient isolation

In the present work, some versions of the latter two approaches will be addressed and studied.

## **2.1 Control of vibration by added damping**

When we add a layer of damping material to a vibrating structure, the energy is dissipated mainly by the fluctuating extensional and shear strains that it undergoes. The direct strain is proportional to the local bending moment, and the shear strain to the local shear force. The damping layers are added to dissipate energy primarily by one type of strain or the other, with different

configurations and material properties being required for each case in order to achieve the best damping efficiency.

In some cases, the damping layer is simply added to the outer surface of the structure, for example when damping needs to be added to an existing structure and this is the most practical application, or the position or accessibility of the location of the structure permits only a superficial application of a damping material. In these cases, the outer surface of the damping layer remains free and unconstrained by any shear stress. When this treatment is added to a vibrating surface, that is vibrating primarily in a bending type of mode, the damping layer is deformed cyclically in tension-compression, dissipating energy [29]. This configuration is known as *unconstrained layer damping*, and it's shown in Figure 6.

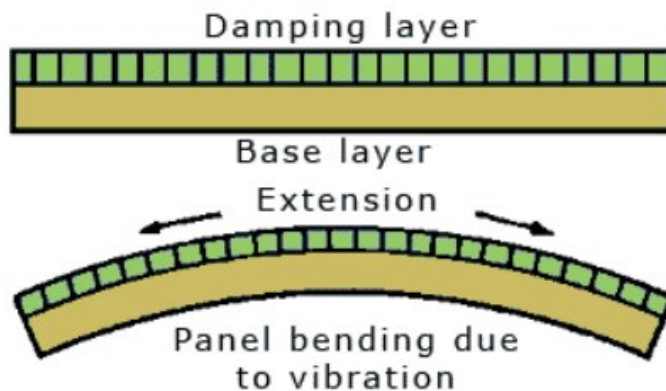


Figure 6 – Unconstrained layer with extensional damping configuration

For any beam or plate, the shear stress, and consequently the shear strain, are greatest at the neutral surface and zero in the outer surfaces. This is why, when damping based on shear strain is needed the best solution is to add a damping layer close to the neutral surface of the plate, which means effectively making a sandwich structure of a damping layer between two plates. When the structure is subjected to cyclic bending, the constraining layer will force the viscoelastic layer to deform in shear. This occurs due to the excessive difference of moduli between the viscoelastic material, the base structure, and the constraining layer [28]. This configuration is known as *constrained layer damping*. It is not essential that the damping layer is placed exactly at the neutral surface of the structure, as long as the layer is sandwiched between two plates, shear stress and strain will be generated in the damping layer [29], there will be a dissipation of energy in the system, and the plate flexural motion will be damped.

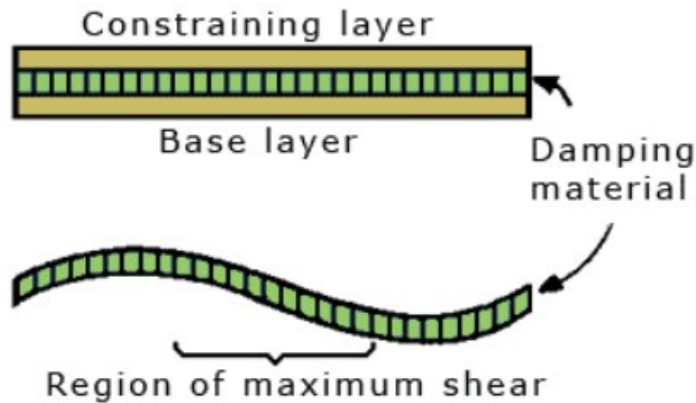


Figure 7 – Constrained layer with shear damping configuration.

These two configurations will be examined in the following sections.

## 2.2 Control of vibration by resilient isolation

When excessive vibration in a system is transmitted through few connection points to another part, these vibrations can be effectively mitigated if the connections are made sufficiently soft. For this purpose, resilient mounts are used.

One of the main sources of vibrations and discomfort on board a ship are the engines, whether they are installed as direct propulsion mechanism, or as generator sets. Other sources are the propellers, bow and stern thrusters, auxiliary machinery, HVAC systems and mooring systems. Moreover, there are also entertainment and human action originated sources to consider [4]. In order to mitigate the acoustic energy transmitted through the structures, the

noise sources should be resiliently mounted. This solution effectively isolates the sources only if the resilient mount system is properly designed and tested [5] [6] [9].

A particular way of isolating the accommodation areas from the acoustic energy transmitted by the structure, is to isolate them with resilient mounts, known as floating floors. These are effective solutions to mitigate impact noise generated by human activities and structure borne noise, generated by machinery [16] [30].

Floating floors are elements that isolate an upper floor from the main structure, in our case, the ship structure. There are two main groups of floating floors for marine applications: continuous layered and resiliently mounted. In the continuous layer floating floors, a continuous layer of decoupling material creates a discontinuity between the ship structure and the upper floor. In the latter, resilient mounts are used as decoupling agents [10]. Both types of floating floors used aboard ships is shown in Figure 8.

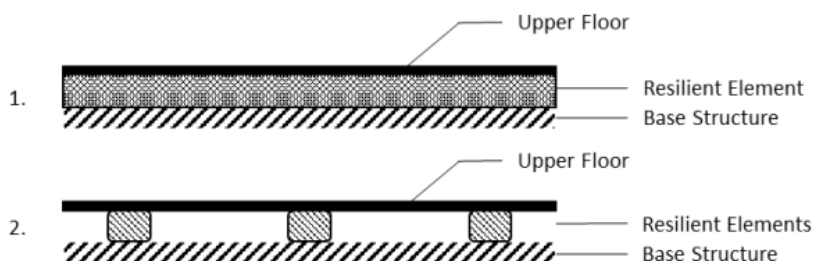


Figure 8 – Continuous floating floor (1) and resiliently mounted floating floor (2)

### **3 Measures of damping**

It is very difficult to come up with a realistic model for damping of a complex piece of equipment operating under several conditions of mechanical interaction. In order to come up with an accurate model of a system, a damping model must be selected, and even after this model is developed, the experimental determination of its parameters could be tedious. One of the difficult aspects is to combine more than one type of damping, such as viscous, structural, fluid, into the same system [22].

There are several ways of defining and measuring the viscously damped SDOF system, in terms of any of the parameters that are used to represent damping, such as specific damping capacity, loss factor, Q-factor and damping ratio, from a measured response behaviour. The damping measurement methods can be divided into two ways, the time-response methods and the frequency-response methods, which use respectively time-response and frequency-response records of the system to estimate damping. The use of these methods varies according to the field of studies. For example, when studying ship stability, due to the magnitude of the motions, time-response methods are used to measure the damping in the roll motion of a ship, such as the logarithmic decrement method. In our case, the nature of the

dynamic motions under study, requires the use of a frequency-response method, such as the half-power bandwidth method.

### **3.1 Complex modulus measurement**

In principle, though rarely in practice, the measurement process of complex modulus properties is simple. An extensional or shear defined deformation is done on the selected sample of subject material, and then the resulting deformations and forces are recorded as functions of time. Different configurations and methods exist for measuring complex modulus properties, like DMA Analysis [31] [32], DMTA Analysis [32], the RSA II analyser [33] [34], Autovibron analyser [35] [36] [37], some of these follow the ASTM E756 standard [38] precisely, or to some extent.

Most of these standardised tests require high precision test specimens and testing fixtures that can represent a high cost [39] if the main activity is not the measurement of the vibration damping properties of materials, or the measurement of many or some of the physical characteristics of materials in general.

The theory in which standards like ASTM E756 are based in, has been developed since the 1950s for non-commercial aerospace applications [40], and originally for plate specimens [41] [42] [43] [44] [45] [46]. In recent years, they were developed for beams, that are closer to being one-dimensional



elements, for which there is no need for making geometrical corrections to take into account the geometry of the specimen under test [23]. However, as the test specimens have grown smaller, any mass added to the specimen, such as load cells, accelerometers, etc., will proportionally become larger and will mean larger errors if appropriate corrections are not made to take into account the precise added mass of the system.

For more practical applications that do not require industrial laboratory precision, the Oberst beam method and the RKU equations, taken as base for the ASTM E756 standard, have been modified, or better said, taken back to their original form. These methods have developed the theory to characterise the complex modulus and the loss factor of the damped system,  $\eta$ , of different configurations of base material and damping layers [41] [42]. These methods, used in reverse can be used to find the complex modulus and loss factor of the damping material,  $\eta_2$ .

### **3.1.1 Unconstrained layer configuration**

This is commonly known as the Oberst beam configuration, in which a viscoelastic material layer is added to a base stiff specimen, as shown in Figure 9, to conform a composite specimen. This is also known as the Free-layer damping treatment. The base specimen provides the necessary stiffness

to the system, and the viscoelastic material layer dissipates the vibration energy.

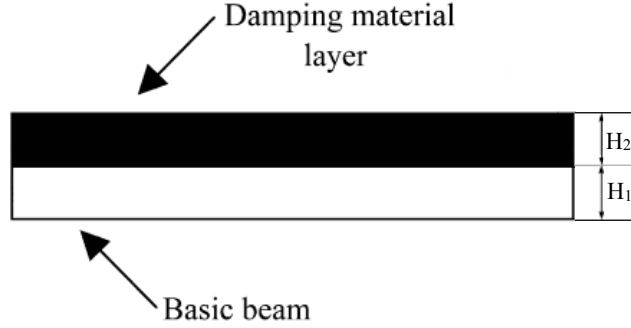


Figure 9 – Representation of a free layer damping system

From Oberst original equation [47], we have:

$$\frac{E_C^* I_C}{E_B I_B} = 1 + e^* h^3 + 3(1 + h)^2 \frac{e^* h}{1 + e^* h} \quad (10)$$

Where:

$$e^* = \frac{E_2^*}{E_1} \quad \text{and} \quad h = \frac{H_2}{H_1}$$

$E_C^*$  is the composite beam complex modulus,  $I_C$  is the composite specimen second moment of inertia,  $E_2^*$  is the complex modulus of the damping layer material,  $E_1$  is the modulus of the base specimen material,  $I_1$  is the second moment of inertia of the base specimen, and  $H_2$  and  $H_1$  are the thicknesses of the damping layer and the base specimen, respectively.

Reversing Oberst equation, we can obtain an equation to calculate the complex modulus of the damping layer material. Setting the bending stiffness ratio:  $Z_u^* = E_c^* I_c / E_1 I_1$ , and rearranging Eq. (10) into a quadratic equation for  $e^*$ , we have:

$$h^4(e^*)^2 + (4h + 6h^2 + 4h^3 - Z_u^*h)e^* + 1 - Z_u^* = 0$$

After solving for  $e^*$  we have:

$$e^* = \frac{-A^*h \pm \sqrt{(A^*h)^2 - 4h^4(1 - Z_u^*)}}{2h^4}$$

Where:

$$A^* = 4 + 6h + 4h^2 - Z_u^* \quad (11)$$

And finally the complex modulus of the damping layer material can be calculated with:

$$E_2^* = \frac{E_1}{2h^3} \left( \sqrt{(A^*)^2 - 4h^2(1 - Z_u^*)} - A^* \right) \quad (12)$$

Equation (12) is the equation that will be used to obtain the complex modulus of the damping material. In order for this equation to have consistent results,  $Z_u^*$  must be higher than 1, the ASTM E756, suggests values higher than 1.01.

In this method, first a base specimen without damping layer is tested to determine the resonance frequencies of the base specimen, and then use them to calculate the Young modulus, which for a cantilever beam specimen we have:

$$E_1 = \frac{48\rho_1\pi^2L^4f_{0n}^2}{H_1^2\xi_n^4} \quad (13)$$

Where  $\rho_1$  is the density of the base beam,  $L$  is the cantilever length,  $f_{0n}$  is the nth resonance frequency and  $\xi_n$  is the nth eigenvalue.

Since the modulus of the composite beam ( $E_C^*$ ) is given by:

$$E_C^* = \frac{48\rho_C\pi^2L^4f_n^2}{(H_1 + H_2)^2\xi_n^4}(1 + i\eta) \quad (14)$$

The resulting equation for  $Z_u^*$  then is:

$$Z_u^* = \left(1 + \frac{\rho_2H_2}{\rho_1H_1}\right) \left(\frac{f_n}{f_{0n}}\right)^2 (1 + i\eta) \quad (15)$$

Using the half-power bandwidth method, we obtain the modal loss factors  $\eta$  from the tests performed on the composite specimens. And then, using Equations (11) and (12), we can obtain the complex modulus of the damping layer material.

Until now, the Oberst equations have been used considering the classical case of a one-dimensional beam with an unconstrained damping layer. If this unconstrained damping layer is applied instead to a two dimensional

plate, the complex flexural rigidity becomes  $D_C^* = D_C'(1 + i\eta)$ , where the flexural rigidity ( $D$ ) of a plate is  $D = EH^3/12(1 - \nu^2)$ . The complex modulus of the damping material is calculated in the same way. The damping layer on a plate undergoes bi-axial stress, but the complex modulus of the damping material is usually taken as that for uni-axial stress conditions. The Poisson ratio can be taken as that for the basic plate material [28] [48].

We have that the complex flexural rigidity of the composite plate is given by [28]:

$$D_C^* = \frac{E_1 H_1^3}{12(1 - \nu^2)} \left[ 1 + e^* h^3 + 3e^* h(1 + h)^2 - 12(1 + e^* h^2) \left( \frac{h_{NA}}{H_1} \right)^2 \right]$$

Where  $h_{NA}$  is the position of the neutral surface of the bending plate, measured from the mid surface of the base plate, and is given by:

$$h_{NA} = \frac{H_1 e^* h(1 + h)}{2(1 + e^* h)}$$

Then, assuming that  $\eta_2^2 \ll 1$  [47], the approximate expression for  $D_C^*$  can be obtained:

$$D_C^* \approx \frac{E_1 H_1^3}{12(1 - \nu^2)} \left[ \frac{1 + 2e^*(2h + 3h^2 + 2h^3) + e^{*2}h^4}{(1 + eh)} \right] \quad (16)$$

Rearranging Equation (16), we obtain:

$$\frac{D_C^*}{D_1} \approx 1 + e^*h^3 + 3(1+h)^2 \frac{e^*h}{1+e^*h} \quad (17)$$

Which has the same form as the original Oberst formula, as shown in Equation (10). Now, since we have that the modulus of the base plate is given by:

$$E_1 = \frac{48(1-\nu^2)\rho_1\pi^2 f_{0n}^2}{H_1^2 k^4} \quad (18)$$

And the modulus of the composite plate given by:

$$E_C^* = \frac{48(1-\nu^2)\rho_C\pi^2 f_n^2}{H_C^2 k^4} (1+i\eta) \quad (19)$$

Where  $H_C = H_1 + H_2$  and  $\rho_C = (\rho_1 H_1 + \rho_2 H_2)/(H_1 + H_2)$ . And so  $Z^*$  becomes:

$$Z_u^* = \left(1 + \frac{\rho_2 H_2}{\rho_1 H_1}\right) \left(\frac{f_n}{f_{0n}}\right)^2 (1+i\eta) \quad (20)$$

Which again, has the same form and is equal to in Equation (15). The difference lies in the calculation of  $E_1$ , that now has a term that includes the Poisson ratio, that since for viscoelastic materials is sometimes still not well understood and consequently not accurately measured [49], it will be taken as for the basic plate material [28].

So now, since Equation (17) is the same as (10), Equation (11) and (12) can be used, together with the with the loss factor of the composite beam ( $\eta_C$ ), that should be obtained using the half-power bandwidth method from tests performed on the composite specimens, to obtain the Young Modulus ( $E_2$ ) and Loss Factor ( $\eta_2$ ) of the damping layer, we have that:

$$E_2 = Re(E_2^*) \quad (21)$$

$$\eta_2 = \frac{Im(E_2^*)}{Re(E_2^*)} \quad (22)$$

### 3.1.2 Constrained layer configuration

In the constrained layer configuration, as shown in Figure 10, developed mainly by Ross, Ungar and Kerwin, in 1959 [42], the following assumptions and limitations are considered:

- The longitudinal inertia is negligible
- The shear deformations in the plate and constraining layer are negligible, which means that the distance between the base layer and the constraining layer is maintained constant.
- The strain energies due to extensions in shear layer are negligible
- The shear strain is uniform through the thickness of the shear layer

- The bonding between the layers is perfect
- The damping comes mainly from the shear deformation occurring in the viscoelastic material in the middle constrained layer

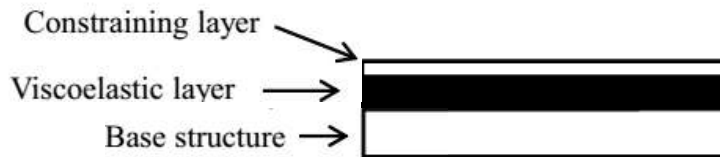


*Figure 10 – Representation of a constrained layer damping system*

With these assumptions, the system may be represented by a single differential equation of sixth order for the longitudinal deformation of the damping or the constraining layer [50], or by a sixth order equation for the beam deflection [51]. Then, Rao [52] identified boundary conditions that are consistent with the sixth order differential equation for deflection, and gave analytical expressions that may be used to obtain loss factors of the constrained layer configuration with general boundary conditions. However, Torvik [48] found that these approximations are limited in their applicability to values of loss factors of the damping material that are much smaller than those in general practice, and also because the “exact” solution from the formulation that Rao found for the beam is extremely difficult to apply in the case of more general boundary conditions, and used a technique developed by



Jones [23]. This approximation however, is for a beam specimen. Shafer [53] has recently given a general overview of the constrained layer configuration theory and application for both beam and plate specimens, and Mead [28] has given exact formulations for the pinned-pinned case of beams and plates in the constrained layer configuration. In order to use the RKU equations for obtaining the loss factor in different boundary conditions, an equivalent length method must be used. This method has been proposed and studied by Torvik [48], to obtain the loss factor of the constrained layer system. Jones [23] has used these equations in reverse to obtain the damping material loss factor. A combination of these methods will be explained, to obtain the loss factor of the damping material from a constrained layer configuration of a free-free plate.

We have that this configuration is governed mainly by three parameters, the structural parameter,  $Y$ , the shear parameter,  $g$ , and the complex flexural rigidity  $D_C^*$ , which have the following form:

$$Y = \frac{h_{321}^2}{D_t(1 - \nu^2)} \left[ \frac{E_1 H_1 E_3 H_3}{E_1 H_1 + E_3 H_3} \right] \quad (23)$$

$$g = \frac{G_2'}{k^2 H_2} \left( \frac{1}{E_1 H_1} + \frac{1}{E_3 H_3} \right) (1 - \nu^2) \quad (24)$$

$$D_C^* = \frac{1}{12(1 - \nu^2)} (E_1 H_1^3 + E_3 H_3^3) \left( 1 + \frac{g^* Y}{1 + g^*} \right) \quad (25)$$

Where:

$$D_t = \frac{E_1 H_1^3}{12(1 - \nu^2)} + \frac{E_3 H_3^3}{12(1 - \nu^2)} \quad \text{and} \quad h_{321} = \frac{H_1 + H_3 + 2H_2}{2}$$

Since for a symmetric constrained layer configuration we have that  $E_1 = E_3$  and  $H_1 = H_3$ , the aforementioned parameters become:

$$Y = \frac{3h_{12}^2}{H_1^2} \quad (26)$$

$$g = \frac{2G_2'(1 - \nu^2)}{k^2 E_1 H_1 H_2} \quad (27)$$

$$D_C^* = \frac{E_1 H_1^3}{6(1 - \nu^2)} + \frac{E_1 H_1 h_{12}^2}{2(1 - \nu^2)} \left( \frac{g^*}{1 + g^*} \right) \quad (28)$$

Where  $h_{12} = H_1 + H_2$  and  $k$  is the wavenumber, that depends on the boundary conditions of the plate.

In the equivalent lengths method, Torvik [48] found that for a simply supported beam to yield the same loss factor than a simply supported plate, the simply supported beam vibrating in the first mode must have an equivalent length,  $L_{EQ}$ , that must be related to the dimensions of the simply supported plate through the latter dimensional eigenvalue in the following manner:

$$\frac{\pi^2}{L_{EQ}^2} = \frac{\pi^2}{1 - \nu^2} \left( \frac{m^2}{a^2} + \frac{n^2}{b^2} \right) \quad (29)$$

Where the left-hand term is the squared dimensional eigenvalue of the first mode of the simply supported beam, and the right-hand term is the squared dimensional eigenvalue of the simply supported plate, being  $a$  and  $b$  the length and width of the plate, respectively, and  $m$  and  $n$  the mode indexes for the simply supported plate.

Then we have that for the desired boundary condition and mode of a determined plate with constrained layer damping treatment, the dimensional eigenvalue,  $k$ , for the plate mode and geometry of interest must be determined and substituted for the dimensional eigenvalue of a simply supported plate, in Equation (29), to find the length of the equivalent simply supported beam from:

$$\frac{\pi^2}{L_{EQ}^2} = \frac{k^2}{1 - \nu^2} \quad (30)$$

The resultant equivalent length must then be used in the shear parameter,  $g$ , to obtain the loss factor of the desired plate with determined boundary conditions.

For a free-free plate, following the Leissa [54] notation, the dimensionless frequencies,  $\lambda$ , are given by:

$$\lambda = \omega a^2 \sqrt{\frac{\rho}{D}} \quad (31)$$

From which we have that the dimensional eigenvalue,  $k$ , of a completely free plate is given by:

$$k^2 = \frac{\lambda}{a^2} \quad (32)$$

Using Equation (32) in Equation (30), to obtain the equivalent length of a free-free plate, and then using it in Equation (27) we have that the shear factor of a free-free plate becomes:

$$g = \frac{2L^2 G_2' (1 - \nu^2)}{\lambda E_1 H_1 H_2} \quad (33)$$

Now that we have all the parameters we need, we take these equations in reverse to come up with equations to obtain the loss factor of the damping material.

An important simplification is to take the young modulus of the damping material ( $E_2^*$ ) as zero. This does not lead to measurable errors, but it allows to invert with ease the RKU equations to obtain the complex flexural rigidity of a symmetric sandwich constrained plate configuration.

In this method first the base specimen, consisting of the two constraining plates taken separately, is tested to determine the resonance frequencies of the base specimen, that can be expressed with the following relation:

$$D_1 = \frac{4\pi^2 \rho_1 H_1 L^4 f_{0n}^2}{\lambda^2} \quad (34)$$

Likewise, for the composite specimen we have that:

$$D_c^* = \frac{4\pi^2 \rho_c H_c L^4 f_{cn}^2}{\lambda^2} (1 + i\eta) \quad (35)$$

And so, we have that the complex flexural rigidity is also given by:

$$\frac{D_c^*}{D_1} = \left( 2 + \frac{\rho_2 H_2}{\rho_1 H_1} \right) \left( \frac{f_{cn}}{f_{1n}} \right)^2 (1 + i\eta) \quad (36)$$

Where the modal loss factor,  $\eta$ , is obtained from the experimental tests, using the half-power bandwidth method. We introduce the parameter  $Z_c^* = D_c^*/D_1$ , and from relating Equation (28) to Equation (36), we obtain the following relation:

$$g^* = \frac{2 - Z_c^*}{Z_c^* - 2 - 6 \left( 1 + \frac{H_2}{H_1} \right)^2} \quad (37)$$

In order for this equation to have consistent results,  $Z_c^*$  must be higher than 2, the ASTM E756, suggests values higher than 2.01.

Finally, we can determine the shear modulus  $G_2$ , and loss factor,  $\eta_2$ , of the damping material since we have that  $G_2^* = G_2(1 + i\eta_2)$ , and:

$$G_2^* = \frac{g^* E_1 H_1 H_2 \lambda}{2(1 - \nu^2) L^2} \quad (38)$$

### 3.1.3 Half-power bandwidth method

As mentioned in the previous sections the modal loss factor,  $\eta_C$ , of both the unconstrained and constrained layer configurations, is calculated using the half-power bandwidth method, that will be described in this section.

This damping measuring method is widely known and used for its simplicity in application. It was developed for single-degree-of-freedom (SDOF) systems [55] [56], because one of its limitations is that for closely spaced modes, the coupling effect can cause errors in the measurement. In certain frequency response functions, it can even be seen that for very close modal frequencies, the half power points that must be taken into account could be absent [57]. However, the use of this method is also extended to multi-degree-of-freedom (MDOF) systems, provided that each of the peaks to analyse is affected only by the mode under study.

Considering the frequency response function (FRF) magnitude of a SDOF system with viscous damping, given by:

$$|X_n(\omega)| = \frac{\omega_n^2}{[(\omega_n^2 - \omega^2)^2 + 4\zeta^2\omega_n^2\omega^2]^{1/2}} \quad (39)$$

For low damping [58], the peak magnitude is given by :

$$Q = \frac{1}{2\zeta} \quad (40)$$

The half-power bandwidth is defined as the width of the frequency response magnitude curve when the magnitude is  $1/\sqrt{2}$  times the peak value. This is usually indicated as  $\Delta\omega$ , as shown in Figure 11. We can obtain  $\Delta\omega$  from Equation (39).

Which for the case of low damping, ( $\zeta < 0.2$ ) [58], since for low damping  $\omega_n \cong \omega_r$ , gives us finally:

$$\zeta = \frac{1}{2} \frac{\Delta\omega}{\omega_r} \quad (41)$$

Equation (41) is accurate when calculated on the displacement frequency response transfer function, for SDOF systems, or MDOF systems with enough space between modes, if the obtained damping values are  $\zeta < 0.2$  [58].

When using the Accelerance frequency response transfer function,  $A(\omega)$ , where the input function is the acceleration of the system, and the output

function is the force of the system, instead of the displacement frequency response transfer function,  $X(\omega)$ , the accuracy of equation (41) is different, and it's applicability reduces to cases in which the obtained damping values are  $\zeta < 0.15$  [58].

If the applicability of the half-power bandwidth method is to be increased, that is, to use it for higher damping values, two methods can be considered: third order correction [58] and the n-dB method [28].

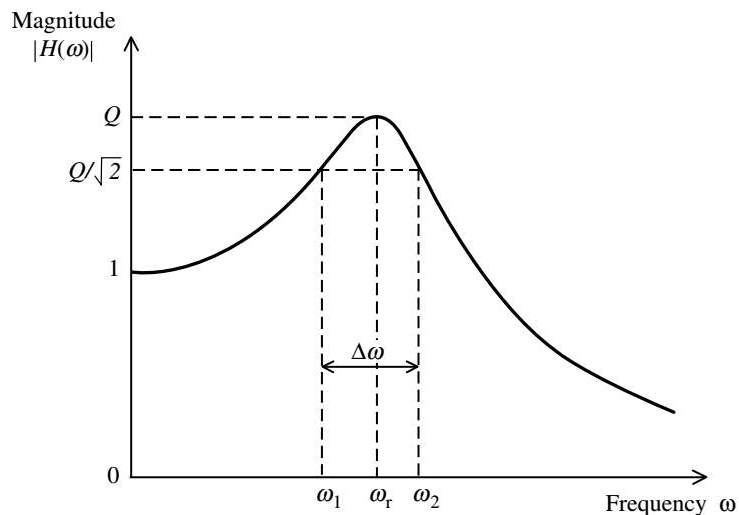


Figure 11 – Half-power bandwidth method



## 4 Motion Transmissibility

For a SDOF system suspended on a moving platform, as shown in Figure 12, we can define the mechanical mobility  $M_m$  of the mass system  $m$  as:

$$M_m = \frac{1}{mi\omega} \quad (42)$$

Where  $\omega$  is the excitation frequency, and the mechanical mobility  $M_s$  of the damper and spring that are connected in parallel as:

$$M_s = \frac{1}{(c + k/i\omega)} \quad (43)$$

Now, since the motion transmissibility  $T_m$  is defined as the ratio between the motion of the system,  $v_m$ , and the applied support motion,  $v$ , for a floating floor system we have:

$$T_m = \left| \frac{v_{floor}}{v_{structure}} \right| = \left| \frac{M_m}{M_m + M_s} \right| \quad (44)$$

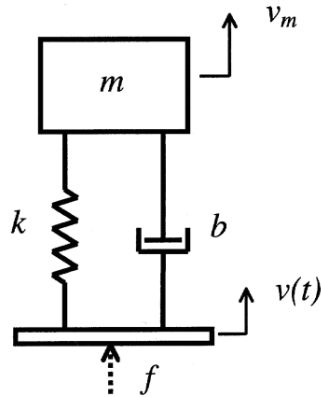


Figure 12 – SDOF system suspended on a moving platform

We can see in Figure 13 the typical motion transmissibility curve for a damped SDOF. In the low frequency range, the motion transmissibility tends to 1. Then, as the exciting frequency increases towards the natural frequency of the system, the transmissibility curve increases up to its maximum value, that depends on the damping ratio. Past this point, the transmissibility curve decreases and tends to 0 as the frequency ratio,  $r = \omega/\omega_n$ , tends to  $+\infty$ .

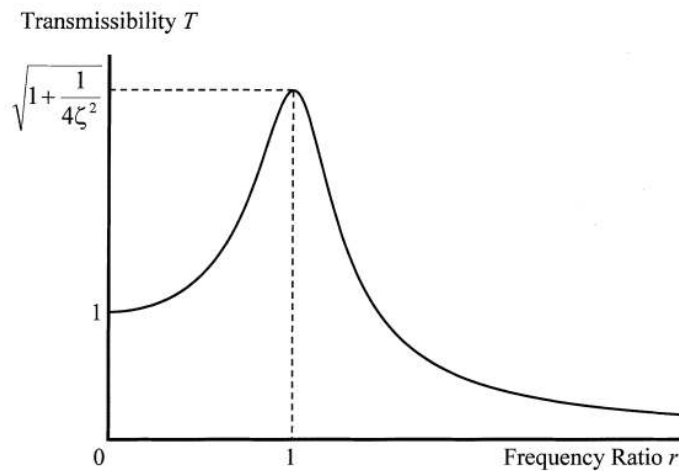


Figure 13 – Typical transmissibility curve of a damped SDOF system with support motion

## 5 Floating Floor performance indicators

Up to date, no international standards exist for testing the quality of structure borne noise isolation. This is why, in order to evaluate the performance of floating floors, in terms of reducing structure borne noise levels, floating floors are tested using a procedure developed by Ødegaard & Danneskiold-Samsøe A/S [59].

### 5.1 Transmission Loss

Several research activities done in recent years have appointed the influence of the dynamic stiffness of the resilient material chosen, on the Transmission Loss curve of the floating floor [60] [61] [62] [63] [64].

The Transmission Loss is one of the parameters that measures the capability of a floating floor to isolate structure borne noise, developed by Ødegaard & Danneskiold-Samsøe A/S [59]. It is often evaluated by researchers [10] [17], by using this method.

It is defined as:

$$TL_v = L_{v,structure} - L_{v,floor} \quad (45)$$

Where  $L_{v,structure}$  is the average velocity level of the deck structure, and  $L_{v,floor}$  is the average velocity level of the upper floor, both measured in

dB ref  $10^{-9}$  m/s and with the floating floor already mounted. The Transmission Loss quantifies the mitigation in the velocity level from the deck structure to the upper floor.

If we combine Equation (44) and Equation (45), we obtain the following relation, that describes the Transmission Loss of a damped SDOF system, also shown in Figure 14:

$$TL_v = 10 \log \frac{v_{structure}}{v_{floor}} = 10 \log \frac{1}{T_m} \quad (46)$$

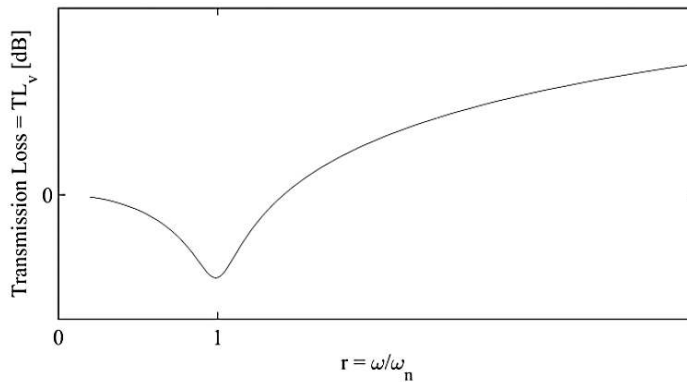


Figure 14 – Transmission Loss curve of a damped SDOF system

From Figure 14 we can see the Transmission Loss behaviour with the variation of frequency range,  $r$ . As it tends to 0, the Transmission Loss also tends to 0. As it approaches towards 1, the Transmission Loss curve drops to a minimum, and at higher frequencies, the curve tends to  $+\infty$  as the frequency ratio tends towards  $+\infty$ .

## 5.2 Insertion Loss

This is another parameter that measures the capability of a floating floor to isolate structure borne noise, developed by Ødegaard & Danneskiold-Samsøe A/S [59].

It is defined as:

$$IL_v = L_{v,0} - L_{v, floor} \quad (47)$$

Where  $L_{v,0}$  is the average velocity level of the deck structure, before the mounting of the floating floor.  $L_{v, floor}$  is again the average velocity level of the upper floor, after the mounting of the floating floor. Both levels, also measured in dB ref  $10^{-9}$  m/s. The Insertion Loss quantifies the improvement of the vibration level on the upper floor obtained by the addition of the floating floor to the system.



## 6 Floating floor optimisation

### 6.1 Background

The mechanical energy involved in a vibrating panel generating noise in its surrounding environment is often generated by remote sources connected to the structure [65]. In the case of ships, the engines and auxiliary machinery generate audio-frequency vibrational energy that is transmitted through the structures to the accommodation decks [9].

The sound pressure level generated in air at standard temperature by a panel excited by audio-frequency vibrational energy in the audio frequency range is obtained [66] by:

$$L_p = L_v + 10 \log(A/4S) - 10 \log \sigma \quad (48)$$

Where  $L_p$  is the sound pressure level, measured in dB ref 20  $\mu\text{Pa}$ ,  $L_v$  is the velocity level of the vibration plate, measured in dB ref  $10^{-9}$  m/s,  $A$  is the equivalent absorption area of the receiving room, measured in  $\text{m}^2$ ,  $S$  is the radiating surface, measured in  $\text{m}^2$ , and  $\sigma$  is the radiation efficiency, obtained according to the following relation [65]:

$$\sigma_e = \frac{W_{radiated}}{\rho c S \langle |v|^2 \rangle} \quad (49)$$

Where  $W_{radiated}$  is the sound power radiating from the vibrating surface, measured in W,  $\rho$  is the air density, measured in  $\text{kg/m}^3$ ,  $c$  is the sound velocity in air, measured in m/s, and  $\langle |v|^2 \rangle$  is the effective value of the velocity of the radiator, averaged over the surface.

If the acoustic characteristic parameters of the receiving room and the radiating panel are constant, namely  $A$ ,  $S$  and  $\sigma$  in Equation (48), then we have that the sound pressure level,  $L_p$ , generated by the vibrating panel depends on the variation of the velocity level  $L_v$ .

For the case of a floating floor, the radiating surface is the upper floor, which radiates sound energy in the receiving room. If the dynamic characteristics of this surface are kept constant, the velocity level  $L_v$  of the upper floor can be controlled by improving the capability of the resilient element to reduce the transmitted vibrational energy.

## 6.2 Optimisation procedure

The research group of the Ship Noise and Vibration Laboratory (NVL) together with the CSNI Lab, have developed a new procedure for the improvement of the isolation capabilities of floating floor resilient mounts.

According to Equation (46), the Transmission Loss of a floating floor can be improved by reducing the transmissibility of its resilient elements. If the damping coefficient,  $c$ , of the resilient elements is constant, this



improvement can be achieved by decreasing the equivalent stiffness,  $k$ , of the resilient mounting system. This decrease in equivalent stiffness, generates a decrease of the natural frequency of the resilient element, that is being considered as a damped SDOF system, and so decreases the resonant frequency of the system, considered as:

$$\omega_r = \omega_n \sqrt{1 - \zeta^2} \quad (50)$$

Where  $\zeta$  is the damping ratio given by:  $\zeta = c/2\sqrt{km}$ .

This implies that the Transmission Loss curve will shift towards the left, as shown in Figure 15. In Figure 15 we can see the typical Transmission Loss curve of a SDOF system, in the solid curve, and in the dashed curve the Transmission Loss curve of a SDOF system with the same inertia,  $m$ , and damping,  $c$ , as the previous system, but a lower stiffness,  $k$ . Following the hypothesis that only the stiffness of the resilient element decreases and that the mass and the damping coefficient are constant, we can notice that the shift of the Transmission Loss curve, leads to an increase in the Transmission Loss curve in the high frequency range. Regarding the low frequency range, there is an increase of the Transmission Loss in correspondence of the resonant frequency. This is due to the fact that the maximum of the transmissibility curve depends on the damping ratio. This can furtherly be explained by noticing that a decrease of the stiffness implies a decrease of the maximum of

the Transmissibility curve, and so, by looking at Equation (46), we can see that this translates into an increase of the Transmission Loss. At frequencies lower than the resonant frequencies, the Transmission Loss decreases and tends to 0.

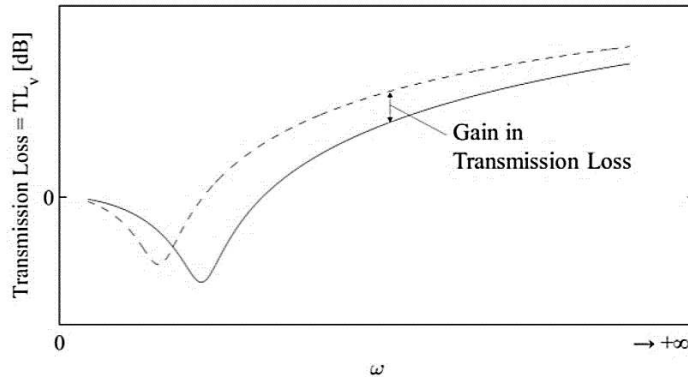


Figure 15 – Transmission Loss curves of two damped SDOF systems with the same inertia,  $m$ , and damping,  $c$ , but different stiffness.

Decreasing the stiffness of the resilient mount implies an increase of the Transmission Loss in the audio frequency range, but it also implies a higher deflection of the floating floor when it is subject to static loads. This is why the static deflection of floating floors must be considered as a design constraint in the optimisation process for the improvement of the dynamic response of resilient elements.

The procedure for the optimisation of resilient elements of a floating floor developed by the research group is the following:

1. Develop different configurations of the floating floor grillage modules

2. Develop finite element models of the floating floor grillage modules
3. Perform static finite element analyses of the different configurations of the floating floor grillage modules subject to the design load
4. Perform experimental tests for measuring the static deflection of the floating floor grillage module prototypes
5. Perform experimental tests for the dynamic characterisation of the floating floor grillage module prototypes

In the first phase of the procedure, different new alternative configurations of the floating floor were developed. The main characteristic to optimise was the capability of the resilient mounts to isolate the structure borne noise. Other parameters taken into account were the feasibility of the resilient element, the ease of assemble ad installation on board and the overall cost for its production. The weight was also controlled in the design of the different configurations of the resilient elements.

The second phase consisted in producing the finite element models of the different configurations of the resilient mounts. These models were later used to verify that the elastic deflection was within the established limits when the design static load was applied on each resilient mount configuration.

In the third phase, an iterative procedure was adopted in order to identify the lowers stiffness of the resilient mount, that would allow the floating floor to comply with the design constraint of maximum deflection under a static compression load. In this phase, a dynamic simulation of the base module was included in the process, to gain a general view of the behaviour of the module in the frequency range of interest, prior to the laboratory tests.

After the finite element analyses, the resilient mounts that complied with the design conditions, were built into prototypes that were tested in the laboratory in phase four. The objective of the first laboratory tests was to validate the numerical simulations and to verify the stiffness of the resilient mounts prototypes.

The final phase of the design optimisation procedure, was to perform tests to evaluate the dynamic characteristics of the resilient mounts in terms of resonant frequencies and Transmission Loss. The resulting Transmission Loss curves for each configuration of resilient mount were then compared to identify the resilient element configuration that shows the highest performance in terms of Transmission Loss.

## **EXPERIMENTAL SETUP**

All the experiments were done in the Ship Noise and Vibration Laboratory (NVL) of the University of Trieste, where in recent years several research activities on the dynamic response of passive vibration control systems have taken place.

The tests done on the plate specimens aimed at obtaining mechanical characteristics of the damping materials of the two configurations studied. As it has been previously explained, for the material characterization the parameters needed were the resonant frequencies, and the damping at each of the measured resonant frequencies. These parameters were obtained by performing experimental modal analysis on the specimens.

The objective of the tests done on the floating floor specimens was to verify the static deflections obtained in the numerical simulations. Also dynamic tests were undertaken to measure the damped natural frequencies and the Transmission Loss of the floating floor prototypes.



## **7 Floating floors experimental procedures**

The procedure presented in Section 6.2 was implemented with the objective to optimise the performance of a new floating floor specifically designed to be installed on board ships. The typical floating floors made for ships are grillages of supporting hollow beams that are elastically suspended on a resilient element. The beams act as a support for both the noise isolation mineral wool panels, which are disconnected from the deck plating, and from the upper floor.

A typical grillage is shown in Figure 16. The hollow beams are made of steel, and are originally 0.6 metres long and have a thickness of 2 mm. The resilient element is continuously distributed beneath the hollow beams.

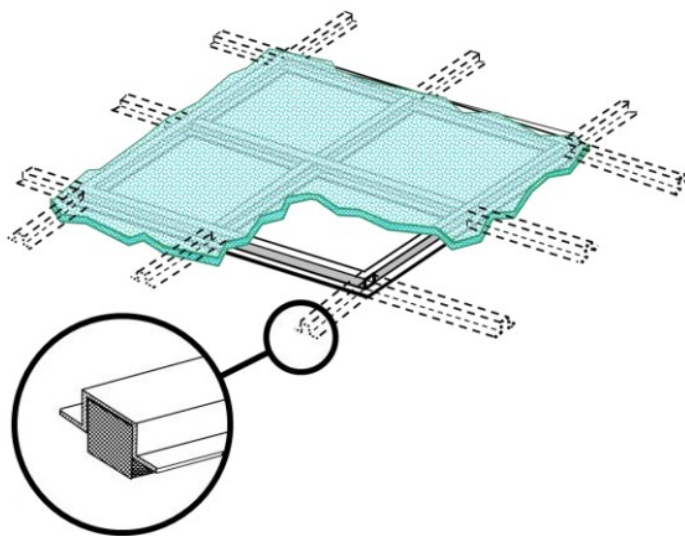


*Figure 16 – Typical floating floor grillage considered as case study, with a detail of the beam section*

## **7.1 Configuration Optimisation**

### **7.1.1 Configurations**

In the first phase of the optimisation, new configurations of the floating floor resilient element were developed. Two different transverse sections of the hollow beam were considered: the original one with an open section, and a new one with a closed section. These two configurations were modelled with the original thickness of 2 mm, and with a new thickness of 1 mm. The two configurations can be seen in Figure 17. The geometric layout of the grillage was considered constant as it was harmonised with the stiffening spacing of a typical deck structure.



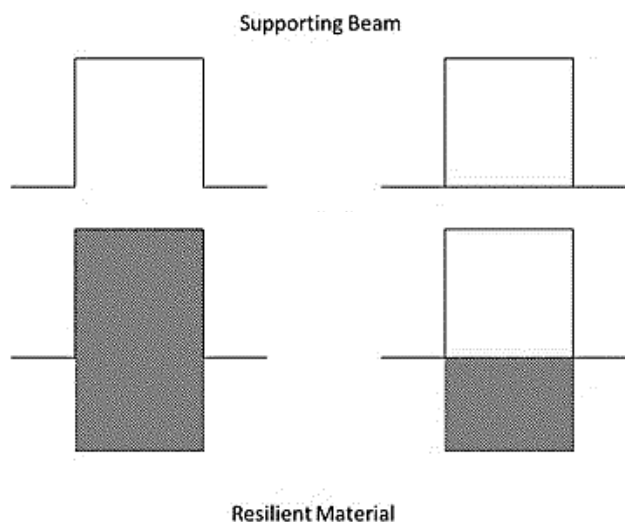












*Figure 17 – Transverse section of the supporting beams with the resilient elements in the original open configuration, and the new closed configuration*

### 7.1.2 Material selection

The original material used in the floating floors under study have a Young modulus,  $E$ , of  $1.45 \text{ MN/m}^2$ . In addition, two different materials were considered for the decoupling element: viscoelastic material and rubber. In an initial analytical analysis, searching for a minimum allowable stiffness of the resilient element subject to the design load, two Young modulus,  $E$ , for the viscoelastic material were proposed:  $0.725 \text{ MN/m}^2$ , and  $0.472 \text{ MN/m}^2$ . These values also take into account the technological limitations in the control of the stiffness of the viscoelastic material during the production phase. Regarding the rubber material, it was selected among products available in the market, and its Young modulus,  $E$ , was selected equal to  $4.4 \text{ MN/m}^2$ . Furthermore, all

the previously mentioned materials were also considered in two different configurations, continuous and discontinuous applications. The latter application was thought of in order to attempt to furtherly reduce the weight of the optimised floating floor. In Table 1, all the configurations are shown.

*Table 1 – Different configurations of floating floor supporting hollow beam taken into account for the optimisation process*

Config.	Beam section	Thickness [mm]	Application	Material
0		2	Cont.	Visco.
1		1	Cont.	Visco.
2		2	Cont.	Visco.
3		1	Cont.	Visco.
4		2	Discont.	Visco.
5		1	Discont.	Visco.
6		2	Cont.	Rubber
7		1	Cont.	Rubber
8		2	Discont.	Rubber
9		1	Discont.	Rubber

### 7.1.3 Design load

The design load chosen for the following numerical simulations and experimental tests was a vertical distributed compression load,  $P_{floor}$ , equal to  $2450 \text{ N/m}^2$ , chosen according to the experience of the research group.

### 7.1.4 Design constraints

The maximum allowable static deflection,  $d_{max}$ , was set equal to 1 millimetre, due to the fact that a higher deflection of the floating floor could

lead to a feeling of discomfort for the passengers and crew members while walking on the floor.

## **7.2 Numerical simulations**

For the second phase of the optimisation procedure, finite elements were developed, in which to perform static simulations to evaluate the stiffness of the resilient material to be used in the floating floor prototypes and a dynamic simulation of the base module to gain a general overview of the behaviour of the module in the frequency range of interest, prior to the laboratory tests. The finite element models were done using specialised software, MSC Patran 2012, and the analysis were performed MSC Nastran 2012.

### **7.2.1 Finite element model description**

Since the grillage system is made of modules, as shown in Figure 16, one single module was modelled.

The materials of the resilient elements and of the support beam were simulated as elastic materials. This assumption is valid since the resilient element is supposed to work under small deformation, and its stiffness does not change during loading. A model of a grillage module corresponding to configuration 3 can be seen in Figure 18, and a model corresponding to configuration 4 can be seen in Figure 19.

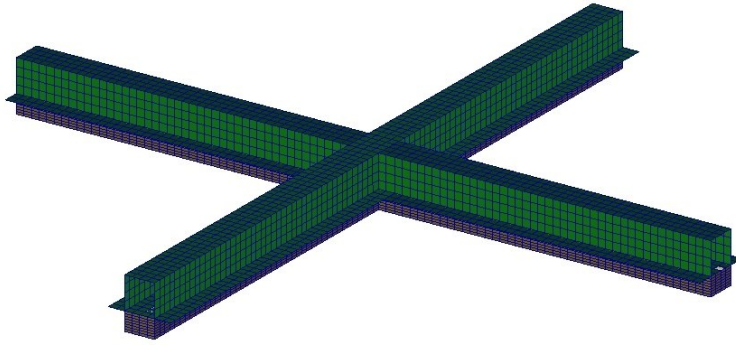


*Figure 18 – Finite element model of a floating floor module with continuous resilient element application*

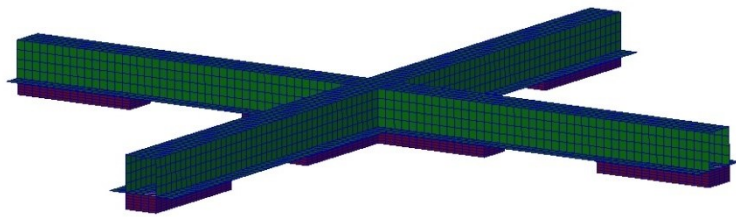


*Figure 19 – Finite element model of a floating floor module with discontinuous resilient element application*

#### **7.2.1.1 Mesh description**

The support beam was modelled with low order quadrilateral shell elements CQUAD4, with four nodes. The support beam was modelled using two different shell element sizes. The top part of the support beam had square shell elements, with 0.0065 metres of side length. The lateral and “wing” elements of the support beam, that have the objective of supporting the mineral wool panels, have been modelled with rectangular shell elements with mesh

size of  $0.007 \times 0.0065$  metres. A portion of the described modelled open beam section can be seen in Figure 20.

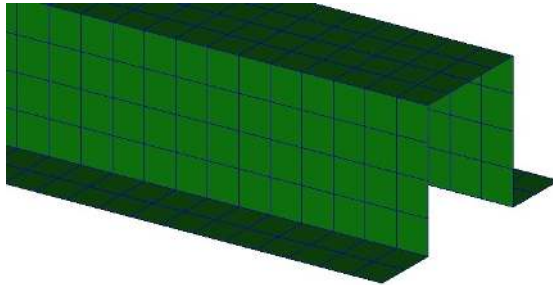


*Figure 20 – Open beam section configuration mesh*

The resilient material was modelled with fully integrated linear brick elements, CHEXA, with eight nodes. For the open section beam configuration, the mesh dimension of the brick elements was of  $0.0065 \times 0.0065 \times 0.008$  metres in the lower portion, below the lower limit of the beam section, and of  $0.0065 \times 0.0065 \times 0.007$  metres in the portion inside the beam section. A portion of the described modelled resilient material can be seen in Figure 21.

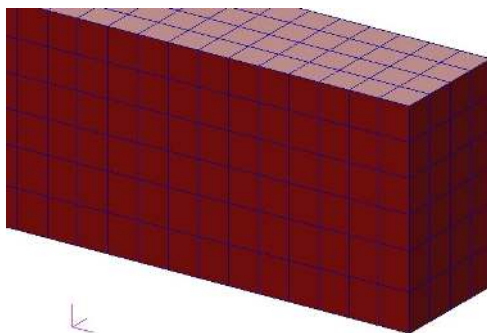


*Figure 21 – Resilient material mesh used for the open beam section configuration*

For the closed section beam configuration, the mesh dimension of the brick elements was of  $0.0065 \times 0.0065 \times 0.002$  metres. A portion of the

described modelled resilient material, together with the associated closed beam section, can be seen in Figure 22.

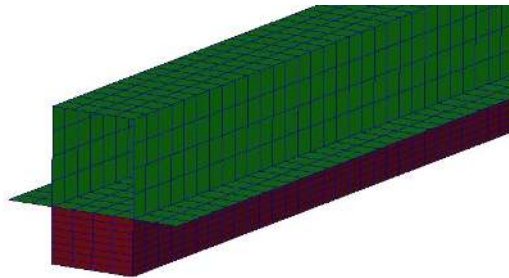


*Figure 22 – Resilient material and closed beam mesh used for the closed beam section configuration*

#### **7.2.1.2 Design loads**

The load received by the single module is of  $882 \text{ N/m}^2$ . For the static simulation, this was applied on the top surface of the module by means of a PLOAD4 entry, that applies a finite force and applies it uniformly along a determined surface. The final pressure applied on each shell element on top of the beam section was of  $28927.9 \text{ N/m}^2$ . The loads applied on each shell element can be seen in Figure 23, represented with light blue vectors.

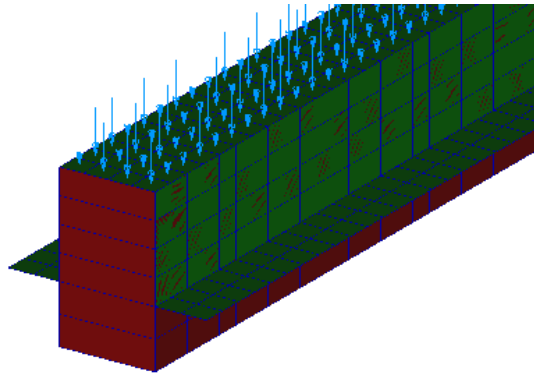


*Figure 23 – Portion of the module depicting the design load applied on each shell element on the top part of the beam section with light blue vectors*

For the dynamic simulations, the load received by the single module, was included in the system by adding a non-structural mass to the elements in the top part of the beam structure.

Also, for the dynamic simulations, a unitary force was applied in the central node of the beam structure of the module, to simulate the vertical excitations that the floating floor undergoes. The force is applied in the vertical direction of the floating floor, as is shown in Figure 24. The read-out node for the frequency transfer function was a node on the top part of one of the extremities of the beam structure, as shown in Figure 25.

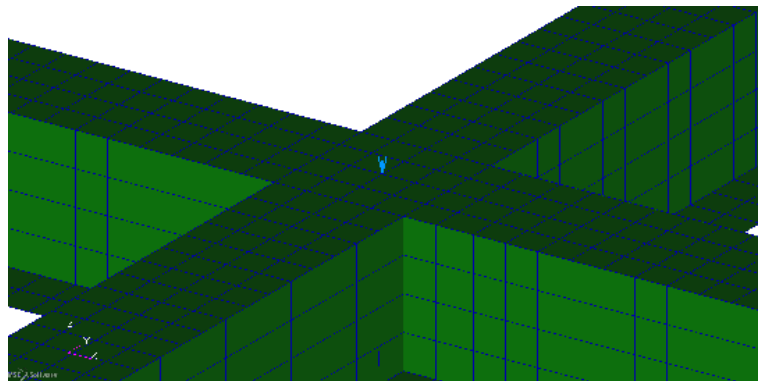


Figure 24 – Central part of the base module depicting the unitary force applied to one of the central nodes for the dynamic simulations with a light blue vector

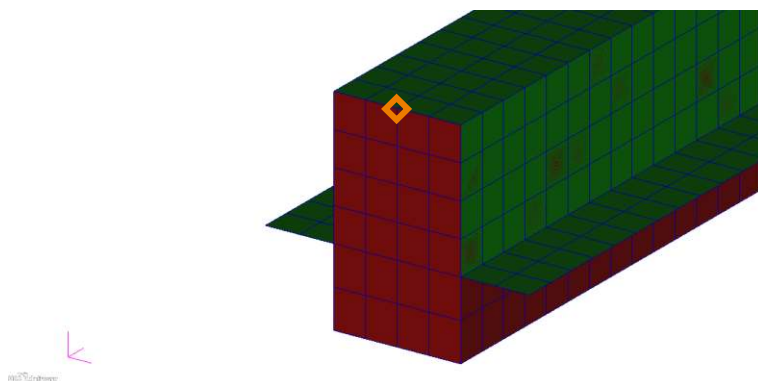


Figure 25 – Extremity of the base module showing the read-out node for the frequency transfer function measurement with an orange rhombus

### 7.2.1.3 Boundary conditions

The boundary conditions of the finite element model of the single module were selected so as to represent correctly the conditions of a whole floating floor grillage in an operational condition.

Three boundary conditions were set on the grillage module. To represent the fixed base of the resilient material to the ship bridge, a vertical translation constraint was set to all the nodes in the lower face of the elements



simulating the resilient material, as can be seen in Figure 26, represented with red vectors.

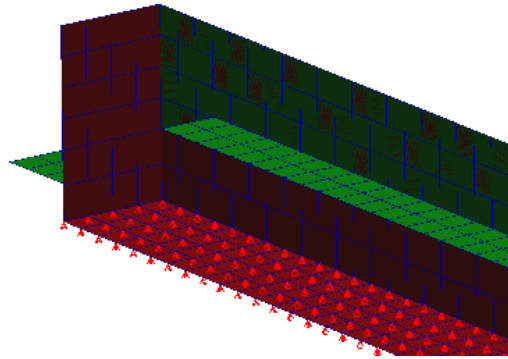


*Figure 26 – Portion of the module depicting the fixed base boundary condition applied to the lower nodes of the solid elements of the resilient material*

To simulate the continuity of the system, that behaves as a whole grillage and not a single module, symmetry constraints were set in the nodes present in the faces of the elements present in the extremities of the module. On the extremities along the X axis, the constraints introduced blocked the translation along the X axis, and the rotation about the Y and Z axis. Likewise, on the extremities along the Y axis, the constraints set in place blocked the translation along the Y axis, and the rotation about the X and Z axis. An example of the constraints applied on one of the extremities along the Y axis can be seen in Figure 27.

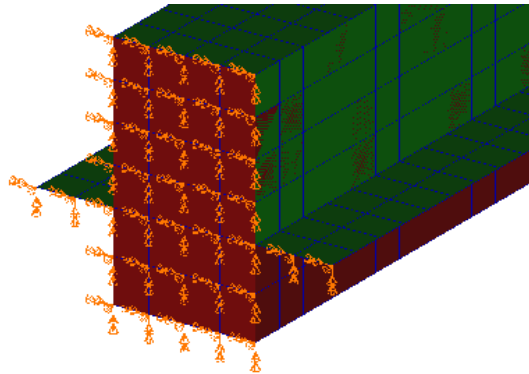


Figure 27 – Portion of the module depicting the symmetry constraint in the Y axis applied to one of the extremities of the module along the Y axis

## 7.2.2 Finite element static simulations results

Linear static finite element simulations of the floating floor modules under a defined static load were undertaken, and the resulting displacements of the different configurations can be seen in Table 2.

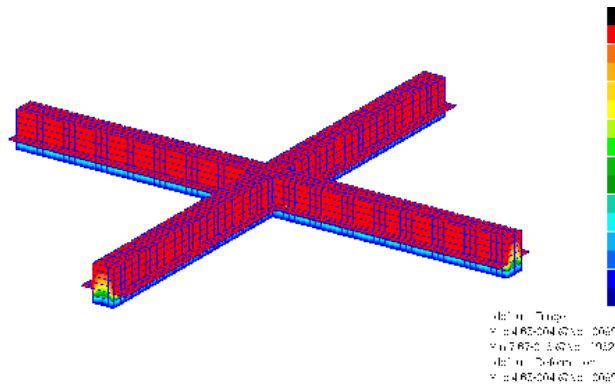






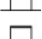
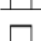
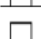









Figure 28 – Linear static simulation of the original floating floor module, showing the deformation and fringe of the structure

*Table 2 – Results of the linear static finite element analyses of the different configurations of the floating floor modules*

Config.	Beam section	Young Modulus ( $E$ ) [MN/m <sup>2</sup> ]	Displacement [mm]
0A		0.73	0.93
<b>0B</b>		<b>0.47</b>	<b>1.43</b>
1A		0.73	0.95
<b>1B</b>		<b>0.47</b>	<b>1.45</b>
2A		0.73	0.64
2B		0.47	0.99
3A		0.73	0.66
<b>3B</b>		<b>0.47</b>	<b>1.01</b>
4A		0.73	0.96
<b>4B</b>		<b>0.47</b>	<b>1.48</b>
<b>5A</b>		<b>0.73</b>	<b>1.52</b>
<b>5B</b>		<b>0.47</b>	<b>1.00</b>
6		4.4	0.18
7		4.4	0.16
8		4.4	0.27
9		4.4	0.24

The configurations that had deflections larger than 1 millimetre are marked in bold font in Table 2. Most of these are the configurations that had a lower stiffness, whether it was because of a low Young modulus,  $E$ , or a lower stiffness of the supporting beam due to the lower thickness of the section.

### 7.2.3 Finite element dynamic simulation results

A forced response dynamic simulation of the floating floor base module under a defined static load was undertaken, and the resulting Mobility frequency response function can be seen in Figure 30 and Figure 30.

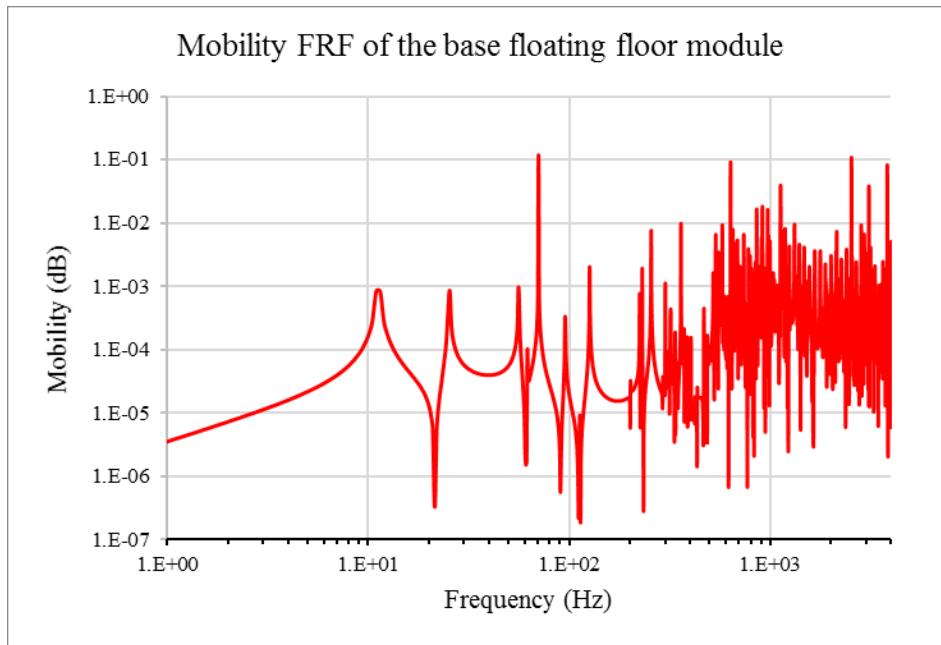


Figure 29 – Mobility FRF of the dynamic simulation taken on the base module, log-log scale

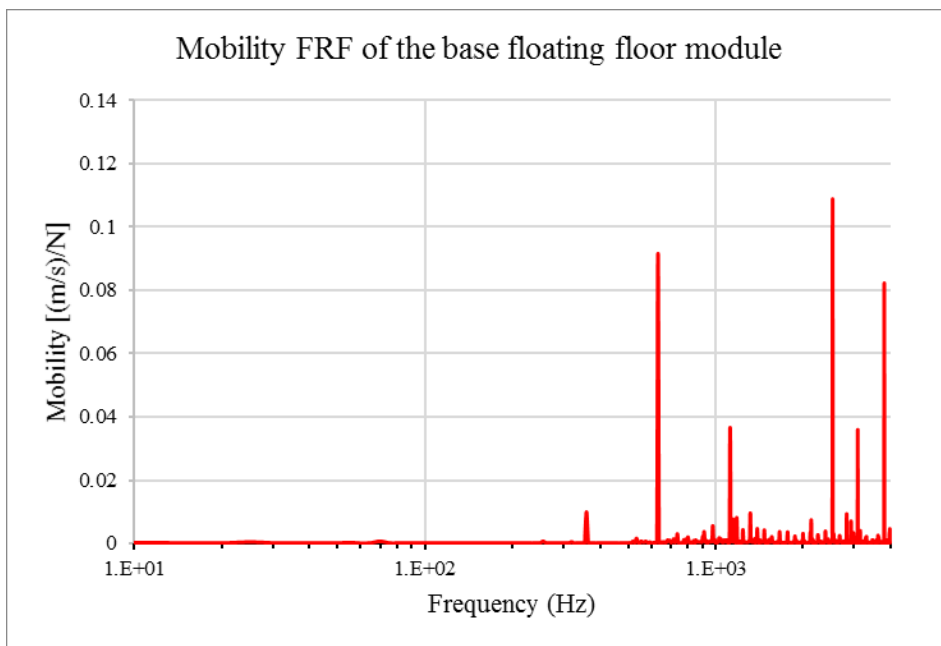








Figure 30 – Mobility FRF of the dynamic simulation taken on the base module, lin-log scale

The simulations show in the log-log graph in Figure 29 that, as is to be expected, on the lower frequencies the function is governed mainly by the first vertical mode, and as the frequencies increase there is also an increase in the amount of modes participating in the motion of the system. In the linear-log graph in Figure 30, we can notice that the modes present around 635 Hz, 2500 Hz and 3800 Hz have higher amplitudes that governing the behaviour of the system.

### **7.3 Static laboratory tests**

The results from the numerical simulations proved useful to identify the minimum allowable stiffness of the resilient material of the floating floor, meaning that a minimum Young Modulus,  $E$ , of the resilient material. From the results of these numerical simulations, six floating floor module prototypes were designed and built to be tested in laboratory. At this point of the research, only prototypes with beam thickness of 2 millimetres were built. The chosen configurations can be seen in Table 3, and an example of a prototype of configuration 4A can be seen in Figure 31.

*Table 3 – Configurations selected for prototype construction*

Configuration	Beam Section	Application
0		Continuous
0A		Continuous
2A		Continuous
4A		Discontinuous
6		Continuous
8		Discontinuous

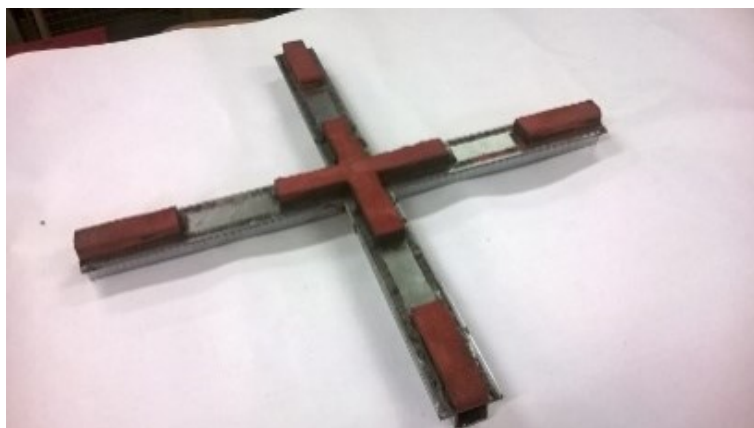


*Figure 31 – A floating floor prototypes built after the numerical simulations*

The first part of the laboratory tests aimed to check the compliance of each of the prototypes with the design specifications on the maximum allowable static deflection,  $d_{max}$ .

### **7.3.1 Static laboratory tests: Setup**

The design static compression load of  $2450 \text{ N/m}^2$  was applied to each prototype, and then the static deflection was measured after 24 hours, in order to allow for the relaxation of the resilient material. The measurements were done with a displacement indicator, set up as shown in Figure 32.



Figure 32 – Setup of the static deflection tests undertaken in laboratory on the floating floor prototypes

### 7.3.2 Static laboratory tests: Results

The results can be seen in Table 4, where the column on the right shows the obtained deflections.

Table 4 – Results for the static deflection tests performed on the floating floor module prototypes undertaken in the laboratory

Configuration	Beam Section	Application	Displacement [mm]
0		Continuous	0.37
0A		Continuous	0.64
2A		Continuous	0.50
4A		Discontinuous	0.80
6		Continuous	0.63
<b>8</b>		<b>Discontinuous</b>	<b>1.48</b>

According to the results, only configuration 8 did not comply with the maximum displacement constraint of 1 millimetre. There is a large discrepancy between the laboratory tests and the numerical simulations. This

can be due to the difficulties in controlling the stiffness of the viscoelastic material during the manufacture process.

#### **7.4 Dynamic laboratory tests**

A series of dynamic tests were performed to the same prototypes to which the static tests were performed on, shown in Table 3.

The first round of tests had the objective to measure the damped natural frequency of the SDOF system made of the floating floor module prototypes and a mass that was selected to simulate the upper floor. The second round of dynamic tests were carried out in order to measure the Transmission Loss of each floating floor prototype module.

##### **7.4.1 Dynamic tests setup: Measurement of resonant frequencies**

The experimental apparatus used to measure the resonant frequency of the system is shown in Figure 33. The resilient element is laying on a rigid plane surface and supports the mass used to simulate the upper surface. The two parts are fastened together using bolted joints. An electrodynamic shaker, connected to the upper mass by a stinger rod, is used to excite the system in the vertical direction. A 12 channel data acquisition system was used to acquire the data measured by ICP piezoelectric accelerometers and by an ICP dynamic load cell that was connected to the stinger rod and the upper mass. The data acquisition system was also used to condition the acquired analogue signal and



to convert it to a digital signal. A computer terminal was used to analyse the signal in the frequency domain and to calculate the Accelerance frequency response functions (FRF). The FRF were calculated in terms of H1 and H2 estimators in order to evaluate the effect of unwanted input vibrations on the measured data. In addition, the coherence functions were calculated in order to verify the quality of the measured data.

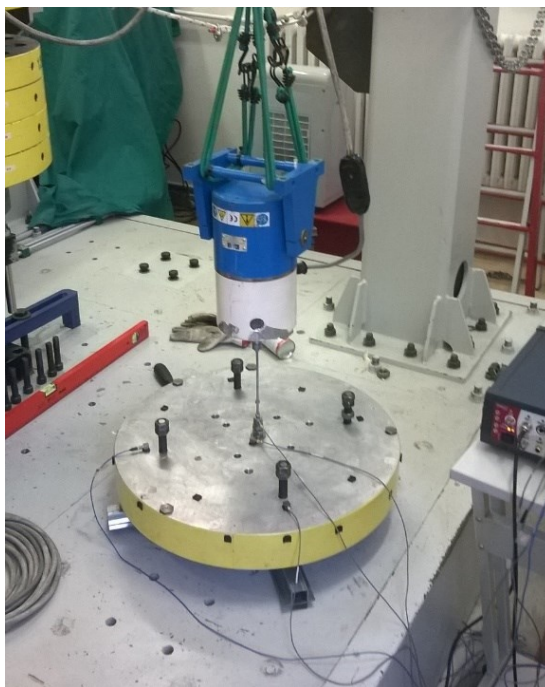


*Figure 33 – Experimental apparatus used for the measurement of the damped natural frequencies of the floating floor prototypes*







Since the calculated natural frequencies ranged between 12 Hz and 36 Hz, a white noise signal, in the frequency range from 1 Hz to 100 Hz, was used to excite the system in the vertical direction, which corresponds to the

–  $Z$  direction of the floating floor, which will be considered as positive for calculation convenience, to avoid negative results.

#### 7.4.2 Dynamic tests results: Resonant frequencies

The results of this first round of dynamic tests can be seen in Figure 34. As can be noticed, the decrease of the resilient material stiffness implies a consequent decrease of the damped natural frequency of the system, considered as a damped SDOF system. This can be seen if we compare Configuration 0, which is the original module that has a resilient material with Young modulus,  $E$ , of  $1.45 \text{ MN/m}^2$ , with Configuration 0A that has the same beam structure but with a resilient material with Young modulus,  $E$ , of  $0.73 \text{ MN/m}^2$ ; for these two configurations there is a reduction of 9 Hz due to the reduction of the resilient material stiffness. The measured resonant frequencies are shown in Table 5.

*Table 5 – Measured damped natural frequency of the prototype modules tested*

Configuration	Beam section	Resonant frequency, $f_r$ [Hz]
0		40.4
0A		31.5
2A		31.9
4A		28.0
6		29.5
8		25.4

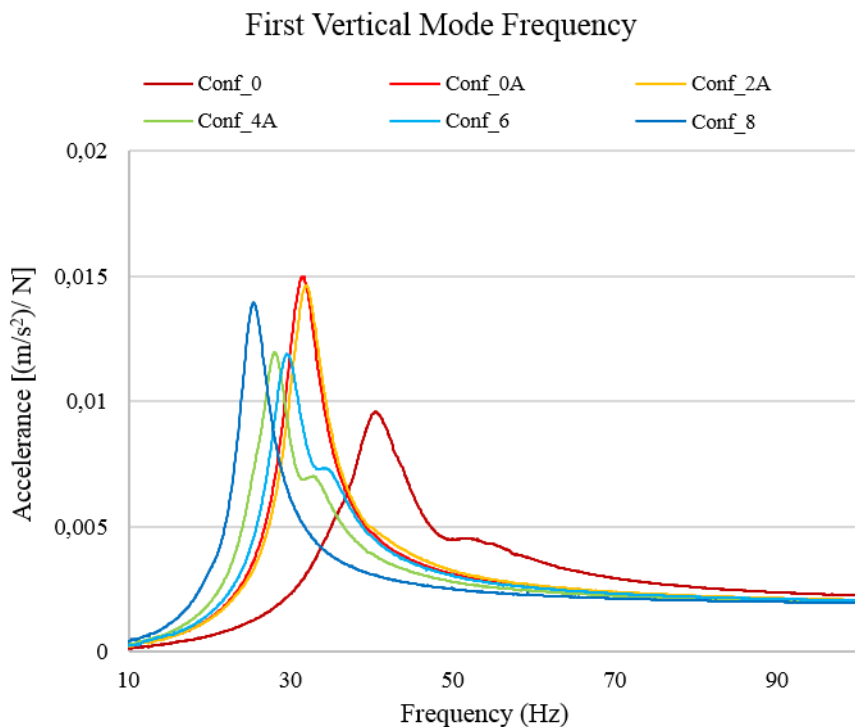
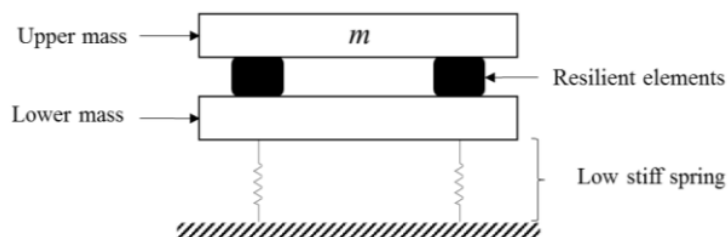


Figure 34 – Accelerance functions in the vertical direction of the floating floor modules

### 7.4.3 Dynamic tests setup: Measurement of Transmission Loss

The setup for these tests, aimed to simulate the condition in which the floating floor will be installed. The setup consisted on an upper mass bolted to the resilient element, which was laying on a lower mass, that was decoupled from the rigid base by means of soft springs. A scheme of the setup is shown in Figure 35. The stiffness of these springs was selected considering that the natural frequency of the SDOF system composed by the lower mass and the soft springs,  $\omega_{nl}$ , should be  $\omega_{nl} \leq 1/3 \omega_n$ , where  $\omega_n$  is the natural frequency of the resilient module and the upper mass, considered a SDOF system. This

guarantees that the system can be considered decoupled from the rigid base [67]. For the tests, each module was loaded with the upper mass, and the dynamic tests were carried out 24 hours afterwards, in order to allow the relaxation of the resilient material.



*Figure 35 – Scheme of the experimental setup for the measurement of the Transmission Loss of the floating floor prototype modules*

The electrodynamic shaker was connected to the lower mass by means of a singer rod, as shown in Figure 36. The data acquisition transducers were 5 ICP piezoelectric accelerometers, that were attached to the upper surface of the upper mass as well as to the lower surface of the lower mass. A 12 channel data acquisition system was used to acquire the data and condition the signals and supply the transducers. The input signal was white noise which ranged from 5 Hz to 5 kHz.

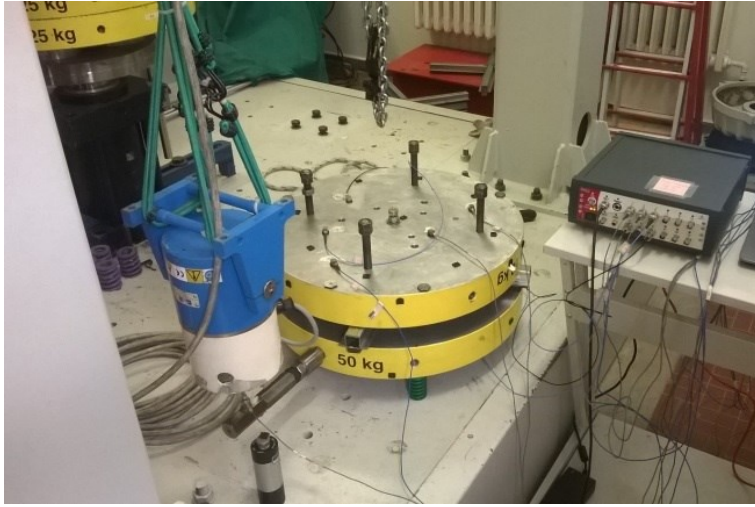


Figure 36 – Experimental apparatus used for the measurement of the Transmission Loss of the floating floor prototype modules

#### 7.4.4 Dynamic tests results: Transmission Loss

The acceleration levels measured by each accelerometer on the upper surface of the upper mass were then averaged in order to evaluate the velocity level on the upper surface, according to the following formula:

$$L_{v, floor} = 10 \log \left( \frac{1}{10} \sum_{i=1}^n 10^{\frac{L_{v,i}}{10}} \right) \quad (51)$$

Where  $L_{v,i}$  is the velocity level, in dB ref  $10^{-9}$  m/s, and measured in the  $i$ -point of the upper surface of the upper mass. Likewise, this formula was used to calculate the average velocity levels,  $L_{v, structure}$ , of the lower surface of the lower mass. Finally, with the use of Equation (45), the Transmission Loss was calculated. The resulting Transmission Loss curves of the floating floor prototype modules is shown in Figure 37, where it can be seen that, according

to the theoretical background previously mentioned, in proximity of the damped natural frequency of each prototype module, the Transmission Loss curves tend to zero. Then, as the frequencies increase, the curves increase about linearly in the log-log graph. Most importantly, we can notice a general trend of the Transmission Loss curves to increase their values as the stiffness of the resilient material decreases. Particularly, Configuration 0 and Configuration 2A, which are the stiffest modules, show to have the lowest Transmission Loss. On the other hand, Configuration 4A and Configuration 8, which have the resilient materials with the lowest stiffness, are characterised by the highest value of Transmission Loss. Later, as the frequencies increase further, the curves deviate from their ideal behaviour and a series of peaks start forming. This is due to the fact that, whereas in the lower frequencies the behaviour of the module is governed by the damped natural frequency of the first mode, in the higher frequencies the system is governed by several other modes. This is why the system no longer behaves as a SDOF system. This has been shown in Section 7.2.3, where the higher frequencies were mainly governed by resonant frequencies at 635 Hz, 2500 Hz and 3800 Hz, which coincide with the peaks formed in the Transmission Loss curve.

The same consideration is valid for the upper floor. In this specific test scenario, an aluminium disk was considered to simulate the presence of the upper floor. The outcome of dynamic simulations performed on this

aluminium disk show that its first mode appears at 1.25 kHz, which reflects on the drop of the Transmission Loss curves in this 1/3 octave band [68].

Furthermore, in the higher frequencies there is a stabilisation of the Transmission Loss curve, as was also expected from the theoretical analysis, and the gain of Transmission Loss between the different module configurations with the increase of frequency is lower.

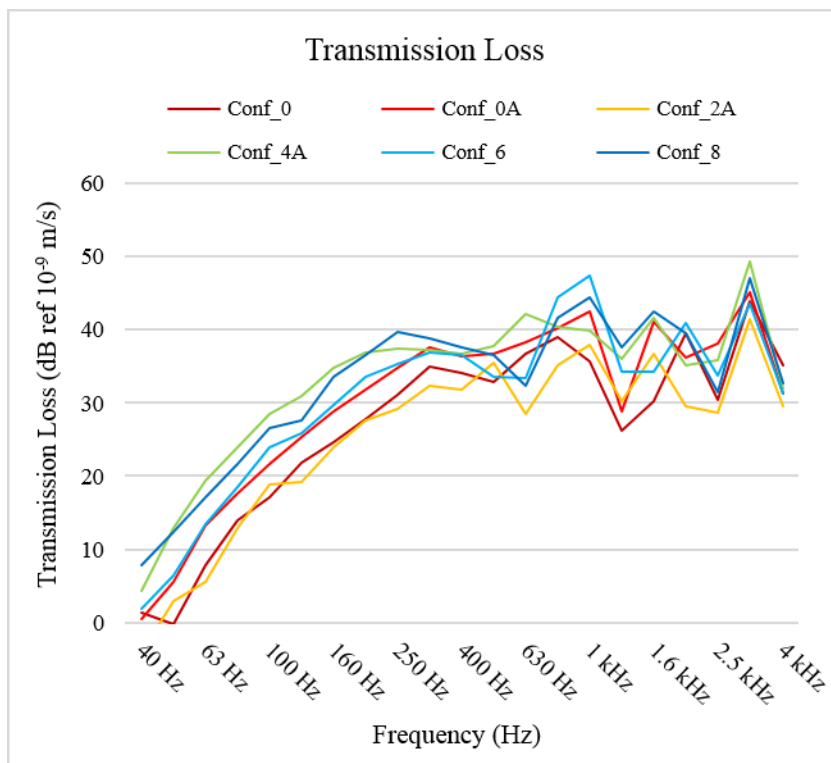


Figure 37 – Transmission Loss curves of the floating floor prototype modules

## 7.5 Conclusion

The Finite Element simulations and the laboratory tests have given very significant results, useful for the consolidation of the proposed optimisation design process.

The original and optimised configuration of the floating floors were modelled with finite elements, using two new materials, while taking into consideration the weight and production process of the whole grillage. The Finite Element simulations performed allowed to do a screening of the configurations that did not comply with the requirements, thus allowing the designers to reduce costs and time in the construction and testing of the prototypes.

After performing the static laboratory tests, a large discrepancy has been noticed between the Finite Element simulations and the laboratory tests, this can be due to difficulties encountered in the control of the stiffness of the resilient materials, presented during the production of the prototypes.

From the first dynamic test round, the damped natural frequencies were obtained. These are important to know the point in which the floating floors cease to work, and as a first touchpoint to understand if the prototype is behaving as theoretically expected.

From the second round of dynamic tests, the Transmission Loss curves were calculated and were found to follow their own theoretical behaviour.



Likewise, differences in the values of the Transmission Loss curves were found, that also follow the theoretical behaviour. The stiffest modules have the lowest Transmission Loss, and the least stiff have the highest Transmission Loss. Moreover, another important finding is that at higher frequencies, the Transmission Loss curve starts showing a series of peaks, due to the fact that the system is governed by several more modes, and it stops behaving as a SDOF system. Beyond this frequencies, the Transmission Loss curve stabilises, and the gain between the different module configurations tends to be smaller as the frequency furtherly increases.



## 8 Plate structure

For non-self-supporting damping materials, the damping properties are evaluated in a two-step process. First, a self-supporting specimen, in our case a uniform isotropic metal plate, called the base plate, is tested to determine its resonant frequencies. Then, the damping material is applied to the base plate to form a damped composite plate specimen, using one of the two configurations shown in Figure 38. These configurations are used to measure the damping due to extensional deformations and are known as the unconstrained layer configuration, or free layer configuration.

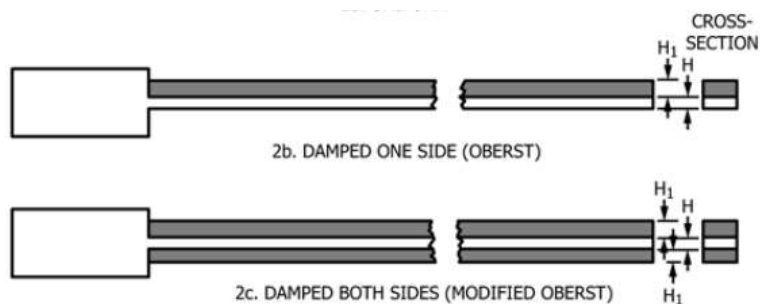


*Figure 38 – Different configurations for the measurement of damping characteristics of non-self-supporting damping materials*

When the shear damping properties of the material are also needed, the damping material layer is constrained within two identical plates, forming a composite plate specimen in sandwich configuration. This configuration is

also known as the constrained layer damping configuration, as stated in the previous sections.

An important factor to consider for the tests, is the thickness of the damping layer to be applied on the base plate. For this we make a plot of Equation (10), we obtain the graph shown in Figure 39. In this graph we can see the dependence of the system Loss Factor ( $\eta$ ) on the thickness and the modulus of the applied viscoelastic layer. From this graph it is clear that for lower values of  $h$ , the system Loss Factor is proportional to the thickness of the viscoelastic layer. For values of  $h$  around the unity, the system Loss Factor depends on the square of the thickness of the viscoelastic layer. When the system Loss Factor arrives to values close to 40% of the viscoelastic material Loss Factor ( $\eta_2$ ), the curves start saturating, and increasing the thickness of the viscoelastic layer, gives no longer additional damping. Also in the graph, we can see that after a thickness ratio ( $h$ ) of 4, all the curves saturate for high system Loss Factor values, which can be the reason why the ASTM E756 standard suggests not to use viscoelastic material thicknesses beyond 4 times as thick as the base plate thickness.

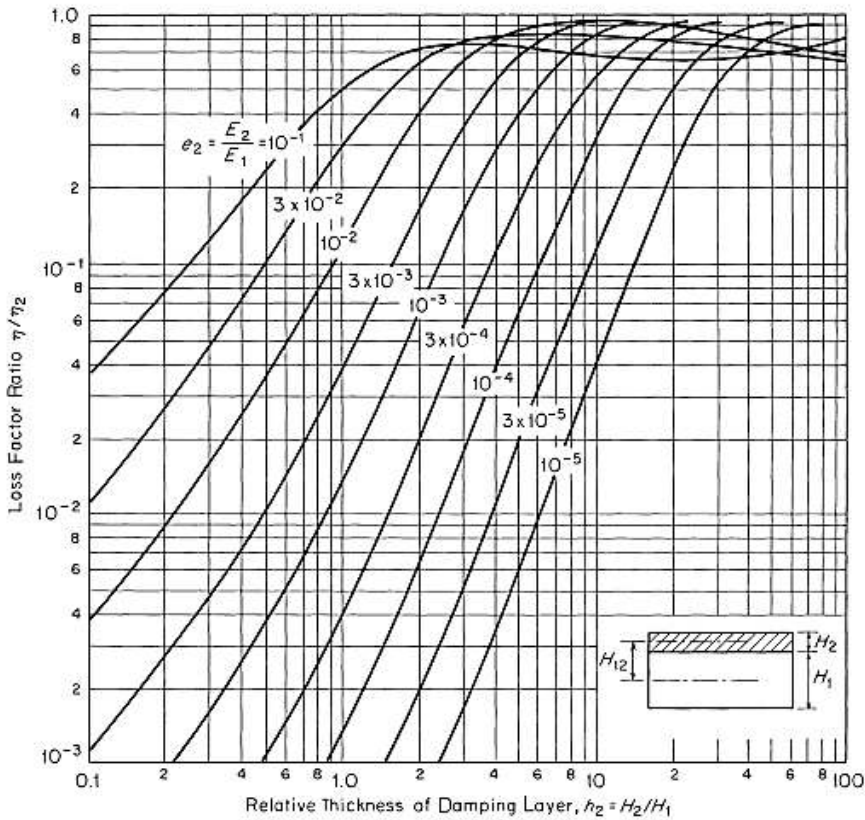


Figure 39 – Dependence of system Loss Factor ( $\eta_c$ ) of a plate with a viscoelastic layer application, on the relative thickness and modulus of the viscoelastic layer

The important thing to consider, is that an appropriate thickness of damping material must be selected, in order to obtain a well-damped response with measurable amounts of damping [38]. For the unconstrained layer configuration, the ASTM E756 standard, suggests a thickness ratio of 1:1 as a starting point, and for the constrained layer configuration, a thickness ratio of 1:10.

Once the plate configuration has been selected, the damped composite specimen is tested to obtain its resonant frequencies and corresponding modal

loss factors over the frequency range of interest. The modal loss factors are obtained using the half-power bandwidth method described earlier.

The elements of the setup are the test specimen, that in our case will be the different plates with diverse passive damping configurations, an impact hammer, to generate the impulse excitation force, the response transducers, to measure the acceleration, a signal analyser, that will provide the data acquisition and signal processing operations and the computer terminal, that is the main element of the test system, with post processing software. The setup elements and scheme can be seen in Figure 40, and will be further described in the next section.



*Figure 40 – Setup for the Experimental Modal Analysis*

The base test specimens are steel plates of two different thicknesses, according to the configuration, that have the characteristics shown in Table 6 and Table 7:

*Table 6 – Characteristics of Base Plate 1*

Base Plate 1 (BP2) – Unconstrained configuration		
Length ( $L$ )	0.5	m
Width ( $b$ )	0.3	m
Thickness ( $h_1$ )	0.002	m
Density ( $\rho_1$ )	7850	Kg/m <sup>3</sup>

*Table 7 – Characteristics of Base Plate 2*

Base Plate 2 (BP5) – Constrained configuration		
Length ( $L$ )	0.5	m
Width ( $b$ )	0.3	m
Thickness ( $h_1$ )	0.005	m
Density ( $\rho_1$ )	7850	Kg/m <sup>3</sup>

The specimens for the unconstrained and constrained configurations have applications of viscoelastic materials that vary in thickness ( $h_2$ ) and type of material. The materials are Plastigel and Viscogel, the latter one with different chemical compositions that are coded as A, B, C and D. The specimens tested, with their different configurations are shown in Table 8, where in  $h_2/h_1$  the suffixes indicate the damping material and the base plate, respectively.

*Table 8 – Specimens tested*

Specimen ID	Damping Material	Configuration	$h_2/h_1$
PL2-FLD	Plastigel	Unconstrained	1
PL4-FLD	Plastigel	Unconstrained	2
PL0.5-CLD	Plastigel	Constrained	0.1
PV2-FLD	Viscogel A	Unconstrained	1
PV4-FLD	Viscogel A	Unconstrained	2
PVA-FLD	Viscogel A	Unconstrained	0.4
PVB-FLD	Viscogel B	Unconstrained	0.4
PVC-FLD	Viscogel C	Unconstrained	0.4
PVD-FLD	Viscogel D	Unconstrained	0.4

The typical constraint suggested by the ASTM E756 standard, is a cantilever connection for a beam. However, the specimens under study are plates in the free-free boundary condition, because the clamped boundary condition was more complicated to obtain for the dimensions of the specimens. The final support for the specimens selected was an elastic suspended link, to better simulate the free-free condition. The final setup scheme can be seen in Figure 41.





*Figure 41 – Final test setup with suspended elastic connections of plate specimen*

## **8.1 Excitation system**

The excitation was done with an APTech instrumental hammer, model AU02-6135. This impulse hammer has a built-in force transducer and several exchangeable hammer tips, made of steel, rubber and nylon, and an extender mass which in different combinations provide better results for different force and frequency ranges. The force transducer has a force range of -1000 to +5000 N, with a resolution of 0.003 N and a sensitivity of 1.5 mV/N (+/- 10%).

The hammer in question with the exchangeable tips and the extender mass can be seen in Figure 42, as shown in the brochure.



*Figure 42 – Impulse Hammer APtech AU02-6135*

When exciting a structure, the position of the impact affects the response of the system. If the impact is done in a nodal line, the modes containing that nodal line will not be excited, which is why, the impact position must be chosen correctly. In order to excite a large amount of modes in a determined frequency range, the impact position must be in a location that ideally does not contain nodal lines for modes in that frequency range, or in which the least amount of nodal lines as possible are present.

In order to select the best exciting position, a modal analysis of the base plate using FEM simulations was made. The mode shapes obtained in the interested frequency range, from 0 Hz to 600 Hz, are shown from Figure 43 to Figure 62.

# Experimental study and numerical simulation of the behaviour of viscoelastic materials to reduce the vibrations on board ships

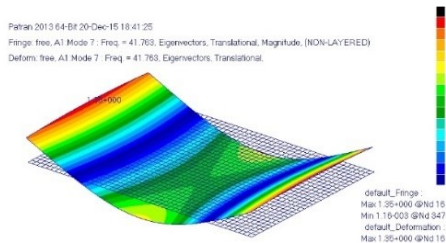


Figure 43 – Mode 1: 41.8 Hz

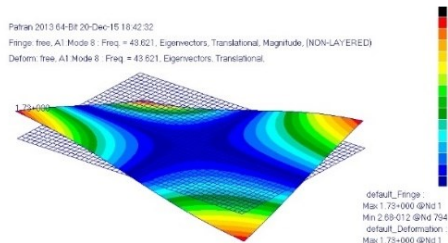


Figure 44 – Mode 2: 43.6 Hz

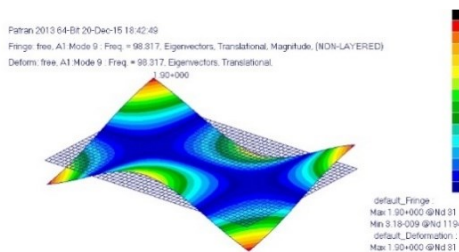


Figure 45 – Mode 3: 98.3 Hz

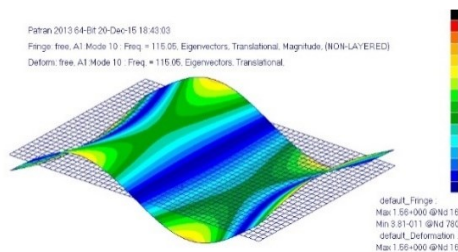


Figure 46 – Mode 4: 115.1 Hz

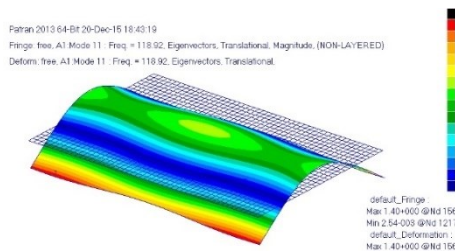


Figure 47 – Mode 5: 118.9 Hz

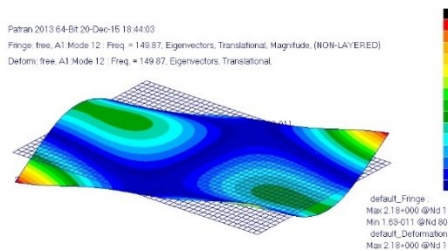


Figure 48 – Mode 6: 149.9 Hz

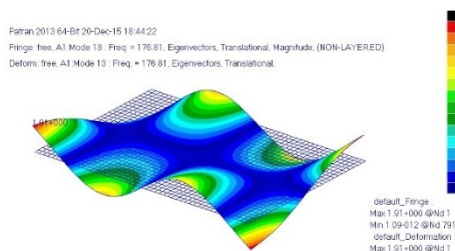


Figure 49 – Mode 7: 176.8 Hz

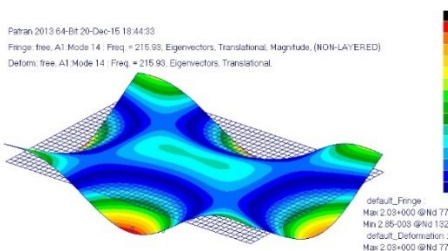
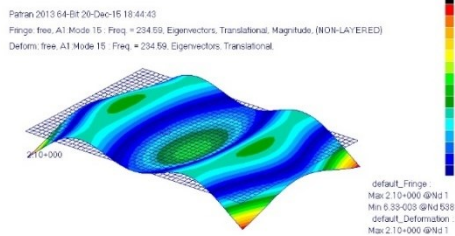
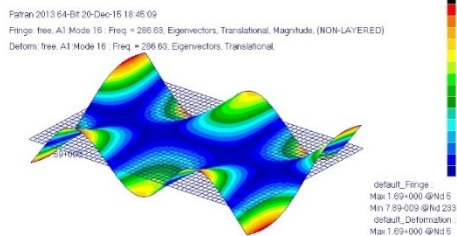


Figure 50 – Mode 8: 215.9 Hz

# Experimental study and numerical simulation of the behaviour of viscoelastic materials to reduce the vibrations on board ships



*Figure 51 – Mode 9: 234.6 Hz*



*Figure 52 – Mode 10: 286.6 Hz*

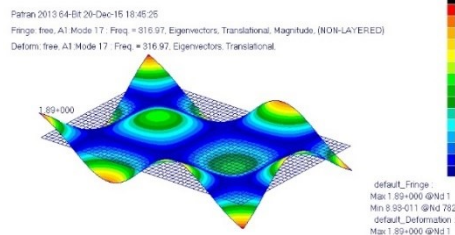


*Figure 53 – Mode 11: 316.7 Hz*

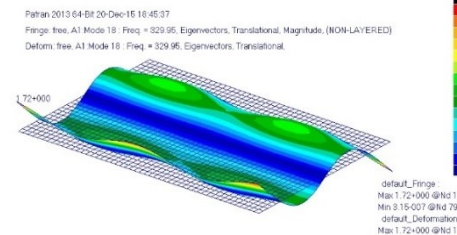


*Figure 54 – Mode 12: 329.9 Hz*

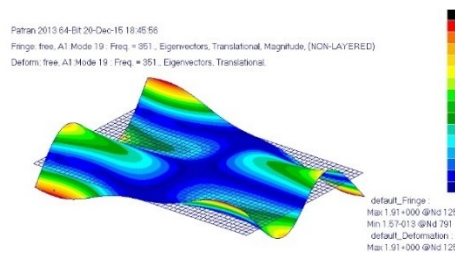


*Figure 55 – Mode 13: 351.0 Hz*

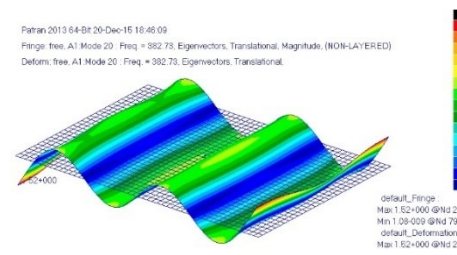


*Figure 56 – Mode 14: 382.7 Hz*

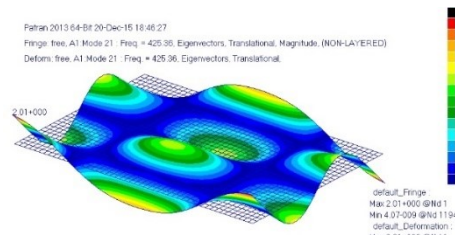


*Figure 57 – Mode 15: 425.4 Hz*

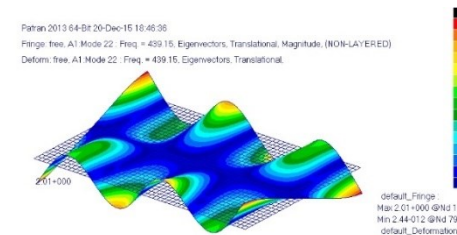


*Figure 58 – Mode 16: 439.2 Hz*

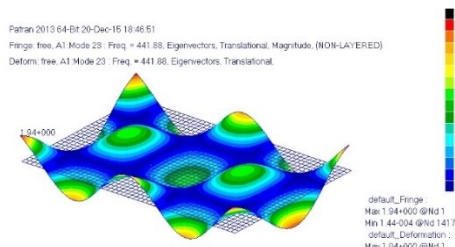


Figure 59 – Mode 17: 441.9 Hz

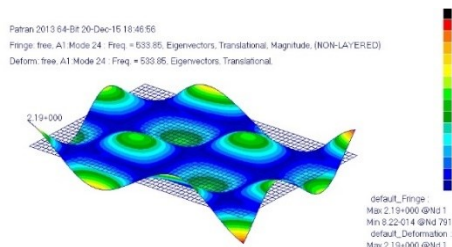


Figure 60 – Mode 18: 533.9 Hz

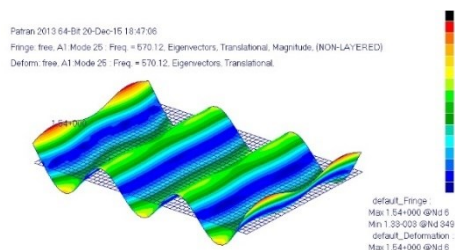


Figure 61 – Mode 19: 570.1 Hz

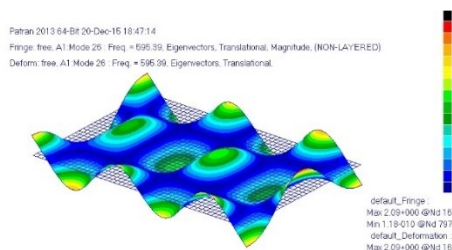
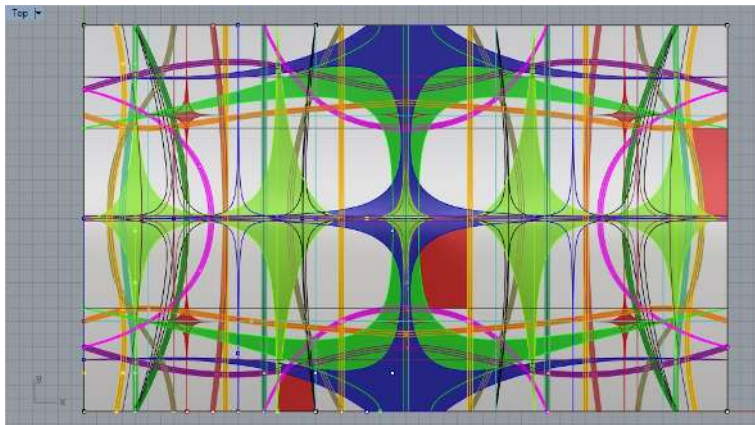
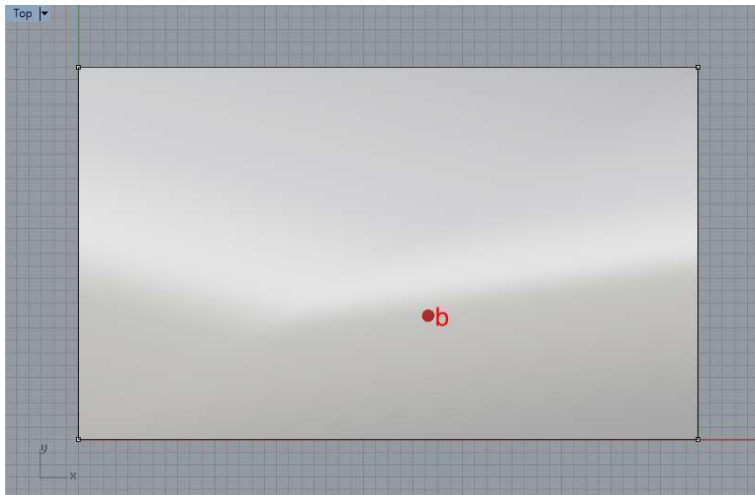


Figure 62 – Mode 20: 595.4 Hz

The obtained modal shapes were superposed using Rhinoceros 5.0 (64-bit version 5.13.60913.21340), to find areas suitable for the impact location. The suitable areas are shown in red shade in Figure 63, and the final impact position is shown in Figure 64. This point is located in position  $x = 0.28 m$  and  $y = 0.13 m$ .



*Figure 63 – Suitable impact areas indicated in red shade*



*Figure 64 – Final impact location, point “b”*

## 8.2 Acquisition system

The test acceleration responses from the different test specimens were measured with piezoelectric accelerometers Brüel & Kjær B&K4507B004, shown in Figure 65a. The data was acquired by a 12-channel signal analysis

data acquisition system, 01dB-Metravib NetdB, shown in Figure 65b, with resident software dBRTA 4.9, and post processing software dBFA 4.9.



Figure 65 – Acquisition system elements

The accelerometers used in the damping material characterisation tests were three. The positions were chosen taking into account the same principle of the location of the impact. Any modes containing nodal lines upon which the accelerometer is put on, will not be identified. This principle, however, can also be used as an advantage, in order to decouple closely spaced modes. While performing initial measurements in all the points in Figure 66, it was noticed that the points on the side opposite to the attachments of the elastic links (points 13, 14 and 15) had generally lower coherences than those on the side of the attachments of the elastic links (points 1, 2 and 3). This is why, as is shown in Figure 41, the accelerometers were placed on the side of the plates where the elastic links were, to avoid potentially low coherence levels in the measurements.

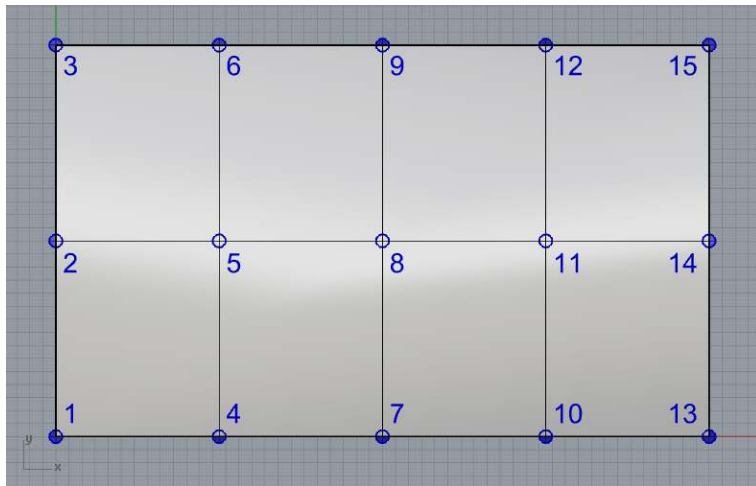


*Figure 66 – Initial accelerometer locations along the base plate*

The chosen position of the accelerometers can be seen in Figure 67. The main accelerometer considered for the measurements was accelerometer in position 1. The measurements from accelerometer in position 2 were used in case decoupling of the modes was needed, and the measurements from accelerometer in position 3 were used as a control on the measurements on accelerometer in position 1, because since they were in symmetrical positions, the resulting responses should be the same.



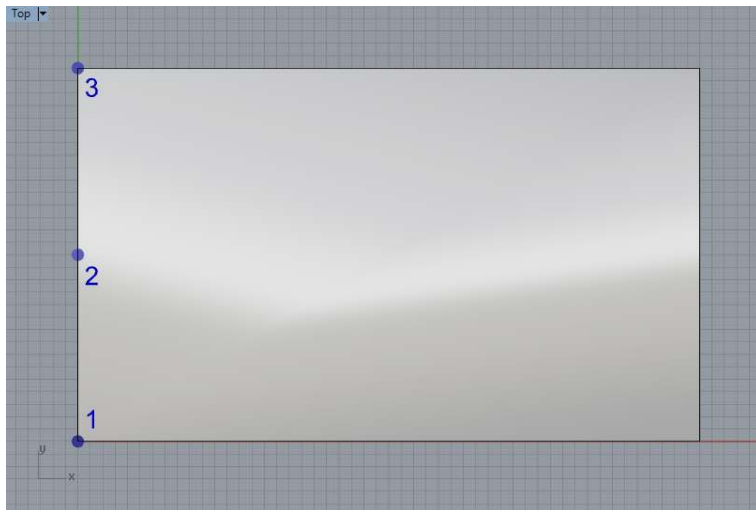


*Figure 67 – Accelerometer locations*

### **8.3 Data processing**

In order to obtain accurate results, a high frequency resolution is needed to better define the FRFs from which, by using the half-power bandwidth method, the modal Loss Factors ( $\eta$ ) will be calculated.

For all the test specimens, an initial base test was done in all the interested frequency range, from 0 Hz to 600 Hz, using fewer spectral lines, and consequently obtaining a lower frequency resolution, of 0.39 Hz. This was done to have an overview of all the interest frequency range, and be able to identify the peak locations. Then the FFT zoom was used. This technique allows the selection of a lower and upper frequency limit, obtaining thus more accuracy by concentrating the measurement points over a narrower band. In

this way, only the frequency ranges that contained the peaks to analyse by the half-power bandwidth method were analysed.

Several tests were done, over the same zoomed frequency ranges, increasing the frequency resolution starting from 0.09 Hz, while trying to obtain acceptable coherences, until 0.02 Hz.

For every test, with the use of the DBFA software, three time records recorded from three impacts were averaged and processed to obtain the acceleration transfer functions in the frequency domain.

#### **8.4 Windowing**

Windowing is necessary in signal analysis to reduce the effects of leakage, though it may never be eliminated completely. When the response decays before the end of the time record, the response window can be used to eliminate the remaining noise in the time record. On the other hand, when the response continues after the end of the time record, the response window is used to force the response signal to decay out [69]. In impact testing, the window used for obtaining both of these results, is the exponential window, shown in Figure 68. A time record signal of the acceleration taken in a measuring point of one the plates analysed is shown in Figure 69.

When the zooming technique is used, a longer time record is used to increase the frequency resolution, while at the same time, capturing the entire

response signal decay. This is why in certain situations, for example with time records of 20 seconds, like shown in Figure 70, the exponential window was not used.

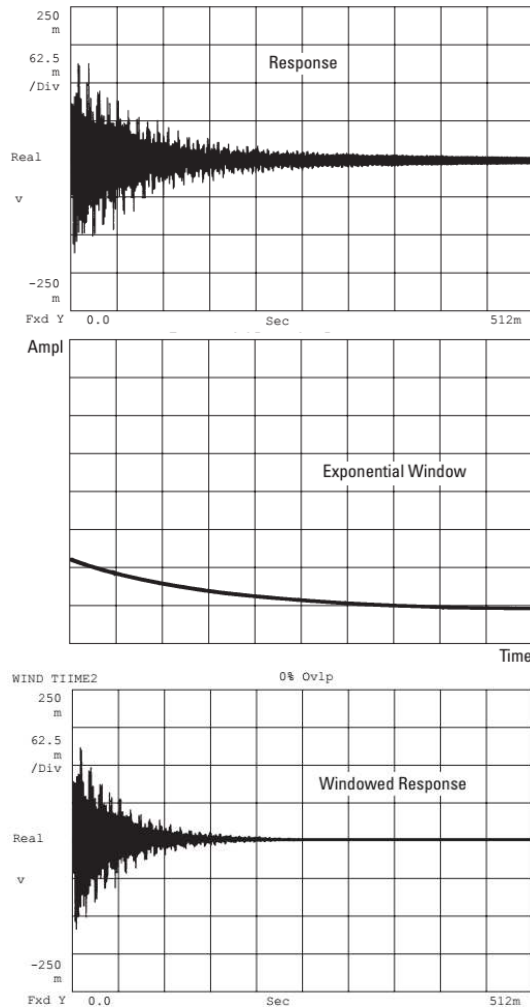
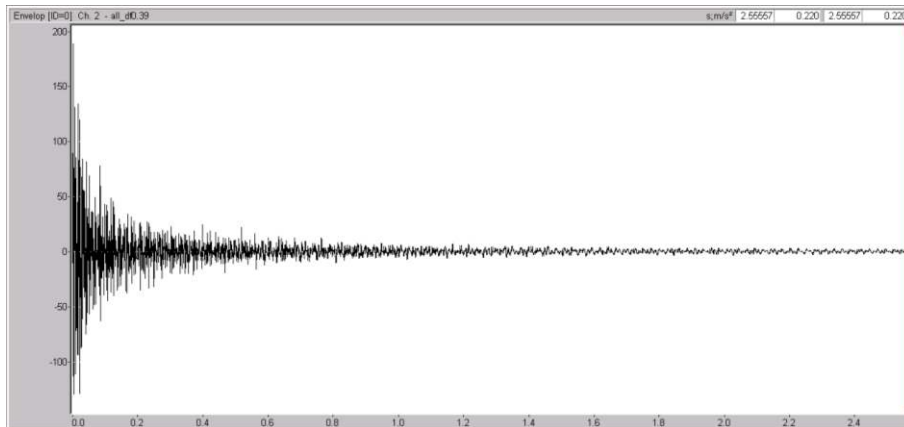
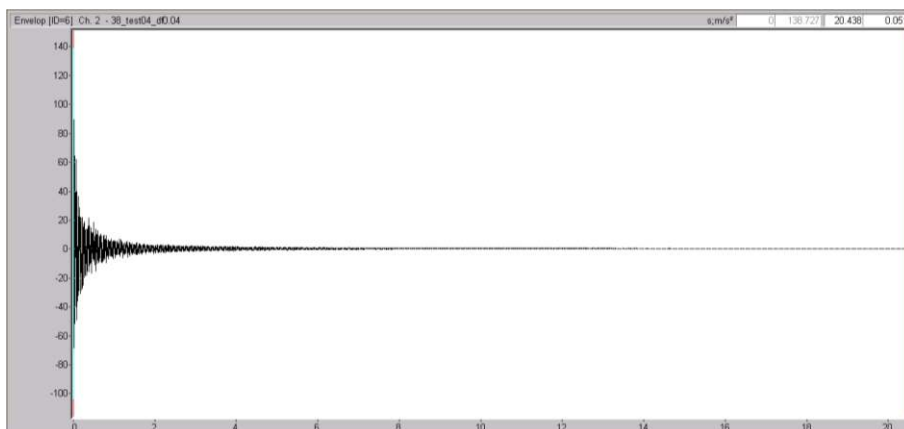


Figure 68 – Typical time response before and after application of an exponential window



*Figure 69 – Time response, Acceleration ( $m/s^2$ ) vs Time (s), used for the initial general identification of peaks, where windowing is needed to force the response to decay*



*Figure 70 – Time response, Acceleration ( $m/s^2$ ) vs Time (s), used for the zooming technique, where windowing is not needed due to the natural decay of the response*

## 8.5 Results

The final results of the tests, shown in Figure 71 until Figure 86, show the frequency response functions of the bare steel plates on the chosen measuring points, and also the frequency response functions of the steel plates with the application of the different damping materials in their two configurations. In addition, the modal loss factor curves of the plates with the application of the different damping materials in their two configurations is shown for every configuration, after their respective frequency response function have been presented. The measurements were undertaken in laboratory conditions.

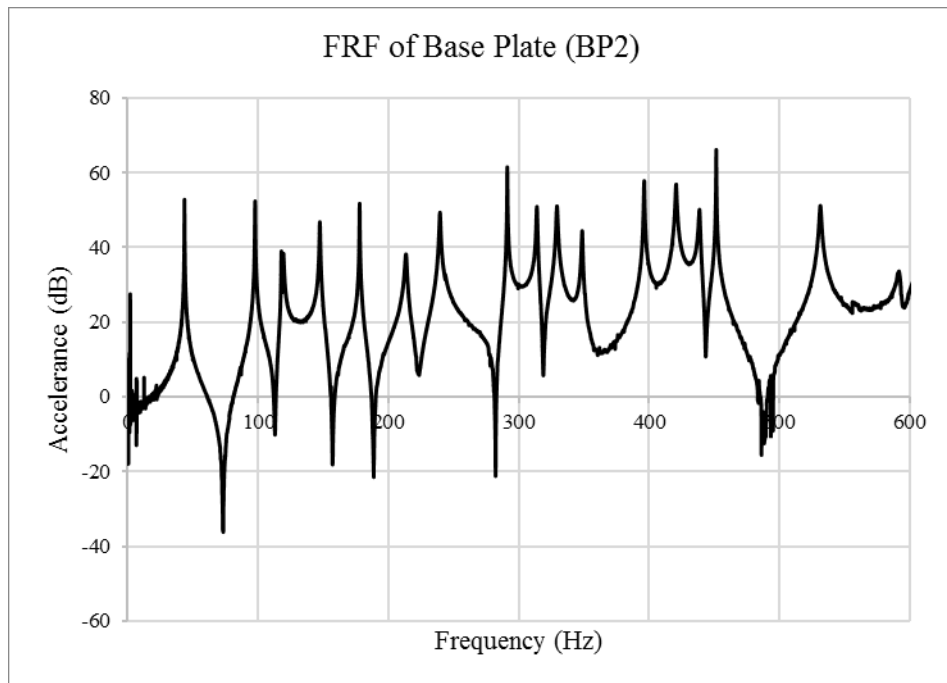


Figure 71 – Accelerance frequency response function of 2mm Base Plate (BP2)

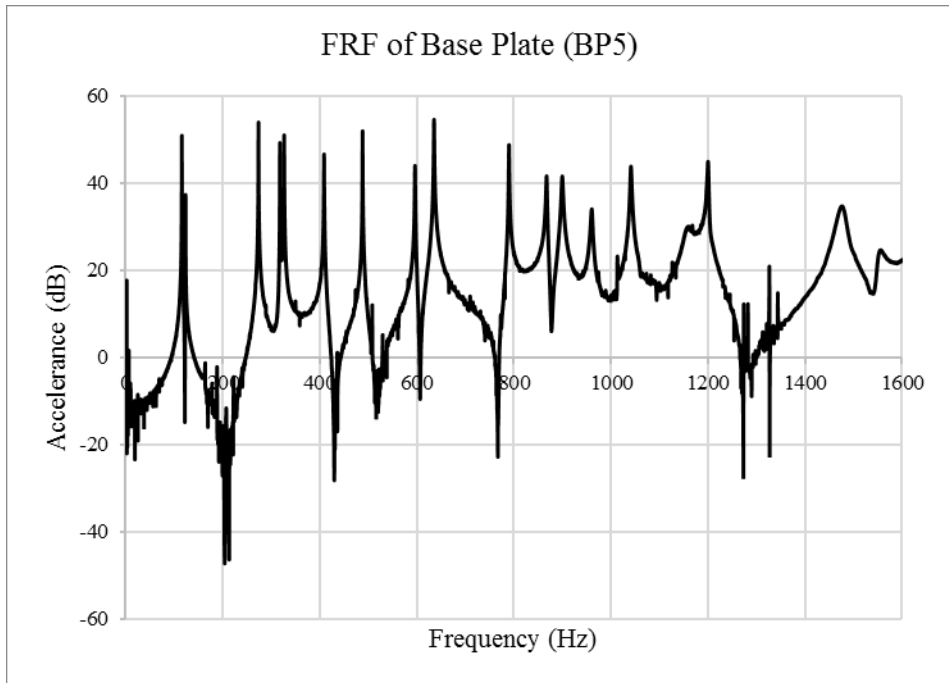


Figure 72 – Accelerance frequency response function of 5mm Base Plate (BP5)

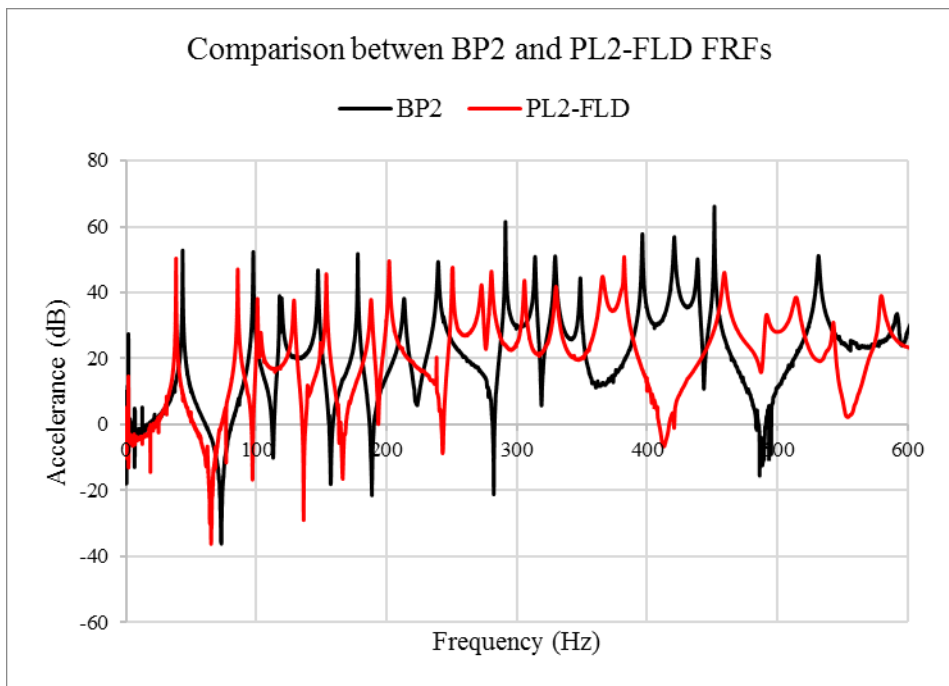
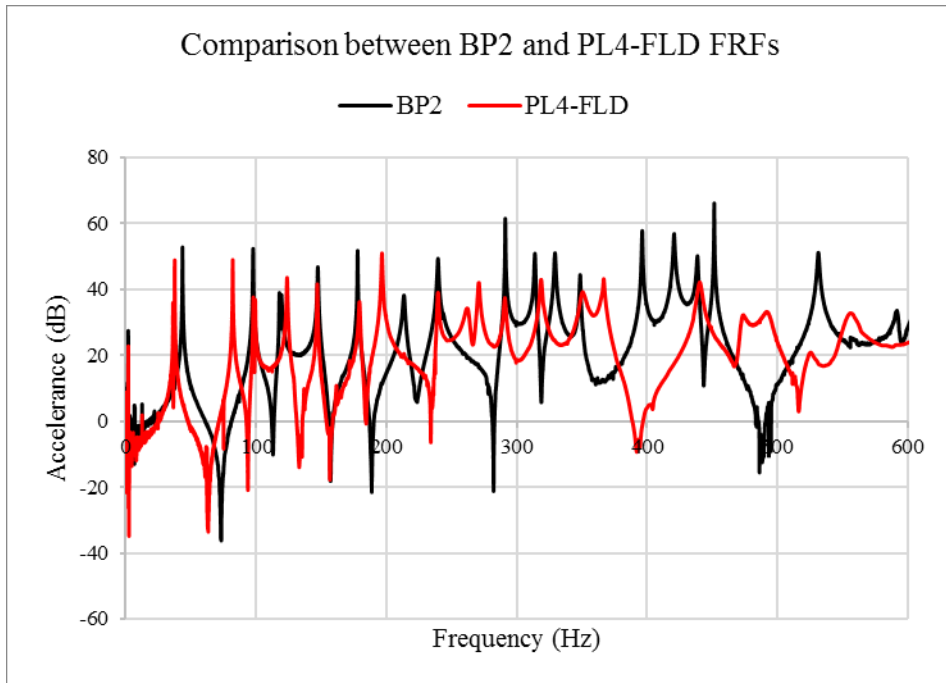
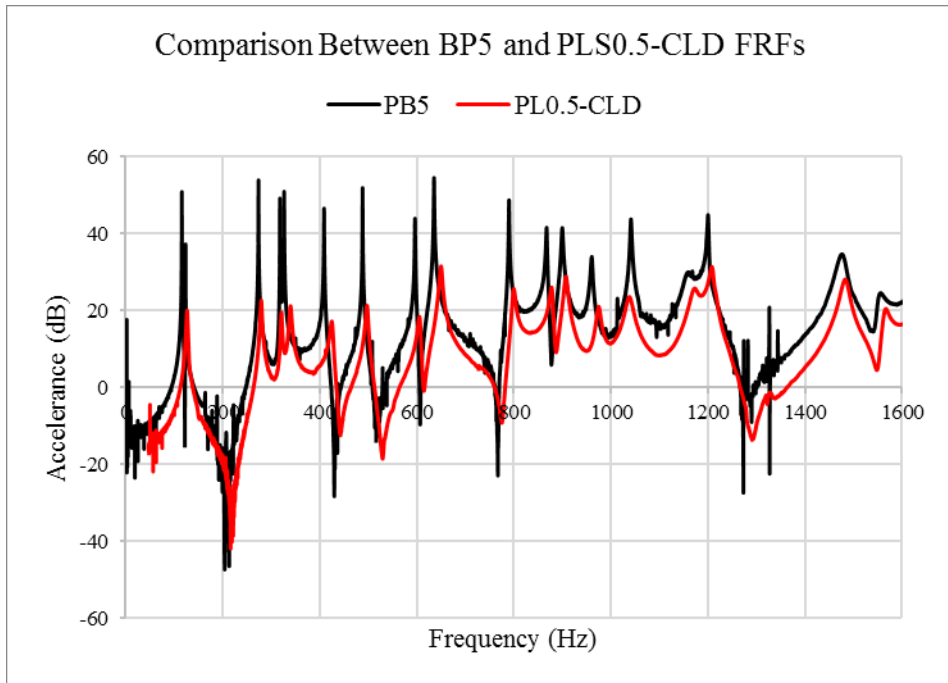


Figure 73 – Comparison of the Accelerance of BP2 and PL2-FLD



*Figure 74 – Comparison of the Accelerance of BP2 and PL4-FLD*

It is evident, by a simple visual analysis of the frequency response functions of the bare plate with a free-layer configuration of Plastigel material shown in Figure 73 and Figure 74, that the application of viscoelastic material, in free-layer configuration, has a positive impact in the behaviour of the plates. The resonant frequencies have been reduced, as expected since there has been an addition of mass. The maximums in the resonant peaks have been reduced, which demonstrates that the damping of the system has been increased.



*Figure 75 – Comparison of the Accelerance of BP5 and PLS0.5-CLD*

In the application of Plastigel material in the constrained layer configuration FRF, shown previously in Figure 75, it can be noticed that the reduction in the peak maximums of the resonant is significantly greater than in the free-layer damping configuration.



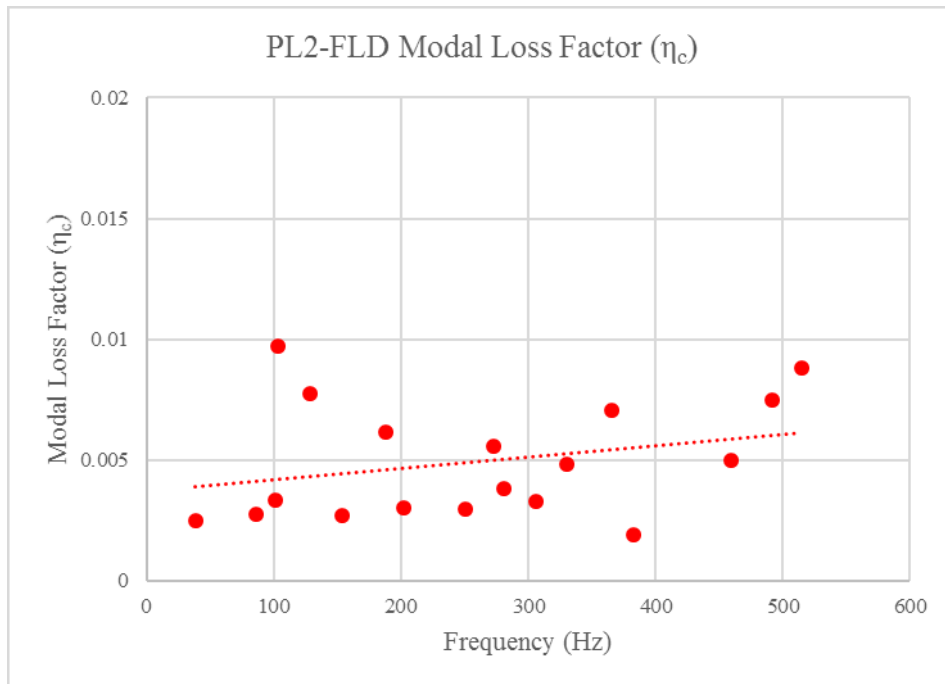


Figure 76 – Modal Loss Factor ( $\eta$ ) of PL2-FLD specimen

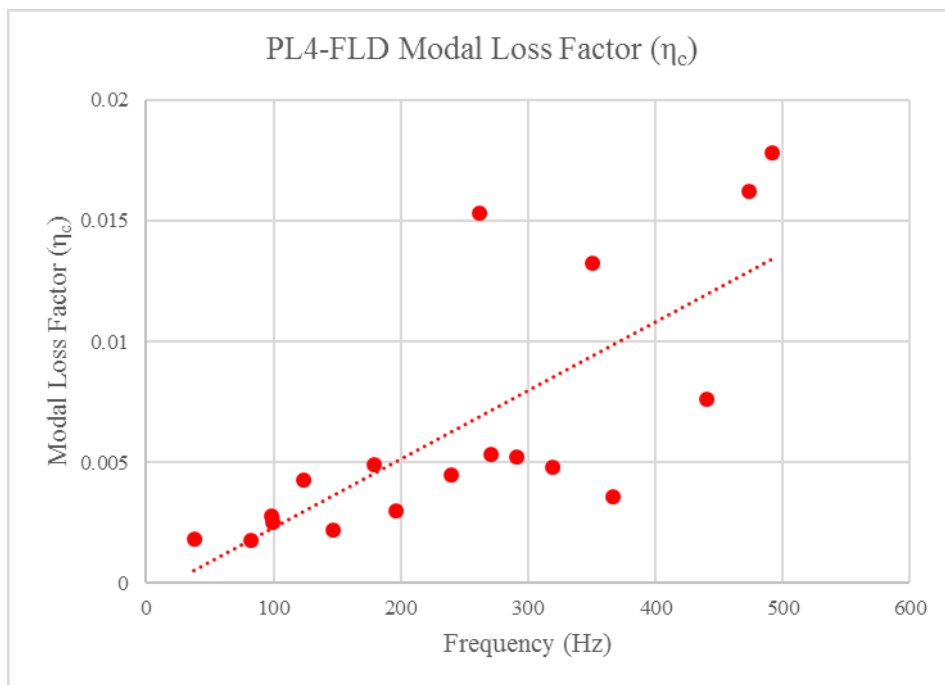
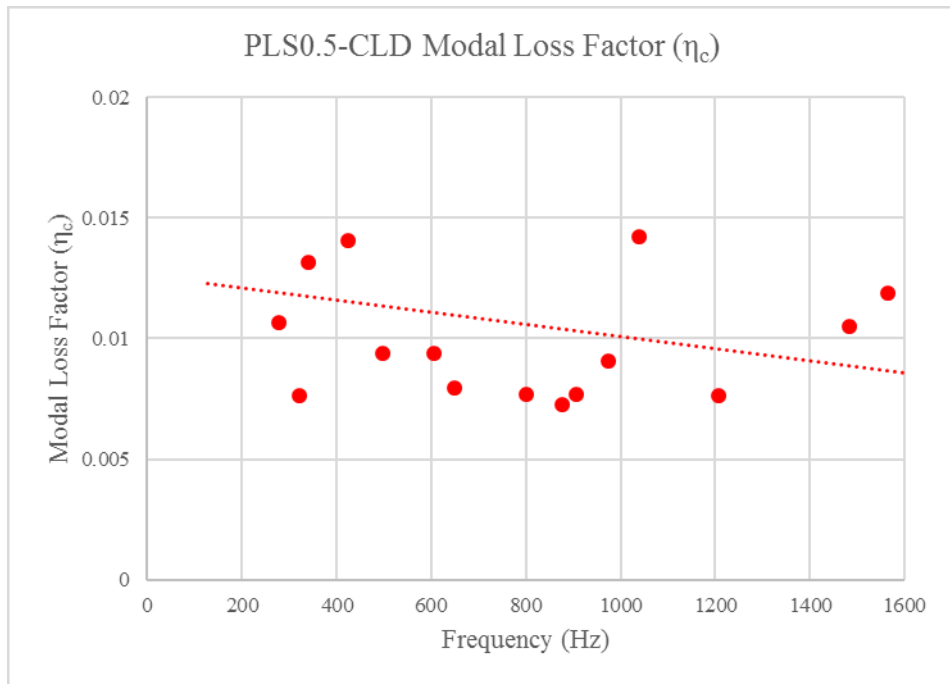


Figure 77 – Modal Loss Factor ( $\eta$ ) of PL4-FLD specimen



*Figure 78 – Modal Loss Factor ( $\eta$ ) of PLS0.5-CLD specimen*

The system modal Loss Factors are in agreement with the behaviour of the acceleration FRFs. Each point corresponds to the calculation of the system Loss Factor for a modal frequency, with the use of the Half-power Bandwidth method, or the n-dB Bandwidth method when needed.

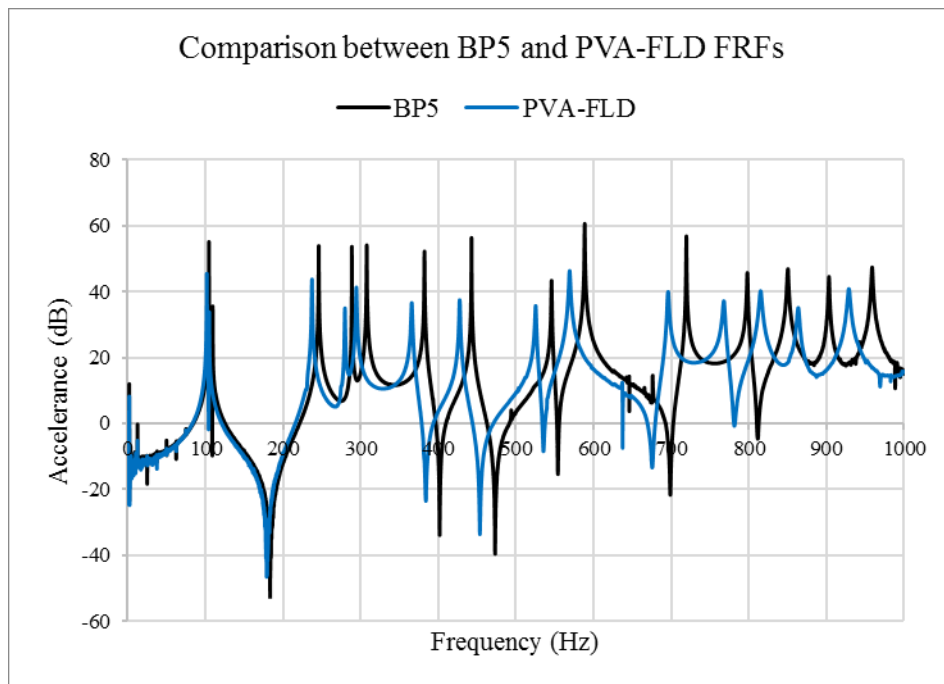


Figure 79 – Comparison of the Accelerance of BP5 and PVA-FLD

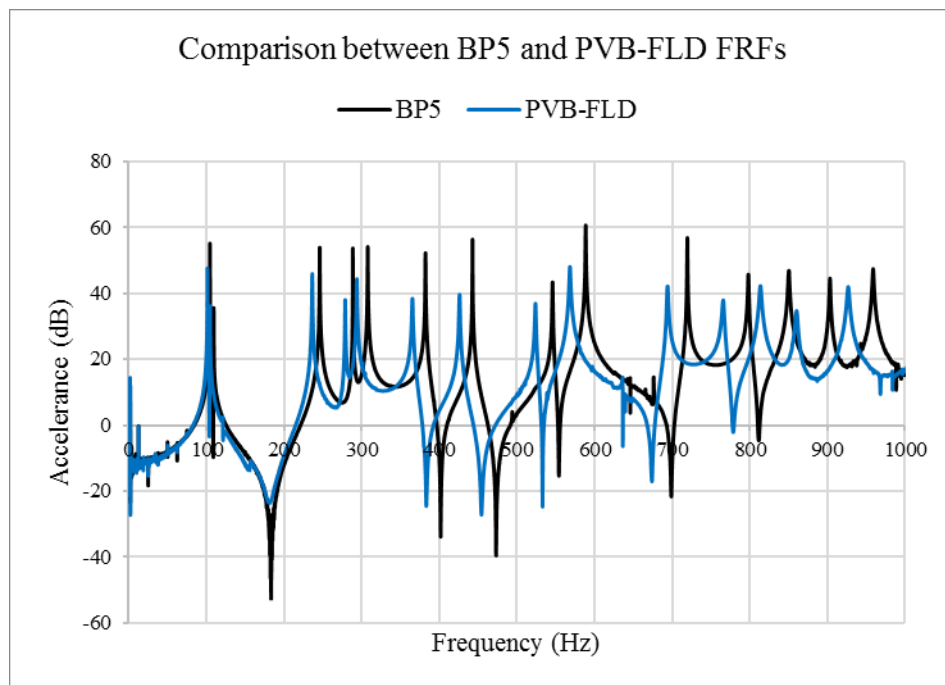


Figure 80 – Comparison of the Accelerance of BP5 and PVB-FLD

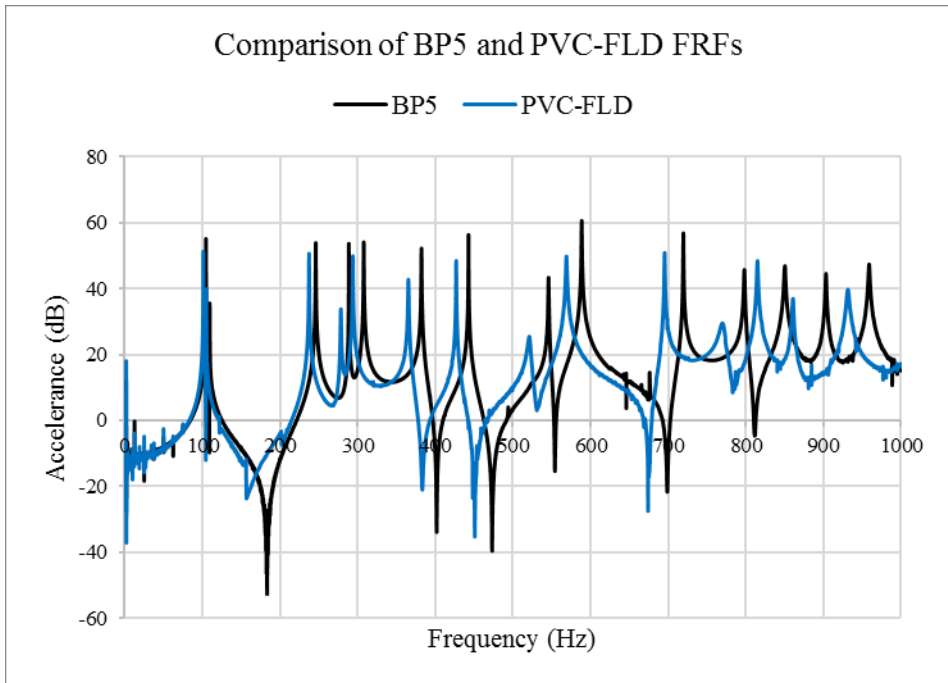


Figure 81 – Comparison of the Accelerance of BP5 and PVC-FLD

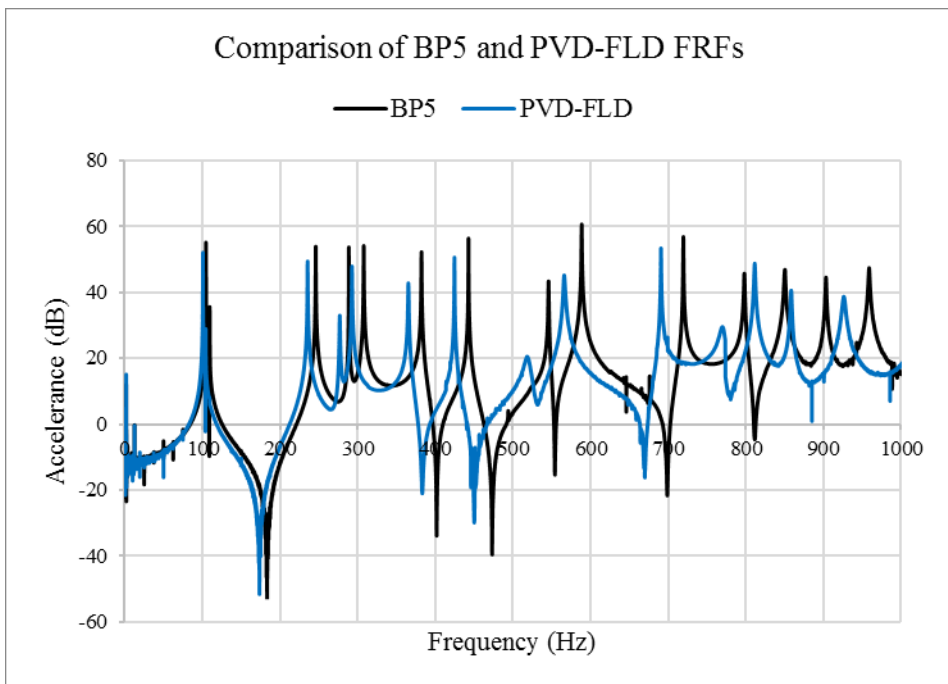
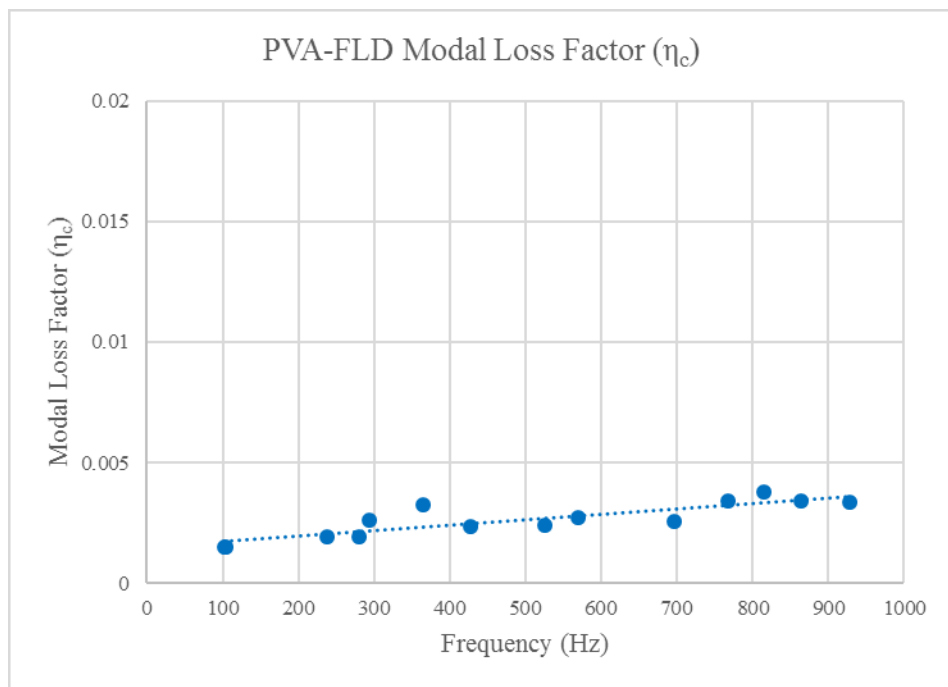


Figure 82 – Comparison of the Accelerance of BP5 and PVD-FLD

From the FRFs of the different Viscogel material application in the free-layer damping configuration, we can see little variations in the behaviour of the system. This evidences the fact that the chemical variations of the material have had little effect in the damping characteristics of the material. This will be more thoroughly shown in the final results.



*Figure 83 – Modal Loss Factor ( $\eta$ ) of PVA-FLD specimen*

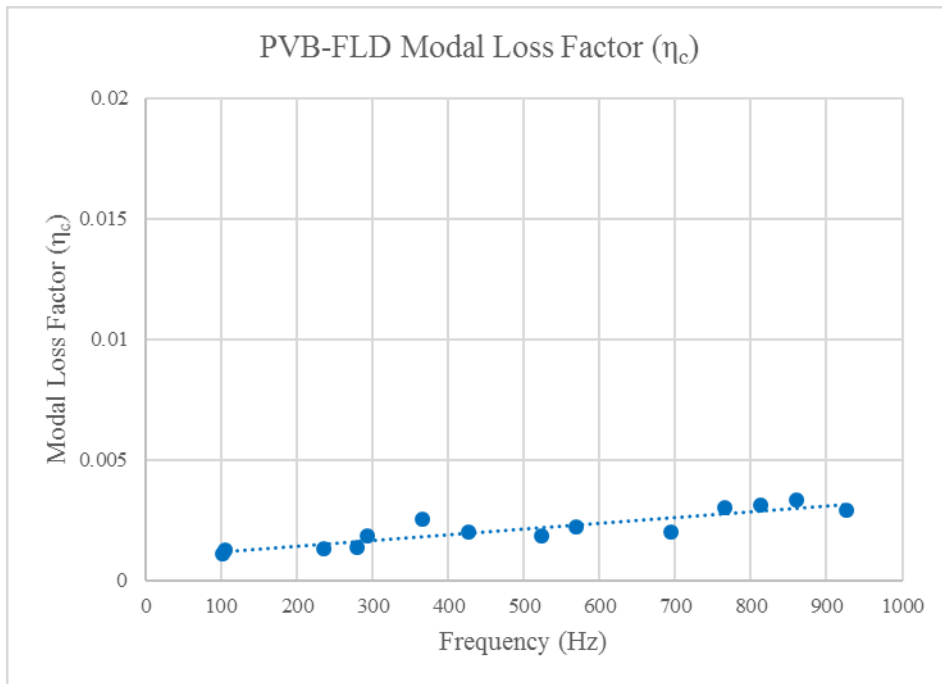


Figure 84 – Modal Loss Factor ( $\eta$ ) of PVB-FLD specimen

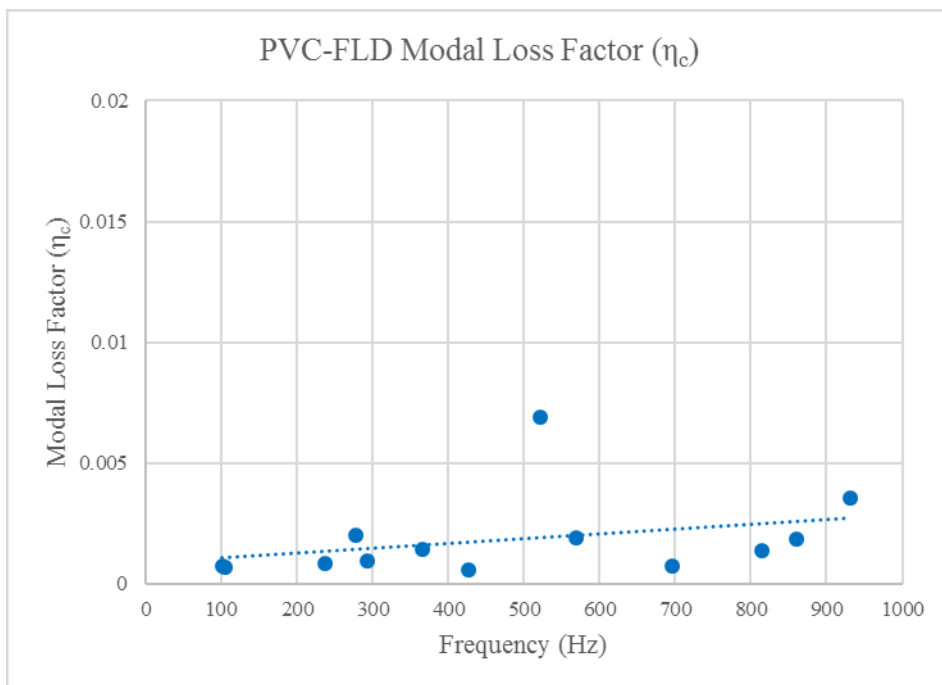


Figure 85 – Modal Loss Factor ( $\eta$ ) of PVC-FLD specimen

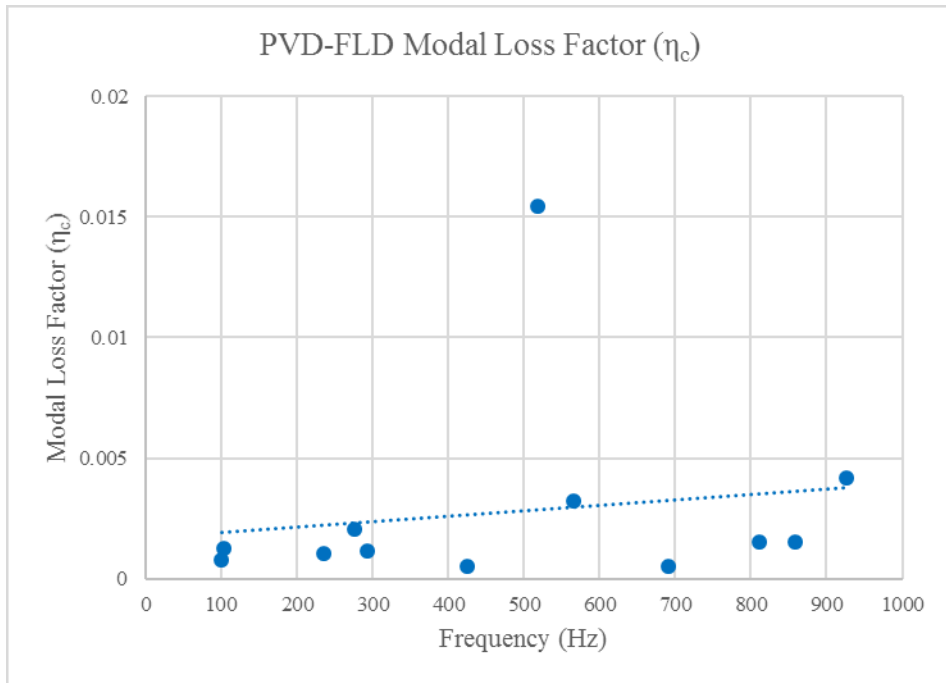


Figure 86 – Modal Loss Factor ( $\eta$ ) of PVD-FLD specimen

For these plate specimens, we can see that mostly the modal Loss Factor is lower. This behaviour is given due to the fact that the ratio between the thickness of the applied viscoelastic layer and the thickness of the base bare steel plate is lower, as shown in Table 8. The ASTM E756 standard suggests a thickness ratio of at least 1 for typical viscoelastic materials, to obtain a properly damped response. The reason that this ratio in the tested specimens was lower, is due to the fact that these were new experimental materials, in which the contraction of the material in the final manufacturing process is not easy to control. This then translates into a density that can result different than the theoretical one, which is why attention should be paid to the

final density of the material, for which laboratory measurements are suggested for its validation.

A possible solution for this issue would be to find plate dimensions that would allow for the manufacturing process to have a better control on the final thickness of the viscoelastic material. Instinctively one would suggest smaller plate dimensions, but the gain in ease of the manufacturing process of a smaller plate and better controllability of viscoelastic thickness control, would be eclipsed by the need of more precise measuring equipment and methods, since in a smaller specimen, the added mass of an accelerometer would make the system prone to larger errors.

There are certain points that fall far from the trend line, as can be seen in the modal Loss Factor graphs shown in Figure 76, Figure 77, Figure 85 or Figure 86. This can be due to several reasons. For example, when two modes are closely spaced, like the case of the points on 100 Hz in Figure 76, it can happen that one of them appears to have a higher modal loss factor, but the equivalent modes in Figure 77 appear to be almost superimposed. These discrepancies will produce values of the material Loss Factor that fall far from the method limitations mentioned in Section 3.1.1 and Section 3.1.2, for the case of a free-layer configuration and a constrained layer configuration respectively, so they will not be considered in the final resulting curve of the material Loss Factor.



## RESULTS AND DISCUSSION

### 9 Resilient Mounts

The experimental tests to obtain the Transmission Loss curves of the floating floor prototype modules allowed for the preparation of the graph shown in Figure 87.

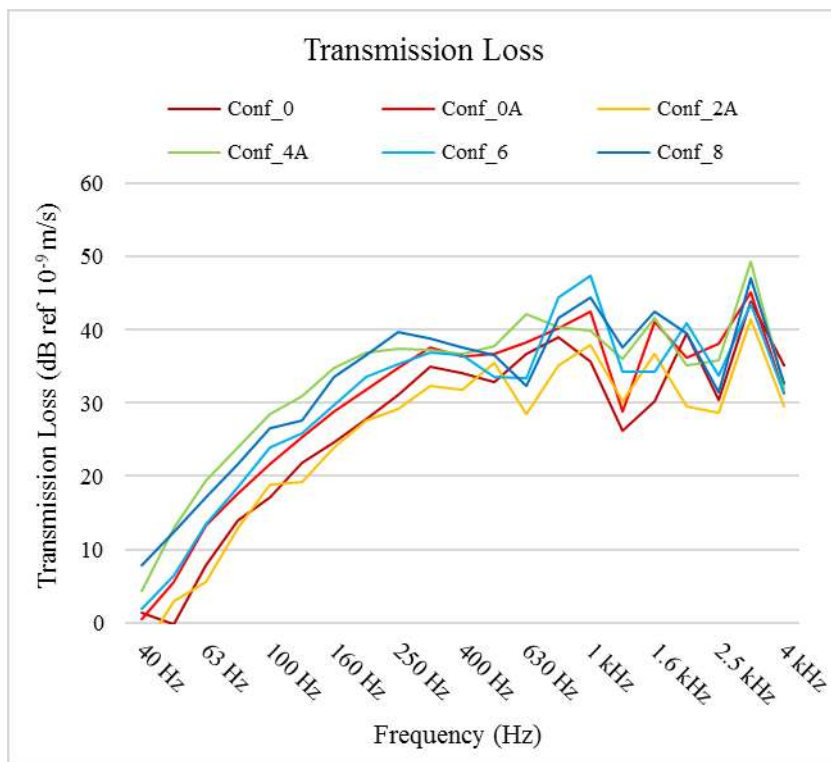


Figure 87 – Transmission Loss curves of the floating floor prototype modules

The Transmission Loss curves behave accordingly to the theory presented previously. The curves tend to zero in proximity of the damped natural frequency of the system. As the frequency increase, the curves increase

about linearly in the log-log graph. In addition, we can see a general trend of the Transmission Loss curves which increase their values as the stiffness of the resilient material decreases. The stiffest floating floor prototype modules, Configuration 0 and Configuration 2A, are the ones showing the lowest Transmission Loss. Au contraire, Configuration 4A and Configuration 8, which have the lowest stiffness among the prototypes are characterised by the highest Transmission Loss values. In the higher frequency range, the curves start showing a series of peaks. This is due to the fact that the system starts being governed also by several other modes, which is why the modules no longer behave as a SDOF system.

In the higher frequency range, the Transmission Loss curves stabilise, and the gain between the different module configurations tend to be smaller as the frequency furtherly increases.

## 10 Material characterisation

Since, as seen in Equation (8) and Equation (9), the Loss Factor is the same for the complex Young modulus and the complex Shear modulus, we can combine the Loss Factor from the different configurations into one final graph of Loss factor in the frequency domain.

As mentioned previously in Section 3.1.1 and Section 3.1.2, in order for the Loss Factor data calculations to be consistent, the ASTM E756 suggests certain limits. The standard suggests that the calculated value of Equation (15) should be greater than 1.01 for a free-layer configuration, and the calculated value of Equation (36), should be greater than 2.01. For pragmatism, Equations (15) and (36) are reported in this section:

$$Z_u^* = \left(1 + \frac{\rho_D h_D}{\rho_B h_B}\right) \left(\frac{f_n}{f_{0n}}\right)^2 (1 + i\eta_C) \quad (15)$$

$$\frac{D_C^*}{D_1} = \left(2 + \frac{\rho_2 h_2}{\rho_1 h_1}\right) \left(\frac{f_{Cn}}{f_{1n}}\right)^2 (1 + i\eta_C) \quad (36)$$

When applying the method described previously, we find that there are several values that do not comply with these limitations, which is why the results of certain modal frequencies are not considered reliable.

Once the points outside the calculation limits are excluded, we obtain the final curve for the material Loss Factor ( $\eta$ ). In Figure 88, we can see the resulting Loss Factor ( $\eta$ ) curve for Plastigel.

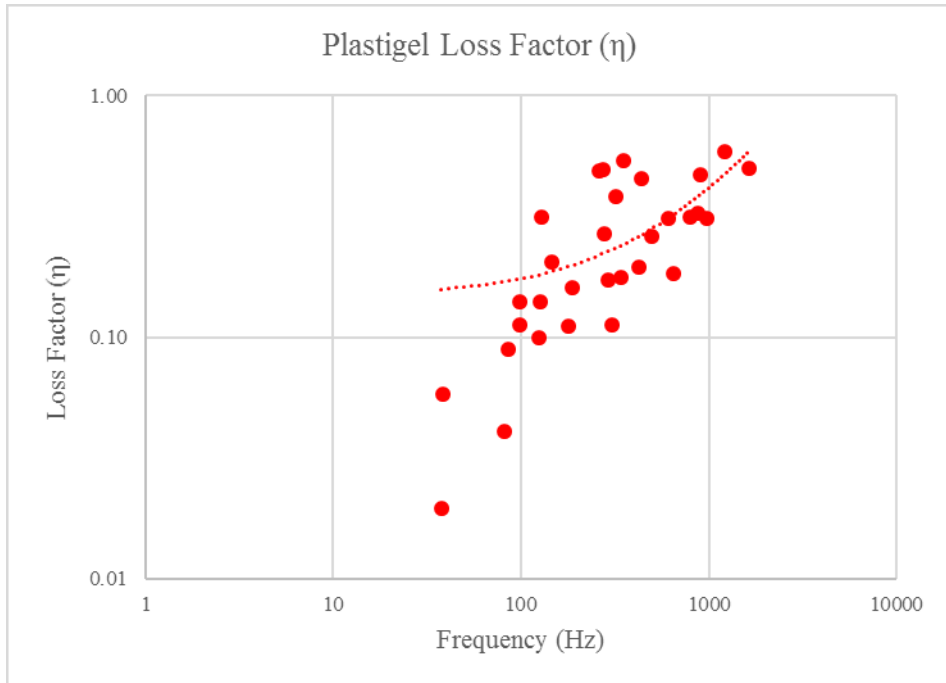


*Figure 88 – Obtained Loss Factor of Plastigel*

The obtained results are in harmony with the behaviour of classical viscoelastic materials in the transition region, shown in Figure 4 and Figure 5.

Also, in Figure 89 a comparison has been made with the Loss Factor obtained with DMA tests of other similar viscoelastic materials. It can be seen that the calculated Loss Factor has a behaviour similar to the other viscoelastic materials.

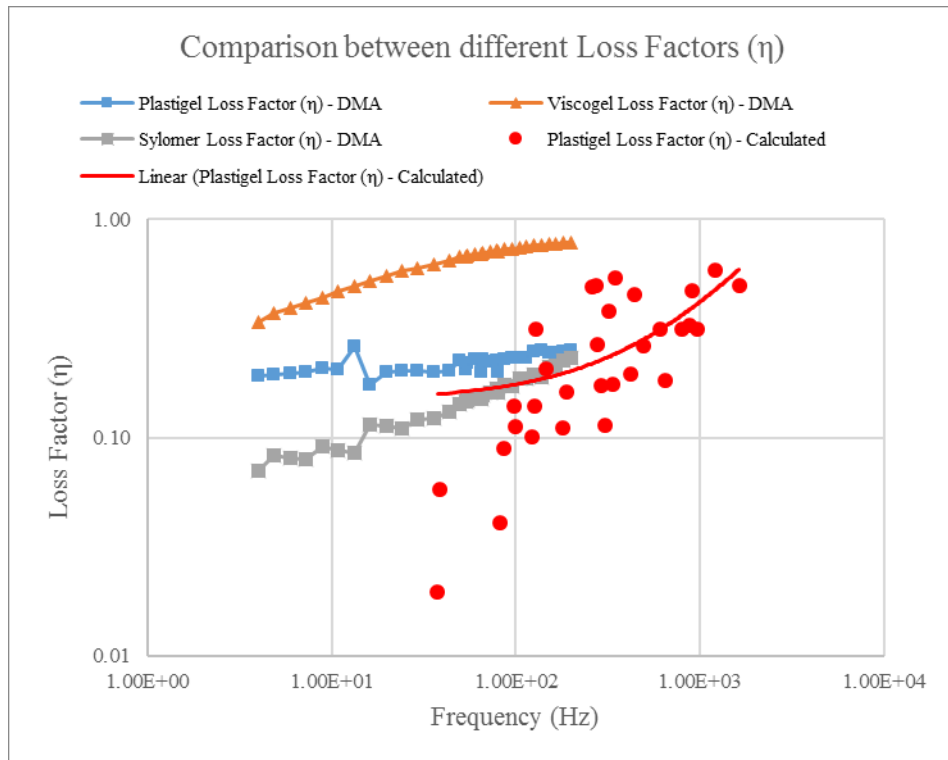


Figure 89 – Comparison graph between the Loss Factor obtained with DMA tests performed on Plastigel, Viscogel and Sylomer, and the Loss Factor calculated with the methods presented in this work



## CONCLUSIONS

The research activities done and presented in this work, have the objective to develop and advise on methods to control noise and vibration on board ships by means of two particular methods, among several existing passive vibration control techniques. These two methods are the use of resilient mounts, such as floating floors, to isolate the receiving structures from structure borne noise as well as from impact noise, and the addition of damping to the system, by the incorporation of damping layers consisting of viscoelastic materials.

As for the first method described, the objective was to propose a design method for the optimisation of floating floors, since there it has been found that no international standards for this means exist. The results have been promising, and the following conclusions can be drawn:

- An optimization method has been set up, that has proven to produce more efficient floating floors. This method has been based on numerical simulations and validated with experimental tests.
- An optimal floating floor design to reduce the structure borne noise generated by human action impacts has been designed.

- The outcome of the measurements of the dynamic tests undertaken to evaluate the Transmission Loss curves show that floating floors can be considered as single-degree-of-freedom systems in the low frequency range.
- The physical characteristics of viscoelastic materials are difficult to control during the manufacturing process. This can impose several difficulties in the specimen and prototype preparation for the tests to be undertaken.
- Due to the variability of the physical properties of viscoelastic materials during the manufacturing process, close attention must be paid to the results of numerical simulations of floating floors, and experimental tests are always suggested to verify the compliance of numerical models.

The second method studied in the present work, aimed at providing a solid theoretical background and a base for further studies on the damping effects of viscoelastic materials involved in the noise and vibration mitigation on board ships, since currently their application on the maritime industry is mainly empirical. The idea was to propose a simple method for measuring the damping capacities of viscoelastic materials. In this aspect, the following conclusions have been achieved:



- A procedure for measuring the Loss Factor of viscoelastic materials has been identified and analytically proposed for obtaining the Loss Factor of viscoelastic materials from plate specimens, based on the Oberst beam theory, the RKU equations, and the equivalence of the length of plates vibrating in the same waveform, for both unconstrained layer configuration and constrained layer configuration of sandwich plates.
- As well as for the floating floor specimen and prototype preparation, the physical characteristics of viscoelastic materials are difficult to control during the manufacturing process. The lack of precise control on the thickness and density ratios required by a specific test can cause several difficulties for the tests to be performed.
- Several tests on several plate specimens have ascertained the fact that the thickness ratio between the viscoelastic material and the base plate is of paramount importance. The thickness of the viscoelastic material must be precisely controlled to obtain thickness ratios that will permit to perform tests that could yield modal Loss Factors and modal frequencies which

together will give optimal values of the  $Z_u^*$  and  $Z_c^*$  parameters, to finally obtain reliable values of the material Loss Factor ( $\eta$ ).

- The study on the measurement of the material Loss Factor using plate specimens can be used as a baseline for future research activities focused on the characterisation of viscoelastic materials for marine applications with the aim of developing design guidelines for the optimisation of the use of viscoelastic materials when applied on marine structures.

## References

- [1] F. De Lorenzo and M. Biot, “Noise and vibration: comfort standards evolving in the wrong direction?,” *Naval Architect*, pp. 36-39, 2006.
- [2] M. Biot and F. De Lorenzo, “Open Issues Regarding Noise and Vibrations On Board Cruise Ships: A Suggested Approach for Measuring Comfort,” in *Institute of Acoustics, Autumn Conference 2007*, Oxford, 2007.
- [3] M. Biot and F. De Lorenzo, “Criteria for designing noise and vibration comfort of passengers on board of ships,” in *XXI Congreso Panamericano de Ingenieria Naval*, Montevideo, 2009.
- [4] M. Biot and F. De Lorenzo, “Some notes on the sound reduction index of pax cabins panels on cruise ships,” in *Acoustics '08 Conference*, Paris, 2008.
- [5] M. Biot, D. Boote, E. Brocco, P. N. Mendoza Vassallo, L. Moro and T. Pais, “Validation of a design method for the simulation of the mechanical mobility of marine diesel engine seating,” in *18th*

- International Conference on Transport Means, TRANSPORT MEANS 2014*, Kaunas, 2014.
- [6] L. Moro, E. Brocco, P. N. Mendoza Vassallo, H. Le Sourne and M. Biot, “Numerical simulation of the dynamic behaviour of resilient mounts for marine diesel engines,” in *Proceedings of the 5th International Conference on Marine Structures, MARSTRUCT 2015*, Southampton, 2015.
- [7] J. S. Tao, G. R. Liu and K. Y. Lam, “Design Optimization of Marine Engine-Mount System,” *Journal of Sound and Vibration*, vol. 235, no. 3, pp. 477-494, August 2000.
- [8] M. Biot and L. Moro, “Experimental study of a resilient mounting for marine diesel engines,” in *International Marine Design Conference, IMDC 2012*, Glasgow, 2012.
- [9] M. Biot, L. Moro and P. N. Mendoza Vassallo, “Prediction of the structure-borne noise due to marine diesel engines on board cruise ships,” in *21st International Congress on Sound and Vibration ICSV 2014*, Beijing, 2014.
- [10] A. Badino and E. Rizzuto, “Innovative de-coupling materials for the isolation of ship cabins,” in *Maritime Technology and Engineering, C.*

- Guedes Soares and T. A. Santos, Eds., Taylor and Francis Group, 2015, pp. 565-573.
- [11] T. Cho, “Vibro-acoustic characteristics of floating floor system: The influence of frequency-matched resonance on low frequency impact sound,” *Journal of Sound and Vibration*, vol. 332, no. 1, pp. 33-42, 2013.
- [12] A. Ferrari and E. Rizzuto, “Modal behaviour of a full scale deck panel with anti-noise treatments,” in *Congress of International Maritime Association of the Mediterranean, IMAM 2005*, Lisbon, 2005.
- [13] N. Bull, T. Riise and B. E. Moen, “Occupational injuries to fisheries workers in Norway reported to insurance companies from 1991 to 1996,” *Occupational Medicine*, vol. 51, no. 5, pp. 299-304, August 2001.
- [14] R. L. Neitzel, B. E. Berna and N. S. Seixas, “Noise exposures aboard catcher/processor fishing vessels,” *American Journal of Industrial Medicine*, vol. 49, no. 8, pp. 624-633, 2006.
- [15] DNV, “Quieter offshore vessels are safer ships says DNV,” *Motor Ship*, vol. 90, pp. 28-30, 2009.

- [16] H.-S. Kim, B.-K. Kim, S.-I. Cha and Y.-S. Kim, "Floor impact noise reduction in ship cabins by means of a floating floor," *Noise Control Engineering Journal*, vol. 54, no. 6, pp. 406-413, 2006.
- [17] L. Moro, E. Brocco, A. Badino, P. N. Mendoza Vassallo, A. Clericuzio and M. Biot, "Design procedure for the development of new floating floors to improve comfort on ships," in *Practical Design of Ships and Other Floating Structures, PRADS 2016*, Copenhagen, 2016.
- [18] J. Fragasso, L. Moro, P. N. Mendoza Vassallo, M. Biot and A. Badino, "Experimental characterization of viscoelastic materials for marine applications," in *Proceedings of the 6th International Conference on Marine Structures, MARSTRUCT 2017*, Lisbon, 2017.
- [19] R. Fan, G. Meng, J. Yang and C. He, "Experimental study of the effect of viscoelastic damping materials on noise and vibration reduction within railway vehicles," *Journal of Sound and Vibration*, vol. 319, no. 1-2, pp. 58-76, 2009.
- [20] M. D. Rao, "Recent applications of viscoelastic damping for noise control in automobiles and commercial airplanes," *Journal of Sound and Vibration*, vol. 262, no. 3, pp. 457-474, May 2003.
- [21] A. Ferrari and E. Rizzuto, "Measuring damping properties of viscoelastic materials for marine applications," in *Proceedings of the 1st*

*International Conference on Marine Structures (MARSTRUCT 2007)*,  
Glasgow, 2007.

- [22] C. W. De Silva, *Vibration: Fundamentals and Practice*, 2nd ed., Boca Raton, FL: CRC Press, 2007.
- [23] D. I. G. Jones, *Handbook of Viscoelastic Vibration Damping*, Chichester, West Sussex: Wiley, 2001.
- [24] W. T. Thomson, *Theory of Vibrations with Applications*, 4th ed., New Jersey: Prentice Hall, 1993.
- [25] M. Stiassnie, "On the application of fractional calculus for the formulation of viscoelastic models," *Applied Mathematical Modelling*, vol. 3, no. 4, pp. 300-302, August 1979.
- [26] R. Bagley and P. Torvik, "A Theoretical Basis for the Application of Fractional Calculus to Viscoelasticity," *Journal of Rheology*, vol. 27, no. 3, pp. 201-210, 1983.
- [27] L. B. Eldred, W. P. Baker and A. N. Palazotto, "Kelvin-Voigt versus fractional derivative model as constitutive relations for viscoelastic materials," *AIAA Journal*, vol. 33, no. 3, pp. 547-550, March 1995.
- [28] D. J. Mead, *Passive Vibration Control*, Chichester: Wiley, 1998, p. 540.

- [29] E. E. Ungar, "Damping of Structures and Use of Damping Materials," in *Handbook of Noise and Vibration Control*, M. J. Crocker, Ed., New Jersey, John Wiley & Sons, Inc., 2007, p. 1569.
- [30] W. A. Cavanaugh, G. C. Tocci and J. A. Wilkes, Eds., *Architectural Acoustics: Principles and Practice*, 2 ed., Wiley & Sons, Inc., 2009.
- [31] Perkin Elmer Inc., "Startup Guide DMA 8000," 2013. [Online]. Available: [https://www.perkinelmer.com/lab-solutions/resources/docs/PRD\\_DMA8000\\_Time\\_Temperature\\_Superposition.pdf](https://www.perkinelmer.com/lab-solutions/resources/docs/PRD_DMA8000_Time_Temperature_Superposition.pdf). [Accessed 13 February 2017].
- [32] Illinois Tool Works Inc., "Dynamic Mechanical Analysis (DMA)," 2017. [Online]. Available: <http://www.instron.us/en-us/our-company/library/glossary/d/dma-dynamic-mechanical-analysis>. [Accessed 13 February 2017].
- [33] CALCE, "Materials Characterization - Dynamic Mechanical Analysis," University of Maryland, 2008. [Online]. Available: <http://www.calce.umd.edu/TSFA/dma.htm>. [Accessed 13 February 2017].
- [34] S. Misra, K. Reed, B. Schafer, K. Ramesh and A. Okamura, "Mechanics of Flexible Needles Robotically Steered through Soft Tissue," *The*



*International Journal of Robotics Research*, vol. 29, no. 13, pp. 1640-1660, November 2010.

- [35] A&D Company Ltd., “Products - Rheovibron Automatic Dynamic Viscoelastometer,” A&D Company Ltd., 2016. [Online]. Available: [http://www.aandd.jp/products/test\\_measuring/ddv/ddv.html](http://www.aandd.jp/products/test_measuring/ddv/ddv.html). [Accessed 13 February 2017].
- [36] D. M. Stoakley, A. K. St. Claire and B. D. Little, “Tensile film clamps and mounting block for the rheovibron and autovibron viscoelastometer”. United States of America Patent 4,864,865, 12 September 1989.
- [37] T. Murayama, “The Measurement of Dynamic Shear Properties of Polymer Melts with a Rheovibron Viscoelastometer,” in *Rheology*, vol. 2, G. Astarita, G. Marucci and L. Nicolais, Eds., Springer, 1980, pp. 255-255.
- [38] ASTM E756-05(2010), Standard Test Method for Measuring Vibration-Damping Properties of Materials, West Conshohocken: ASTM International, 2010.
- [39] Perkin Elmer Inc, “Dynamic Mechanical Analysis (DMA),” 2017. [Online]. Available:

- <https://www.perkinelmer.com/it/category/dynamic-mechanical-analysis-dma>. [Accessed 13 February 2017].
- [40] E. E. Ungar, D. Ross and E. J. M. Kerwin, "Damping of Flexural Vibrations by Alternate Visco-Elastic and Elastic Layers," Wright Air Development Center, Wright-Patterson Air Force Base, Ohio, Declassified in 1960.
- [41] E. M. Kerwin, "Damping of Flexural Waves by a Constrained Viscoelastic Layer," *The Journal of the Acoustical Society of America*, vol. 31, no. 7, pp. 952-962, July 1959.
- [42] D. Ross, E. E. Ungar and E. M. Kerwin, Jr., "Damping of Plate Flexural Vibrations by Means of Viscoelastic Laminae," *Structural Damping, ASME Publication*, pp. 49-87, December 1959.
- [43] T. Tarnóczy, "Vibration of metal plates covered with vibration damping layers," *Journal of Sound and Vibration*, vol. 11, no. 3, pp. 299-307, 1970.
- [44] C. V. R. Reddy, N. Ganesan and B. V. A. Rao, "Response of unconstrained layer panels to random excitation at a point," *Journal of Sound and Vibration*, vol. 73, no. 3, pp. 419-427, 1980.
- [45] C. V. R. Reddy, N. Ganesan, B. V. A. Rao and S. Narayanan, "Response of plates with unconstrained layer damping treatment to random acoustic

- excitation. Part I: Damping and frequency evaluations,” *Journal of Sound and Vibration*, vol. 69, no. 1, pp. 35-43, 1980.
- [46] G. Parthasarathy, C. V. R. Reddy and N. Ganesan, “Partial coverage of rectangular plates by unconstrained layer damping treatments,” *Journal of Sound and Vibration*, vol. 102, no. 2, pp. 203-216, 1985.
- [47] H. Oberst and K. Frankenfeld, “Über die Dämpfung der Biegeschwingungen dünner Bleche durch fest haftende Beläge,” *Acta Acustica united with Acustica*, vol. 2, no. 6, pp. 181-194, 1952.
- [48] P. J. Torvik and B. D. Runyon, “Estimating the Loss Factors of Plates with Constrained Layer Damping Treatments,” *AIAA Journal*, vol. 45, no. 7, pp. 1492-1500, 2007.
- [49] N. Tschoegl, W. G. Knauss and I. Emri, “Poisson's Ratio in Linear Viscoelasticity – A Critical Review,” *Mechanics of Time-Dependent Materials*, vol. 6, no. 1, pp. 3-51, March 2002.
- [50] R. A. Di Taranto, “Theory of Vibratory Bending for Elastic and Viscoelastic Layered Finite-Length Beams,” *Journal of Applied Mechanics*, vol. 32, no. 4, pp. 881-886, 1965.
- [51] D. J. Mead and S. Markus, “The Forced Vibration of a Three-Layered, Damped Sandwich Beam with Arbitrary Boundary Conditions,” *Journal of Sound and Vibration*, vol. 10, no. 2, pp. 163-175, 1969.

- [52] D. K. Rao, "Frequency and Loss Factors of Sandwich Beams under Various Boundary Conditions," *Journal of Mechanical Engineering Science*, vol. 20, no. 5, pp. 271-282, 1978.
- [53] B. M. Shafer, "An overview of constrained-layer damping theory and application," in *Proceedings of Meetings on Acoustics*, Montreal, 2013.
- [54] A. W. Leissa, "The Free Vibration of Rectangular Plates," *Journal of Sound and Vibration*, vol. 31, no. 3, pp. 257-293, December 1973.
- [55] R. E. D. Bishop and G. M. L. Gladwell, "An Investigation into the Theory of Resonance Testing," *Philosophical Transactions of the Royal Society*, vol. 255, no. 1055, pp. 241-280, January 1963.
- [56] J. W. Pendered and R. E. D. Bishop, "A Critical Introduction to Some Industrial Resonance Testing Techniques," *Journal of Mechanical Engineering Science*, vol. 5, no. 4, pp. 345-367, December 1963.
- [57] H. P. Yin, "A new theoretical basis for the bandwidth method and optimal power ratios for the damping estimation," *Mechanical Systems and Signal Processing*, vol. 22, no. 8, pp. 1869-1881, November 2008.
- [58] G. A. Papagiannopoulos and G. D. Hatzigeorgiou, "On the use of the half-power bandwidth method to estimate damping in building structures," *Soil Dynamics and Earthquake Engineering*, vol. 31, no. 7, pp. 1075-1079, July 2011.

- [59] Ødegaard, “Sound insulation properties of marine flooring constructions manufactured by Sika Cufaden A/S,” Technical Report, Fredensborg, 2004.
- [60] G. Ramorino, D. Vetturi, D. Cambiaghi, A. Pegoretti and T. Ricco, “Development in dynamic testing of rubber compounds: assessment of non-linear effects,” *Polymer Testing*, vol. 22, no. 6, pp. 681-687, 2003.
- [61] T. R. Lin, N. H. Farag and J. Pan, “Evaluation of frequency dependent rubber mount stiffness and damping by impact test,” *Applied Acoustics*, vol. 66, no. 7, pp. 829-844, 2005.
- [62] P. Ladislav, P. Ludek, V. Frantisek and C. Jan, “Laboratory measurement of stiffness and damping of rubber element,” *Engineering Mechanics*, vol. 14, no. 1/2, pp. 13-22, 2007.
- [63] V. M. Kulik, B. N. Semenov, A. V. Boiko, B. M. Seoudi, H. H. Chun and I. Lee, “Measurement of dynamic properties of viscoelastic materials,” *Experimental Mechanics*, vol. 49, pp. 417-425, 2009.
- [64] A. Schiavi, A. Pavoni Belli, F. Russo and M. Corallo, “Dynamic stiffness of resilient materials: some consideration on the proposed revision of ISO 9052-1 standard,” in *20th International Congress on Acoustics, ICA 2010*, Sidney, 2010.

- [65] F. Fahy, “Foundation of engineering acoustics,” Elsevier Academic Press, San Diego, 2005.
- [66] L. Cremer, M. Heckl and B. A. T. Petersson, *Structure-Borne Sound*, 3 ed., Berlin: Springer-Verlag Berlin Heidelberg, 2005, p. 608.
- [67] L. Moro, M. Biot, N. Mantini and C. Pestelli, “Solutions to improve accuracy in experimental measurements of the dynamic response of resilient mountings for marine diesel engines,” in *4th International Conference on Marine Structures, MARSTRUCT 2013*, Espoo, 2013.
- [68] L. Moro, *Structure borne noise due to marine diesel engines: Experimental study and numerical simulation for the prediction of the dynamic behaviour of resilient mounts*, PhD Thesis, Trieste: University of Trieste, 2014, p. 165.
- [69] Agilent Technologies, *The Fundamentals fo Modal Testing*, Agilent Technologies, 2000, p. 56.
- [70] D. Roylance, “Linear Viscoelasticity,” Massachusetts Institute of Technology, 24 October 2001. [Online]. Available: <http://web.mit.edu/course/3/3.11/www/modules/visco.pdf>. [Accessed 16 January 2017].
- [71] J. Vincent, *Structural Biomaterials*, 3rd ed., Princeton, New Jersey: Princeton University Press, 2012, p. 240.

- [72] R. R. Craig and A. J. Kurdila, *Fundamentals of Structural Dynamics*, 2nd ed., New Jersey: John Wiley & Sons, Inc., 2006.
- [73] A. Ferrari and E. Rizzuto, “Vibrational behaviour of a deck panel of a fast ferry,” in *Proceedings of 7th International Conference on Fast Sea Transportation (FAST2003)*, Ischia, Italy, 2003.